FACULDADE DE ENGENHARIA DA UNIVERSIDADE DO PORTO

Relaxed Branch Flow Model Applied to Renewable Energy Communities

Gonçalo Fernando Sousa Coelho

FEUP FACULDADE DE ENGENHARIA
UNIVERSIDADE DO PORTO

Mestrado em Engenharia Eletrotécnica e de Computadores

Supervisor: Prof. Doutor Tiago André Teixeira Soares

July 28, 2026

Resumo

A crescente penetração de Fontes de Energia Renovável (RES) distribuídas, a eletrificação dos consumos finais e o surgimento dos prosumidores têm vindo a reforçar o papel das Comunidades de Energia Renovável (RECs) como elementos-chave da transição energética. Estas comunidades promovem a geração local, o autoconsumo e a partilha justa de benefícios, contribuindo para um sistema energético mais sustentável e descentralizado. No entanto, a maioria dos modelos de otimização atualmente utilizados na gestão de RECs apresenta limitações na aplicação a contextos reais, uma vez que frequentemente dependem de representações simplificadas das redes que desconsideram as restrições operacionais e físicas das redes de distribuição.

Com o objetivo de ultrapassar estas limitações e melhorar a precisão técnica da otimização das RECs, esta dissertação centra-se no estudo, formulação e aplicação de um Modelo de Fluxo de Ramo Relaxado (RBFM) como uma estrutura que incorpora explicitamente as restrições da rede de distribuição, preservando a eficiência computacional. Com base em investigações anteriores sobre técnicas de relaxação convexa e formulações de Fluxo de Potência Ótimo (OPF), o estudo analisa como estas abordagens podem ser adaptadas no contexto das comunidades de energia.

A abordagem proposta foi integrada à ferramenta de RECs do INESC TEC, Optimal Scheduling Tool for Energy Communities (OSTEC), um sistema interno de simulação e otimização de transações energéticas comunitárias que permite a formulação de uma operação comunitária explicitamente condicionada pelas restrições da rede. Adicionalmente, são apresentados o enquadramento teórico, a formulação matemática adotada, a arquitetura de implementação e a análise de cenários de operação com e sem consideração explícita da rede de distribuição.

Os resultados demonstram a importância de modelar explicitamente a rede de distribuição na otimização da operação de RECs. Embora a desconsideração das restrições da rede reduza o custo de operação da comunidade em aproximadamente 33% (de $9,476$ € para $6,308$ €), o despacho obtido provoca sobrecargas em quatro ramos da rede, com o mais crítico atingindo 130,8% do seu limite térmico. Em contraste, a consideração da formulação com restrições de rede mantém todos os ramos dentro dos respetivos limites, ao custo de cerca de 640 kWh de corte de carga durante o pico noturno de consumo. A representação da rede foi validada de forma independente por meio de um fluxo de potência não linear em Corrente Alternada (AC) e de um simulador comercial de sistemas elétricos, apresentando uma concordância da ordem de $10^{-5}\%$, o que confirma a precisão física da formulação relaxada.

Em suma, este trabalho contribui para o desenvolvimento de uma base conceptual, metodológica e computacional para sistemas de gestão energética comunitária mais realistas, tecnicamente consistentes e robustos, adequados à operação de redes de distribuição com elevada penetração de recursos energéticos distribuídos (DERs).

Palavras-chave: Comunidades de Energia Renovável, Transações Peer-to-Peer, Otimização com Restrições de Rede, Fluxo de Potência Ótimo, Modelo de Fluxo de Ramo Relaxado, Relaxações Convexas, Redes de Distribuição.

Abstract

The increasing penetration of distributed Renewable Energy Sources (RES), end-use electrification, and the emergence of prosumers have reinforced the role of Renewable Energy Communities (RECs) as key enablers of the energy transition. Such communities promote local generation, self-consumption, and fair benefit sharing, contributing to a more sustainable and decentralized power system. Nevertheless, most optimization models currently used for RECs management are limited in their real-world applicability, as they frequently rely on simplified network representations that neglect the operational and physical constraints of distribution grids.

To overcome these limitations and improve the technical accuracy of REC optimization, this dissertation focuses on the study, formulation, and application of a Relaxed Branch Flow Model (RBFM) as a framework that explicitly incorporates distribution network constraints while preserving computational efficiency. Building on previous research in convex relaxation techniques and Optimal Power Flow (OPF) formulations, the study explores how these methods can be adapted to the context of RECs.

The proposed approach was integrated into INESC TEC's REC tool, referred to as the Optimal Scheduling Tool for Energy Communities (OSTEC), an internal simulation and optimization system for community energy transactions, which enables a community operation formulation explicitly constrained by distribution network limitations. Additionally, the theoretical framework, the adopted mathematical formulation, the implementation architecture, and the analysis of operational scenarios with and without the explicit consideration of the distribution network are presented.

The results demonstrate the importance of explicitly modeling the distribution network when optimizing REC operation. While neglecting network constraints reduces the community operating cost by approximately 33% (from 9476 € to 6308 €), the resulting dispatch overloads four branches, with the most critical reaching 130.8% of its thermal limit. The consideration of the network-constrained formulation, in contrast, keeps all branches within their ratings at the cost of around 640 kWh of demand response curtailment during the evening peak. The underlying network representation was independently validated against a nonlinear Alternating-Current (AC) power-flow analysis and a commercial power-system simulator, showing agreement to within 10^{-5}%, thereby confirming the physical accuracy of the relaxed formulation.

Overall, this work contributes to the development of a conceptual, methodological, and computational foundation to support the creation of more realistic, technically consistent, and robust community energy management systems suitable for the operation of distribution networks with high penetration of Distributed Energy Resources (DERs).

Keywords: Renewable Energy Communities, Peer-to-Peer Trading, Network-Constrained Optimization, Optimal Power Flow, Relaxed Branch Flow Model, Convex Relaxations, Distribution Networks.

UN Sustainable Development Goals

The United Nations Sustainable Development Goals (SDGs) define an ambitious and comprehensive framework to guide global development towards environmental sustainability, social equity, and economic resilience. As illustrated in Figure 1, these 17 interconnected goals address a diverse set of global challenges, including climate change mitigation, sustainable resource management, inclusive economic growth, and the development of resilient infrastructure.

Figure 1: UN SDGs [1]

Within this framework, the present dissertation aligns particularly with the following goals:

SDG 7 Ensure access to affordable, reliable, sustainable, and modern energy for all

SDG 9 Build resilient infrastructure, promote inclusive and sustainable industrialization, and foster innovation

SDG 11 Make cities and human settlements inclusive, safe, resilient, and sustainable

SDG 12 Ensure sustainable consumption and production patterns

SDG 13 Take urgent action to combat climate change and its impacts

In the context of energy systems, these SDGs highlight the transition to low-carbon energy generation, efficient resource management, and the development of robust and innovative infrastructures.

The following table summarizes the SDG targets addressed, the nature of the contribution, and the performance indicators that can be used to assess the impact of the proposed methodology.

Table 1: SDG targets, contributions, and performance indicators

SDG	Target	Contribution	Performance Indicators
7	7.2	Increase renewable integration in RECs while ensuring network-feasible operation.	Local renewable utilization; self-consumption/self-sufficiency rate; renewable curtailment reduction.
	7.3	Improve energy efficiency through coordinated DER scheduling under network constraints.	Community cost reduction; peak import/export reduction; network loss reduction (%).
	7.B	Enhance use of existing distribution infrastructure via voltage and thermal constraint internalization.	Avoided voltage violations; line/transformer loading margin; hosting capacity proxy.
9	9.4	Provide a scalable, computationally efficient optimization framework that improves the sustainable operation of grid infrastructure under high DER penetration.	Solver runtime; scalability with number of nodes/time periods; feasibility rate across scenarios.
	9.5	Contribute with methodological and implementation advances (integration of RBFM-based constraints into an operational REC tool).	Reproducibility (open test cases); quality of relaxation (optimality gap/relaxation tightness indicators, when applicable).
11	11.6	Reduce adverse environmental impacts associated with inefficient grid operation by avoiding constraint violations and unnecessary losses in local energy sharing.	Loss reduction; reduction of congestion events; reduction in energy imported from upstream grid (proxy).
12	12.2	Improve efficient management of local energy resources (Photovoltaic generation, storage, flexibility) within community operation.	Increased utilization of local generation; reduced waste of available flexibility; reduced energy spillage/curtailment.
	12.5	Avoid wasteful operational actions by incorporating network-aware schedules.	Reduced battery cycling cost/degradation proxy; fewer infeasible schedules requiring post-correction; reduced re-dispatch/penalty events.
13	13.2	Support low-carbon energy planning through secure high-RES community operation.	CO_2 reduction potential (emission factor); increased RES share; reduced upstream dependency.

Acknowledgements

First, I would like to express my sincere gratitude to my supervisor, Prof. Dr. Tiago Soares, and to my advisor within INESC TEC, António Sérgio Faria, for their continuous availability, guidance, and support throughout the development of this dissertation. Their constructive feedback and willingness to help at every stage of this work were invaluable, and I couldn't be more thankful for the time they dedicated to discussing ideas, addressing challenges, and helping shape the direction of this research.

I would also like to thank the Faculty of Engineering of the University of Porto (FEUP) for providing an outstanding academic environment and high-quality education. The knowledge I acquired, the friends I made along the way, and the challenges I overcame throughout this journey have played a fundamental role in shaping both my academic and personal development.

To my parents, Ana and José, I am deeply grateful for your unconditional love, support, and encouragement throughout my entire academic path. Your sacrifices and dedication made this achievement possible, and I will always remember and value everything you have done for me.

A special acknowledgment goes to my sister, Rita, whose encouragement, motivation, and ability to cheer me up during the toughest times were invaluable. Your support often made difficult days much easier to overcome.

Finally, I would like to thank my closest friends, Marco, Madalena, and Patrícia, for their friendship, motivation, and support. Thank you for brightening my days.

To everyone who, in one way or another, contributed to this achievement, my sincere thank you.

Gonçalo Coelho

"Success is the sum of small efforts, repeated day in and day out"

Robert Collier

Contents

List of Figures

List of Tables

List of Abbreviations and Acronyms

AC	Alternating-Current
ADMM	Alternating Direction Method of Multipliers
APP	Auxiliary Problem Principle
BESS	Battery Energy Storage System
BFM	Branch Flow Model
CBM	Community-Based Market
CEC	Citizen Energy Community
CHP	Combined Heat and Power
DC	Direct-Current
DER	Distributed Energy Resource
DSO	Distribution System Operator
EGAC	Managing Entity of Collective Self-Consumption (Entidade Gestora do Autoconsumo Coletivo)
ERSE	Energy Services Regulatory Authority (Entidade Reguladora dos Serviços Energéticos)
EU	European Union
EV	Electric Vehicle
HV	High-Voltage
HVAC	Heating, Ventilation, and Air Conditioning
IMD	Internal Market Directive
LEM	Local Energy Market
LV	Low-Voltage
MILP	Mixed-Integer Linear Programming
MIPGap	Mixed Integer Programming Gap
MMR	Mid-Market Rate
MV	Medium-Voltage
NP-hard	Nondeterministic Polynomial-time hard
OLTC	On-Load Tap Changer
OPF	Optimal Power Flow
OSTEC	Optimal Scheduling Tool for Energy Communities
P2P	Peer-to-peer
PTDF	Power Transfer Distribution Factor
PV	Photovoltaic
QC	Quadratically Convex
QCQP	Quadratically Constrained Quadratic Program
R/X	Resistance-to-Reactance ratio
RBFM	Relaxed Branch Flow Model
REC	Renewable Energy Community

RED II	Renewable Energy Directive II
RES	Renewable Energy Sources
SDG	Sustainable Development Goal
SDP	Semidefinite Programming
SOC	Second Order Cone
SoC	State of Charge
SOCP	Second Order Cone Programming
TOU	Time-of-Use

List of Symbols

Indices and Sets

$t \in T$	Set of discrete time intervals over the optimization horizon
$n \in N$	Set of community members (each associated with a non-slack network bus)
$\mathscr{N}$	Set of all network buses (community members, junction buses, and slack)
N^{PV}	Set of buses containing PV generation
N^{W}	Set of buses containing wind generation
N^{CHP}	Set of buses containing CHP units
$s \in S$	Set of battery storage systems associated with each member
$ev \in EV$	Set of electric vehicles associated with each member
$(n,m) \in \mathscr{E}$	Set of directed distribution network branches (lines)
$j \in N$	Index of a bus where an active power injection is applied (sensitivity analysis)

Parameters

$\hat{E}^{C}_{n,t}$	Electrical consumption of n at t (kWh)
$\hat{E}^{G}_{n,t}$	Forecasted (non-dispatchable) behind-the-meter renewable generation (PV and wind) of n at t (kWh)
$\hat{E}^{G,PV}_{n,t}$	Forecasted behind-the-meter PV generation of n at t (kWh)
$\hat{E}^{G,W}_{n,t}$	Forecasted behind-the-meter wind generation of n at t (kWh)
$P^{C}_{n,t}$	Active power consumption of n at t (p.u.)
$Q^{C}_{n,t}$	Reactive power consumption of n at t (p.u.)
$\hat{\lambda}^{buy}_{n,t}$	Retail electricity purchase tariff for n at t (€/kWh)
$\hat{\lambda}^{sell}_{n,t}$	Retail electricity selling tariff for n at t (€/kWh)
$\hat{\lambda}^{marketbuy}_{t}$	Market-indexed electricity purchase tariff at t (€/kWh)
$\hat{\lambda}^{marketsell}_{t}$	Market-indexed electricity selling tariff at time t (€/kWh)
$\hat{\lambda}^{grid}_{t}$	Grid access tariff for self-consumption at t (€/kWh)
$\hat{\lambda}^{EXTRA}$	Fictitious very high penalty tariff applied upon violation of $\hat{P}^{CPE,max}_{n}$ (€/kW)
$\hat{\lambda}^{DR}$	Penalty tariff associated with demand-response curtailment (€/kWh)
$\hat{\lambda}^{GC}$	Penalty tariff associated with generation curtailment (€/kWh)
$\hat{\lambda}^{\Delta Y}$	Penalty coefficient associated with the no-worse-off slack variable ΔY_n
$\hat{\lambda}^{deg}_{n,s}$	Estimated degradation cost of battery s of n (€/kWh)

$\hat{\lambda}_t^{p2p}$	Fictitious local energy price at t (€/kWh)
$\hat{\lambda}_n^{CHP}$	Marginal generation cost of the CHP unit of n (€/kWh)
$\hat{P}_n^{CHP,max}$	Maximum electrical generation capacity of the CHP unit of n (kW)
$\hat{P}_n^{CPE,max}$	Contracted power limit of n at the metering point (kW)
$\hat{E}_{n,s}^{B,N}$	Nominal capacity of battery s of n (kWh)
$\widehat{SoC}_{n,s}^{B,min}$	Minimum allowable state of charge of battery s of n (%)
$\widehat{SoC}_{n,s}^{B,max}$	Maximum allowable state of charge of battery s of n (%)
$\hat{P}_{n,s}^{B,max}$	Maximum input/output power of battery s of n (kW)
$\hat{\eta}_{n,s}^{B,C}$	Charging efficiency of battery s of n
$\hat{\eta}_{n,s}^{B,D}$	Discharging efficiency of battery s of n
$\hat{C}_n^{ind}$	Individual energy cost of n obtained in Stage 1 (€)
Δt	Duration of each time interval (h)
$\hat{M}$	Large positive constant used in binary linearization
$\hat{E}_{n,ev,t}^{Trip}$	Energy consumed by vehicle ev of n at t (kWh)
$\hat{E}_{n,ev}^{EV,MinCharge}$	Minimum required stored energy for vehicle ev of n (kWh)
$\hat{E}_{n,ev}^{EV,BatCapacity}$	Battery energy capacity of vehicle ev of n (kWh)
$\hat{\eta}_{n,ev}^{EV,C}$	Charging efficiency of vehicle ev of n
$\hat{\eta}_{n,ev}^{EV,D}$	Discharging efficiency of vehicle ev of n
$\hat{P}_{n,ev}^{EV,ChargeLimit}$	Maximum charging power of vehicle ev of n (kW)
$\hat{P}_{n,ev}^{EV,DischargeLimit}$	Maximum discharging power of vehicle ev of n (kW)
$\hat{X}_{n,ev,t}^{EV}$	Binary parameter indicating if vehicle ev of n is plugged in at t
$R_{n,m}$	Resistance of distribution line (n,m) (p.u.)
$X_{n,m}$	Reactance of distribution line (n,m) (p.u.)
V_n^{min}	Minimum voltage magnitude at node n (p.u.)
V_n^{max}	Maximum voltage magnitude at node n (p.u.)
$I_{n,m}^{max}$	Maximum current magnitude in line (n,m) (p.u.)
ρ	Regularization coefficient applied to the squared branch current magnitudes
ε	Regularization coefficient applied to the gross bilateral purchase volume
ε^{SOC}	Numerical tolerance used in SOC constraint violation detection
$S_{n,j}^{V}$	Sensitivity of the voltage magnitude at bus n to an active power injection at bus j
$S_{(n,m),j}^{I}$	Sensitivity of the current magnitude in branch (n,m) to an active power injection at bus j

Decision Variables

$E_{n,t}^{SUP,retail}$	Energy supplied by n from its retailer at t (kWh)
$E_{n,t}^{SUR,retail}$	Energy surplus sold by n to its retailer at t (kWh)
$E_{n,t}^{SUP,market}$	Energy purchased by n in the external market at t (kWh)
$E_{n,t}^{SUR,market}$	Energy surplus sold by n in the external market at t (kWh)
$E_{n,t}^{PUR}$	Energy purchased within the REC through peer-to-peer transactions, by n at t (kWh)

$E_{n,m,t}^{PUR}$	Energy purchased by member n specifically from member m at t, with $m \neq n$ (kWh)
$E_{n,t}^{SALE}$	Energy sold within the REC through peer-to-peer transactions, by n at t (kWh)
$E_{n,t}^{DR}$	Demand-response curtailment applied to n at t (kWh)
$E_{n,t}^{GC}$	Generation curtailment applied to the renewable generation of n at t (kWh)
ΔY_n	Non-negative slack variable associated with the no-worse-off constraint (€)
$E_{n,t}^{G,CHP}$	Dispatchable CHP electrical generation of n at t (kWh)
$E_{n,t}^{CMET}$	Net energy consumption at the metering point of n at t (kWh)
$E_{n,t}^{SLC}$	Self-consumed energy behind the meter by n at t (kWh)
$P_{n,t}^{EXTRA}$	Excess power above the contracted limit ($\hat{P}_n^{CPE,max}$) at t (kW)
$\delta_{n,t}^{SUP}$	Auxiliary binary variable preventing n from simultaneously buying and selling to the retailer at t
$E_{n,s,t}^{B}$	Energy stored in battery s of n at t (kWh)
$SoC_{n,s,t}^{B}$	State of charge of battery s of n at t (%)
$E_{n,s,t}^{B,C}$	Energy charged into battery s of n at t (kWh)
$E_{n,s,t}^{B,D}$	Energy discharged from battery s of n at t (kWh)
$\delta_{n,s,t}^{B,C}$	Auxiliary binary variable preventing battery s of n from charging and discharging simultaneously at t
$E_{n,ev,t}^{EV,Stored}$	Energy stored in vehicle ev of n at the end of period t (kWh)
$E_{n,ev,t}^{EV,Charge}$	Energy charged into vehicle ev of n at t (kWh)
$E_{n,ev,t}^{EV,Discharge}$	Energy discharged from vehicle ev of n at t (kWh)
$P_{n,m,t}$	Active power flow in line (n,m) at t (p.u.)
$Q_{n,m,t}$	Reactive power flow in line (n,m) at t (p.u.)
$l_{n,m,t}$	Squared current magnitude in line (n,m) at t (p.u.^{2})
$v_{n,t}$	Squared voltage magnitude at node n at t (p.u.^{2})
$P_{n,t}^{inj}$	Net active power injection at node n at t (p.u.)
$Q_{n,t}^{inj}$	Net reactive power injection at node n at t (p.u.)
$Q_{n,t}^{G,PV}$	Reactive power generated by PV units of n at t (kVArh)
$Q_{n,t}^{G,W}$	Reactive power generated by wind units of n at t (kVArh)
$Q_{n,t}^{G,CHP}$	Reactive power generated by CHP units of n at t (kVArh)

Chapter 1

Introduction

This chapter presents the context, motivation, and goals of the work developed in this dissertation. Initially, the main drivers behind the increasing relevance of Renewable Energy Communities (RECs) are introduced, along with the key challenges associated with their operation and the limitations of existing optimization approaches. The chapter then explains what this research aims to achieve and defines its overall scope, followed by a mention of other related projects and publications. Finally, an overview of the document's structure is provided.

1.1 Context and Motivation

The global energy landscape is currently undergoing a deep transformation, provoked by the urgent need to decarbonize energy systems and reduce dependence on fossil fuels [2]. At the same time, recent European legislation has increasingly promoted the active participation of end-users in electricity markets through concepts such as active customers and energy communities [3, 4].

Over the past few years, this transition has been reflected in the increasing penetration of distributed Renewable Energy Sources (RES), the end-use sectors electrification (i.e., the replacement of fossil-fuel-based, such as transport and heating devices, with electricity-powered options like Electric Vehicles (EVs), heat pumps, and Heating, Ventilation, and Air Conditioning (HVAC) systems), and the emergence of prosumers, entities capable of both consuming and producing electricity. Supported by evolving regulatory frameworks, these developments eventually made RECs indispensable to the energy transition, promoting local generation, community resilience, and the equitable sharing of collective benefits [5].

From a regulatory perspective, Directive 2018/2001, under European Union (EU) law, established the conceptual and legal foundations for the development of RECs across European Member States, defining principles for individual and collective self-consumption, as well as Peer-to-Peer (P2P) energy trading [3, 5]. Its transposition into national legislation, such as in Portugal and Spain, has enabled the development of operational frameworks that allow end-users to cooperatively manage local energy resources and interact with the Distribution System Operator (DSO) to ensure grid compatibility [5].

In parallel, the rapid proliferation of Photovoltaic (PV) generation, storage systems, and flexible loads at the Low-Voltage (LV) distribution level is fundamentally reshaping power flows within distribution networks, transforming traditionally passive consumers into active participants in the energy system.

However, the increasing integration of Distributed Energy Resources (DERs) introduces significant operational challenges, including voltage rise, reverse power flows, line congestion, and transformer overloads [6, 7]. These issues are not merely theoretical, as studies show that uncoordinated P2P trading at high PV penetration can lead to voltage fluctuations and increased system losses, highlighting the need to align market mechanisms with the network's physical constraints [7].

Within this context, RECs require coordinated mechanisms not only for energy sharing and asset management, but also for ensuring fair and transparent allocation of costs and benefits among participants. At the same time, the increasing reliance on flexible resources further reinforces the need for robust operational frameworks capable of handling variability and uncertainty [8, 9].

Nonetheless, several challenges arise when attempting to operate RECs in a technically and economically coherent manner. The variability of internal energy transaction prices, the risk of network congestion, and the difficulty of ensuring equitable benefit sharing constitute key barriers to their large-scale adoption [5].

A fundamental issue underlying these challenges is the disconnect between economic decision-making and the physical behavior of distribution networks. Many existing approaches rely on simplified or unconstrained network representations, neglecting voltage limits, line thermal ratings, and power losses [10, 11]. While these simplifications reduce computational complexity, they may yield solutions that are economically attractive yet physically infeasible in real-world operation.

This gap motivates the development of optimization frameworks that explicitly incorporate network constraints into community-level decision-making. By ensuring that energy transactions and scheduling decisions respect the underlying grid limitations, it becomes possible to enhance both the technical reliability and the economic efficiency of REC operation, avoiding the need for corrective actions by the DSO [12]. In this regard, network feasibility can be ensured either by embedding the network constraints directly within the optimization or by applying a corrective step after the economic schedule is obtained, a distinction that is also examined in this work.

In this context, Optimal Power Flow (OPF) formulations play a central role in explicitly representing network constraints. However, due to the non-convexity of the Alternating-Current (AC) power-flow equations, OPF problems are generally computationally challenging. To address this issue, convex relaxation techniques have been widely studied in the literature, including Second-Order Cone Programming (SOCP) and Semidefinite Programming (SDP), which can provide tractable approximations and, in some cases, globally optimal solutions under specific network conditions [13, 14].

To address these challenges, this dissertation proposes an optimization framework that integrates Relaxed Branch Flow Model (RBFM)-based network constraints into REC operation, enabling network-aware decision-making while maintaining computational tractability.

1.2 Objectives

The increasing complexity of REC operations, driven by the high penetration of DERs and the need to ensure secure distribution network operation, requires optimization frameworks that jointly address both the economic and physical aspects of community operations.

In this context, the main objective of this dissertation is to develop a network-constrained optimization framework for REC operation based on the RBFM, explicitly accounting for voltage constraints, line capacities, and network losses within the optimization process. The proposed framework is subsequently integrated into INESC TEC's community management platform, Optimal Scheduling Tool for Energy Communities (OSTEC), enabling its application to the coordinated management of RECs.

By combining market mechanisms with a physically consistent representation of the distribution network, the proposed framework aims to improve the technical feasibility and operational efficiency of REC operation while supporting network-aware decision-making and contributing to secure distribution system operation.

The main scientific contribution of this dissertation lies in the integration of the RBFM within a community energy management framework, enabling optimization decisions that explicitly account for distribution network constraints in RECs.

To achieve this goal, the following specific objectives are addressed:

- Develop and integrate an RBFM-based network-constrained optimization formulation for REC operation;
- Implement the proposed formulation within the OSTEC platform, enabling the coordinated optimization of energy transactions, distributed generation, and flexibility resources;
- Assess the impact of explicitly modeling network constraints on REC operation, comparing results with approaches based on simplified or unconstrained network representations;
- Validate the proposed model through comparison with an AC power flow benchmark, an external simulation tool, and an alternative sensitivity-based network representation;
- Evaluate the operational and economic performance of the proposed framework under different operating scenarios, quantifying the trade-offs between economic efficiency and technical feasibility.

1.3 Related Projects and Publications

The work developed in the scope of this dissertation partially concerns the objectives and results of three research projects, namely:

- ENPOWER - Energy Activated Citizens and Data-Driven Energy-Secure Communities for a Consumer-Centric Energy System- European Union's Horizon 2020, No. 101096354;

- PVSmile - Digitalizing the Lifecycle of Community-Integrated PV Systems for Smart Grid-Ready and Inclusive Energy Communities - Horizon Europe, No. 101235645;
- EMPEDOFLEX - EMpowering Positive Energy District Optimal FLEXibility provision, DOI: https://doi.org/10.54499/CETP/0007/2024.

The developed work has resulted in the writing of one scientific paper for journal publication. The following should be referred to:

- Gonçalo Coelho, António Sérgio Faria and Tiago Soares, "A Network-Constrained Optimization Framework for Renewable Energy Communities Based on the Relaxed Branch Flow Model", submitted to Electric Power Systems Research journal.

1.4 Structure of the Dissertation

This dissertation is organized into five chapters, each addressing a distinct stage of the research process, from the problem contextualization to the development and validation of the proposed methodology.

Chapter 1 introduces the topic and motivation for the work, defines the main goals, and outlines the overall structure of the dissertation.

Chapter 2 presents the fundamental background and an extensive review of the main OPF formulations considered in distribution networks, as well as convex relaxation techniques and their main applications. The chapter also delves into the concept of RECs, their regulatory context, and existing market structures, concluding with a review of how convex relaxation techniques have been applied in community-scale optimization, alongside the identification of research gaps.

Chapter 3 describes the mathematical formulation behind the operation of the proposed approach. It presents the integration of a network-constrained model based on the RBFM into the REC optimization framework implemented in OSTEC, detailing the objective function, constraints, and overall structure of the problem.

Chapter 4 presents the simulation studies used to evaluate the proposed framework, structured into two complementary case studies. The first study focuses on model validation using a controlled 10-bus radial distribution system, verifying the tightness of the Second Order Cone (SOC) relaxation and the physical consistency of the network response under parametric stress. The second study constitutes the main contribution of the dissertation, applying the validated framework to a more realistic distribution network with fully integrated REC dynamics to quantify the impact of network constraints on community operation and assess the trade-offs between economic performance and technical feasibility.

Finally, Chapter 5 summarizes the key findings of the dissertation, discusses the contributions and limitations of the proposed approach, and outlines directions for future work.

Chapter 2

Background and State-of-the-Art

This chapter provides fundamental background concepts necessary to understand how RECs are optimized under real-world network conditions and how these can be adapted to improve power flow and grid resilience. It also presents a comprehensive review of the state of the art in different OPF formulations applied to energy communities, aiming to provide a clearer understanding of their advantages and limitations.

In the first place, the core modeling principles for power flow in distribution networks will be introduced, with a particular focus on models that address the integration of DERs and the physical constraints of real-world grids. Building upon these principles, the chapter then examines the emergence of RECs, discussing their regulatory background, operational principles, and the challenges associated with local energy optimization.

Subsequently, it will be explored how convex relaxation techniques have been used to overcome the non-convexity of the AC-OPF problem, facilitating the development of scalable and accurate solutions, including the RBFM. Such models are especially applicable to radial networks and form a core component of the proposed methodology.

Finally, the chapter presents different distributed optimization architectures and their relevance for decentralized REC management, followed by a review of recent advances in uncertainty handling and sustainability assessment in community-based energy models.

2.1 OPF Models in Distribution Networks

Renewable-rich distribution systems require OPF tools to ensure both economic efficiency and technical feasibility in power system operations. These tools optimize an objective, such as generation cost, prosumer surplus, or losses, subject to power-balance equations and network constraints [13]. In contrast to transmission grids, distribution systems are generally radial, with higher Resistance-to-Reactance ratios (R/X) and more integrated DERs, such as PV systems and batteries [13].

This is especially true in RECs, where local generation and P2P trading can introduce voltage and congestion issues if OPF constraints are not properly managed [5]. Indeed, many early community energy market designs neglected network constraints, prioritizing computational tractability over model fidelity, and thereby increasing the risk of unsafe grid conditions.

Existing REC optimization frameworks generally differ in how they incorporate network constraints into the market-clearing process. While some approaches decouple economic scheduling from network validation by performing an OPF as a post-processing stage, others directly embed network constraints within the optimization problem. For instance, [5] proposes a three-stage REC management model, in which, after energy sharing, the DSO executes an OPF to resolve any local voltage or thermal violations, ensuring grid feasibility yet decoupling technical constraints from market decisions. Conversely, [12] embeds an OPF distribution into a community market-clearing framework to prevent constraint violations, although this integration increases computation time by approximately eight times.

To address these challenges, several OPF formulations have been proposed for distribution networks, ranging from full nonlinear AC formulations to simplified linear approximations and convex relaxations. The following review focuses on their underlying modeling assumptions, computational characteristics, and suitability for network-constrained REC optimization, thereby motivating the selection of the RBFM adopted in this dissertation.

2.1.1 AC-OPF (Full Nonlinear Formulation)

The AC-OPF is the classic and most comprehensive model, which makes use of the full set of nonlinear power flow equations to represent network physics [13]. It includes Kirchhoff's voltage and power equations for active and reactive power at each bus, expressed in terms of trigonometric functions of voltages, phase angles, and power flows [13]. For instance, the active and reactive power injections are given respectively by:

$$P_i = |V_i| \sum_{j \in \mathcal{N}} |V_j| \big(G_{ij} \cos(\theta_{ij}) + B_{ij} \sin(\theta_{ij}) \big) \tag{2.1}$$

$$Q_i = |V_i| \sum_{j \in \mathcal{N}} |V_j| \big(G_{ij} \sin(\theta_{ij}) - B_{ij} \cos(\theta_{ij}) \big) \tag{2.2}$$

where G_{ij} and B_{ij} represent the (i, j) elements of the conductance and susceptance matrices, respectively, while V_i and V_j denote the voltage magnitudes at nodes i and j [13].

These equations ensure accurate modeling of losses and voltage drops [13]. However, when expressed mathematically, the AC-OPF takes the form of a Quadratically Constrained Quadratic Program (QCQP), a nonconvex type of OPF. It is therefore considered Nondeterministic Polynomial-time hard (NP-hard), even for radial network topologies, demanding high computational requirements for large systems [13].

The non-convexity of AC-OPF is often illustrated using feasible region plots. Figure 2.1 presents a known example of the feasible region for a simple three-bus network under AC power flow equations. Although the system's structure is simple, its resulting feasible space is highly nonconvex and folded, making global optimization difficult. This motivates the widespread interest in convex relaxation techniques, which approximate the feasible region with outer bounds that are computationally more tractable [13].

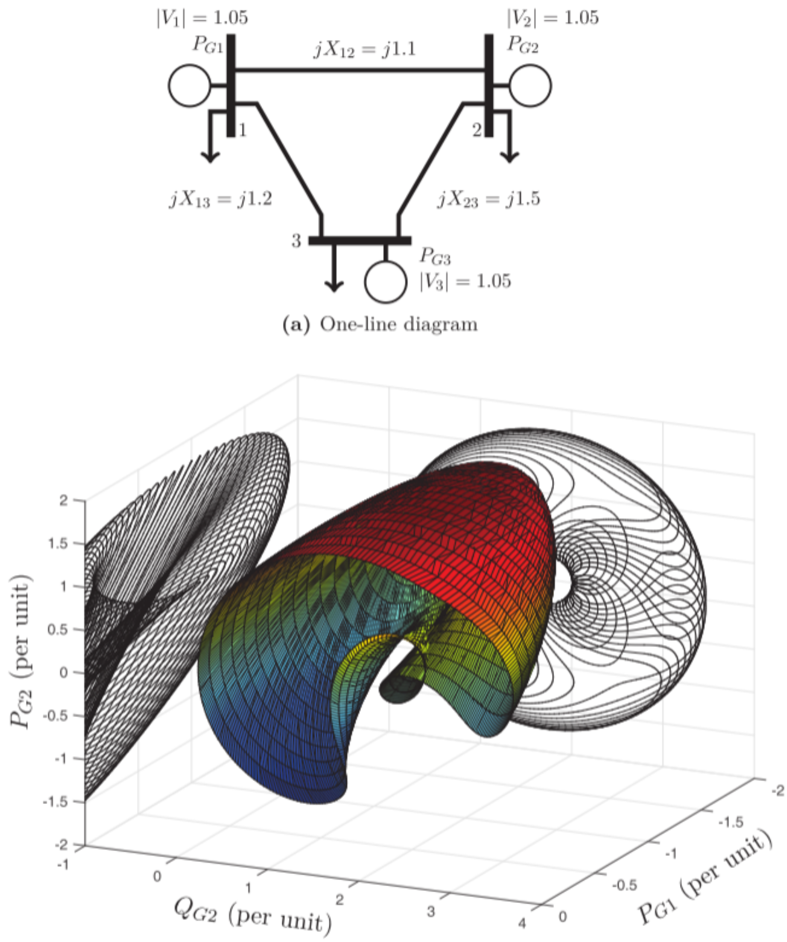

(a) One-line diagram

(b) Feasible space

Figure 2.1: Feasible region of AC power flow for a three-bus example system with fixed voltage magnitudes. The network diagram (a) corresponds to the plotted nonconvex surface (b), illustrating active and reactive power injections [13].

While AC-OPF is computationally demanding, it serves as an important benchmark since it captures the underlying physical network constraints [13]. For example, in REC applications, using AC-OPF means the optimization of the community directly considers voltage magnitudes, thermal limits, and losses, leading to solutions that do not need any further adjustment by network operators and, therefore, improving the fairness and reliability of energy sharing outcomes, as all grid constraints are internalized [5, 12]. However, solving a full AC-OPF for every market interval or control action in a community can be impractical [13].

These limitations have motivated the development of alternative formulations that seek to preserve the physical accuracy of AC-OPF while reducing computational complexity, as discussed in the following subsections.

2.1.2 DC-OPF (Linearized Approximation)

In order to enhance tractability, several studies have examined the implementation of the Direct-Current (DC)-OPF model. This formulation provides a linear approximation of the AC power flow equations by assuming negligible reactive power, small angle differences, and unit voltage magnitudes, thereby effectively decoupling active power flow from voltage magnitude [13].

This simplification derives from a Taylor series expansion of the active power flow equations around the flat voltage profile $V_i = 1\angle 0°$, for any $i \in \mathcal{N}$, assuming no line resistances, small angle differences, and neglecting reactive power flows [13]. The resulting matrix formulation can be compactly written as:

$$P = A_{\text{inc}} \cdot \text{diag}(b) \cdot A_{\text{inc}}^{\top} \cdot \theta \tag{2.3}$$

where A_{inc} is the network incidence matrix (i.e., a matrix that encodes the network topology and direction of active power flows) and b is the vector of line susceptances [13].

Although DC-OPF remains the preferred formulation for transmission-level market clearing due to its computational efficiency, its simplifying assumptions significantly limit its applicability to active distribution networks. In particular, the higher R/X ratios, bidirectional power flows introduced by DERs, and greater voltage variability characteristic of distribution systems reduce the accuracy of the linear approximation. Furthermore, neglecting reactive power and voltage constraints may lead to operating points that violate thermal or voltage limits, making the formulation less suitable for network-constrained REC optimization [13].

To overcome some of these limitations, several extensions of the classical DC-OPF have been proposed. For example, Hong et al. [15] introduced a relaxed PV bus model that incorporates an approximation of voltage regulation at generator buses, a feature omitted in the standard DC-OPF formulation. Such enhancements improve the representation of inverter-based DERs and are particularly relevant for RECs, where PV systems actively contribute to local voltage regulation. Nevertheless, these models remain linear approximations of the nonlinear behavior of AC networks and therefore cannot fully capture the electrical characteristics of active distribution networks.

Despite these refinements, these models remain simplifications of the nonlinear AC behavior. As illustrated in [5] 's third-stage OPF correction, the use of DC-OPF in REC coordination may still require a posterior AC feasibility check. Furthermore, [13] shows that empirical error patterns of DC-OPF vary significantly across scenarios, making it harder to generalize its validity. Alternative DC model variants, including Power Transfer Distribution Factor (PTDF)-based formulations and Hot-Start, offer incremental improvements but do not fully resolve the fundamental absence of reactive power modeling or the inability to represent voltage magnitude variability [13].

In summary, DC-OPF offers computational speed and simplicity and remains attractive for large-scale tasks, but must be applied with caution in distribution scenarios, especially within RECs, unless supplemented by techniques that mitigate its inaccuracies.

2.1.3 Branch Flow Model

The Branch Flow Model (BFM) is an alternative formulation of the AC power-flow equations that represents the network in terms of branch variables rather than bus-voltage phase angles. It focuses on the quantities flowing through the lines of the system, namely active and reactive power, voltages, and currents, which makes it particularly suitable for distribution networks and for deriving convex relaxations, where power typically flows from an upstream slack node towards downstream loads [13, 14]. The model explicitly represents the electrical behavior of each branch (i,k) through Ohm's law and complex power definitions, that is:

$$S_{ik} = V_i I_{ik}^*, \quad V_k = V_i - z_{ik} I_{ik}, \tag{2.4}$$

where S_{ik} is the complex power from bus i to k, V_i is the complex voltage at bus i, I_{ik} is the current from bus i to k, and z_{ik} is the line impedance [16, 17].

In the context of radial feeders, the BFM is expressed using active and reactive power flows, namely P_{ik} and Q_{ik}, squared current magnitudes $\ell_{ik} = |I_{ik}|^2$, and squared voltage magnitudes $v_i = |V_i|^2$. In the formulation presented later in Chapter 3 of this dissertation, the squared current magnitude is denoted by l for notational simplicity, and the index pair (i,k) is replaced by (n,m) to denote directed branches, consistently with the community member index $n \in N$ used throughout the optimization framework. This widely adopted formulation, originally obtained from the Baran-Wu *DistFlow* representation, as detailed in [18], establishes the relationship between power balance and voltage drops along each branch [13, 16]. The corresponding mathematical equations are:

$$P_{ik} = R_{ik}\ell_{ik} - P_k + \sum_{m\,:\,k\to m} P_{km}, \tag{2.5}$$

$$Q_{ik} = X_{ik}\ell_{ik} - Q_k + \sum_{m\,:\,k\to m} Q_{km}, \tag{2.6}$$

$$v_k = v_i - 2(R_{ik}P_{ik} + X_{ik}Q_{ik}) + (R_{ik}^2 + X_{ik}^2)\ell_{ik}, \tag{2.7}$$

together with the nonlinear current-power relation:

$$\ell_{ik} = \frac{P_{ik}^2 + Q_{ik}^2}{v_i}, \qquad \forall (i,k) \in \mathscr{E} \tag{2.8}$$

where:

- R_{ik} and X_{ik} denote the resistance and reactance of the branch (i,k);
- P_k and Q_k are the net active and reactive power injections at bus k;

- Equation (2.8) expresses that the squared current magnitude is equal to the ratio between the squared apparent power flow and the voltage magnitude at the upstream node.
- The set $\mathscr{E}$ represents the collection of directed branches (i,k) composing the network topology, with i and k being the upstream and downstream of each branch, respectively.

Unlike the conventional bus-injection formulation used in AC-OPF, the BFM explicitly represents power flows, voltages, and currents at the branch level. This branch-oriented representation is particularly well suited to radial distribution networks, where power naturally flows from an upstream source towards downstream loads. Consequently, the BFM accurately captures voltage drops and line losses while providing a mathematical structure particularly well-suited to deriving convex relaxations [13, 14].

The quadratic relation described in equation (2.8) makes the branch flow formulation nonconvex. To address this limitation, several convex relaxations, such as SOCP formulations, have been developed to obtain tractable OPF models, as will be discussed in the following subsection [14, 16].

2.1.4 Convex Relaxations

Addressing the AC-OPF problem continues to be significantly challenging, primarily due to the nonlinear and nonconvex nature of the underlying power flow equations. Consequently, convex relaxations have emerged as an essential methodological tool, facilitating the derivation of tractable OPF formulations and enabling the application of efficient convex optimization algorithms that offer global optimality guarantees for the relaxed problem [13].

These relaxations operate by expanding the feasible region of the original AC-OPF via convex supersets of the nonlinear constraints, thereby making it computationally tractable while still capturing most of the relevant physical constraints. This conceptual idea is illustrated in Figure 2.2, where a convex relaxation (blue region) offers a tighter and more systematic outer-approximation of the nonconvex feasible space compared to a simple linear approximation (red region) [13].

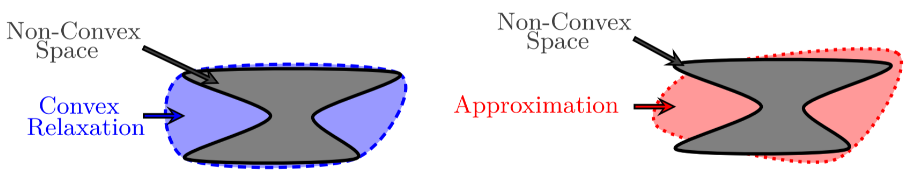

Figure 2.2: Conceptual illustration of a convex relaxation (blue region) and an approximation (red region) for the feasible space [13].

Among different relaxation techniques presented in the literature, three main sets have emerged as particularly prominent, such as (i) SDP-based OPF relaxations, (ii) SOCP-based OPF relaxations, and (iii) Quadratically Convex (QC) relaxations. Each method presents a distinct balance between relaxation tightness, computational scalability, and suitability for radial or meshed networks [13, 14].

2.1.4.1 SDP Relaxation

The SDP-OPF relaxation reformulates the AC power flow equations by representing the voltage phase angles in a lifted Hermitian matrix variable, represented by $W = vv^H$. This transformation converts nonlinear products such as $V_i V_j^*$ into linear terms of W [13]. The nonconvex rank-one constraint $\text{rank}(W) = 1$ is then relaxed by requiring W to be positive semidefinite, leading to a convex SDP-OPF formulation.

SDP relaxations are known as one of the tightest relaxations available, and in several classes of radial networks, they are even guaranteed to be exact [14]. Moreover, recent work, such as the decentralized SDP variant based on the BFM proposed by [17], demonstrates that an SDP-based OPF can be solved efficiently even in large distribution networks, using accelerated Alternating Direction Method of Multipliers (ADMM) schemes. Their experiments on the modified IEEE 123 and 8500 bus systems revealed that the SDP relaxation can produce globally optimal solutions while remaining computationally practical [17].

2.1.4.2 SOCP Relaxation

SOCP relaxations make use of the BFM structure presented earlier. That is, following the application of angle relaxation, the quadratic current-power relation (Equation (2.8)) remains as the only source of non-convexity, being then relaxed, in the SOCP approach, to the SOC inequality:

$$\ell_{ik} \geq \frac{P_{ik}^2 + Q_{ik}^2}{v_i}, \qquad \forall (i,k) \in \mathscr{E}. \tag{2.9}$$

The resulting formulation is known as the RBFM, a convex relaxation that preserves the structure of the original power equations [14, 16].

As described in [16], a foundational theoretical insight shows that for radial networks without upper bounds on loads, both the angle and SOC relaxations are exact solutions. As a result, the RBFM returns the global AC-OPF optimum, enabling precise recovery of voltages and power flows. Notably, even for meshed networks, the SOC relaxation remains exact. However, angle recovery may fail if cycle consistency is not maintained. In such cases, the strategic placement of phase shifters outside a spanning tree can restore convexity [16].

Building upon prior results, [19] established additional guarantees by deriving a sufficient condition (C1) for exactness under practical system constraints, such as line limits and generator and voltage bounds. Essentially, C1 is intended to limit reverse power flows, thereby preventing simultaneous back-feeding of active and reactive power. When the condition is satisfied, the feasible sub-injection region (i.e., the set of all physically admissible active and reactive power injections at every non-slack bus) becomes convex. This ensures that the solution obtained from the SOCP relaxation can always be mapped to an AC-feasible solution.

SOCP-based relaxations have also been used in more advanced formulations. For example, the work developed in [20] incorporates the RBFM into a robust multi-period optimization framework, coordinating active and reactive power, voltage-regulation devices, and storage. Their mixed-integer SOCP formulation (i.e., a SOCP-relaxed OPF that includes discrete decision variables, such as tap positions of On-Load Tap Changers (OLTCs) or capacitor-switching states) incorporates additional linear cuts to tighten the relaxation under high DER conditions. Furthermore, [21] extends the SOCP-based OPF to decentralized operation using an adaptive-core Auxiliary Problem Principle (APP), demonstrating faster convergence and improved accuracy compared with classical APP approaches.

Overall, this balance between reduced tightness and a faster computation makes SOCP relaxations particularly well-suited for real-time operation, large-scale scheduling, and community energy management.

2.1.4.3 QC Relaxation

Ultimately, the QC-OPF relaxation can be used to approximate the nonlinear AC-OPF equations by constructing convex envelopes for the bilinear and quadratic terms present in power flow modeling. These envelopes represent the tightest convex sets that contain the original nonlinear relations, allowing the effective replacement of difficult bilinear terms with tractable convex inequalities without losing excessive accuracy [13]. As a result, the QC-OPF formulation provides a balance between tightness (typically tighter than standard SOCP relaxations) and scalability (lighter than SDP-based models), making it well-suited for distribution-level optimization where computational efficiency is important [13].

Generally, QC relaxations exhibit superior performance when voltage magnitudes are maintained within relatively narrow operational ranges, a common scenario in regulated distribution grids [13]. Consequently, the QC-OPF formulation can serve either as a robust, standalone convex approximation or as an intermediate relaxation that facilitates warm-starting more computationally intensive OPF algorithms [13].

Although QC relaxations are less frequently adopted in REC-specific studies, they remain a useful modeling alternative in scenarios where the aim is to preserve high accuracy while avoiding the scalability limitations of SDP formulations.

Table 2.1 summarizes the main characteristics of the OPF formulations reviewed throughout this section. AC-OPF provides the most accurate representation of the electrical network but is computationally demanding due to its nonlinear nature, whereas DC-OPF achieves excellent scalability at the cost of neglecting reactive power and voltage constraints. Convex relaxations bridge these two approaches by preserving the main physical characteristics of the network while remaining computationally tractable. Among them, SOCP relaxations based on the BFM offer a particularly attractive compromise for radial distribution networks, combining an accurate network representation with moderate computational complexity. For this reason, the RBFM is adopted in this dissertation as the foundation of the proposed optimization framework.

Table 2.1: Comparison of the main OPF formulations for distribution network optimization.

Formulation	Network Model	Convex	Reactive Power	Voltage Constraints	Computational Complexity	Suitability for Radial Networks
AC-OPF	Full AC	No	Yes	Yes	High	Good[1]
DC-OPF	Linear Approximation	Yes	No	No	Very Low	Limited
SDP Relaxation	Full AC (relaxed)	Yes	Yes	Yes	Very High	Excellent
SOCP (RBFM)	Full AC (relaxed)	Yes	Yes	Yes	Moderate	Excellent
QC Relaxation	Full AC (relaxed)	Yes	Yes	Yes	Moderate–High	Good

[1] Accurate but computationally demanding. Rarely used for large-scale or repeated scheduling.

2.2 RECs and Local Energy Sharing

RECs are often conceptualized as organizational models that enable end-users, such as consumers and prosumers, to actively interact with the electric system. Described in the literature as groups equipped with DERs, such as PV generation, batteries, and flexible loads, RECs collaborate to optimize local energy resource utilization, reduce energy costs, enhance self-sufficiency, and contribute to a more sustainable and resilient electricity system [5].

These communities stretch beyond technical frameworks, also incorporating organizational and socio-economic principles that require coordination, fairness, digital platforms, and appropriate market mechanisms to ensure effective local energy sharing [8, 10]. Furthermore, recent studies highlight that flexibility assets and differences in member preferences influence how communities operate and how long members stay involved [11, 22]. Consequently, the design of an REC is not only determined by the available DERs but also by the adopted market architecture and coordination mechanism, which directly influence both economic performance and the ability to incorporate distribution network constraints.

2.2.1 Prosumers, Community Structure and Collective Objectives

Prosumers are the most active end-users in RECs, being responsible for a variety of duties such as consumption, generation, storage, and, in some cases, flexible demand management, making them active agents in energy decision-making [6, 10, 11]. Their motivations usually include cost reduction, energy autonomy, sustainability, balanced benefit-sharing, and a desire for greater control over their energy footprint [8, 9]. This observed active behavior is significantly different from the traditional centralized operation of electric systems, helping to explain why community energy models have gained increasing relevance over the past few years.

Elaborating on this theme, the internal structure of a community is essential for defining how local energy sharing is carried out, as members of these communities can contribute with different resources, preferences, and levels of flexibility. As a result, RECs can adopt various organizational arrangements. In many implementations, a community manager is responsible for collecting information from members, coordinating internal energy allocation, conducting market clearing, and interacting with the DSO when required [10, 11].

Meanwhile, fully decentralized arrangements, which are typical in P2P energy trading, allow each prosumer to autonomously negotiate with others and directly participate in local trading decisions [6, 23]. Despite the different levels of coordination, these organizational models share the common goal of utilizing local resources to optimize collective benefits for community members [8, 11]. These organizational differences strongly influence how network constraints are incorporated into the optimization process, as discussed in the following subsections.

2.2.2 Local Energy Sharing Models

As previously mentioned, the way energy is exchanged between community members is an extremely important aspect in defining a REC. Since prosumers differ in their contributions, a community must acquire a coordination mechanism that determines how surplus renewable generation is shared and how local deficits are compensated, thereby influencing economic outcomes, fairness perceptions, operational stability, and the level of engagement of community members, depending on the type of sharing model chosen [8, 10, 22].

Building on these considerations, there are three main categories of local energy sharing models, varying primarily in their levels of decentralization and the degree of coordination involved: P2P trading markets, Community-Based Markets (CBMs), and Hybrid Models (i.e., structures that combine features of both approaches).

From an optimization perspective, these market architectures differ primarily in the degree of centralization used to coordinate community resources. This distinction is particularly relevant because centralized formulations facilitate the direct incorporation of network constraints within the optimization problem. In contrast, decentralized approaches generally require distributed coordination algorithms to ensure technical feasibility.

2.2.2.1 P2P Trading markets

P2P trading is the most decentralized approach to local energy sharing, characterized primarily by direct negotiations between prosumers. Within this framework, the referred participants engage in bilateral contracts or even distributed matching algorithms, allowing them to specify preferences for price, trading partners, and quantities exchanged [6, 10]. This high level of autonomy supports robust local balancing and offers significant flexibility to participants.

Figure 2.3 illustrates a conceptual overview of a full P2P market, in which prosumers exchange energy through multiple bilateral interactions [10]. As shown in this context, the market depends heavily on information exchanges among peers, which run in parallel with the physical power flows in the distribution network. These interactions require digital platforms capable of managing bids, validating trades, and ensuring transparency among participants.

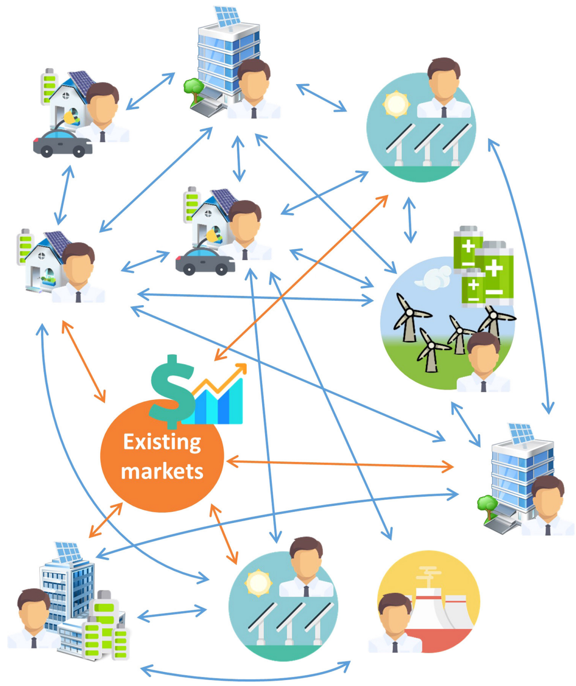

Figure 2.3: Illustration of a full P2P market architecture [10].

This conceptual distinction between the physical and virtual layers of the market is crucial to P2P design. Furthermore, as shown in Figure 2.4, physical power continues to flow according to the distribution grid's topology and its electrical limitations. At the same time, the virtual layer manages information exchange, market operations, and pricing mechanisms [6]. To facilitate decentralized decision-making and ensure compatibility with the underlying distribution network, these structures are crucial.

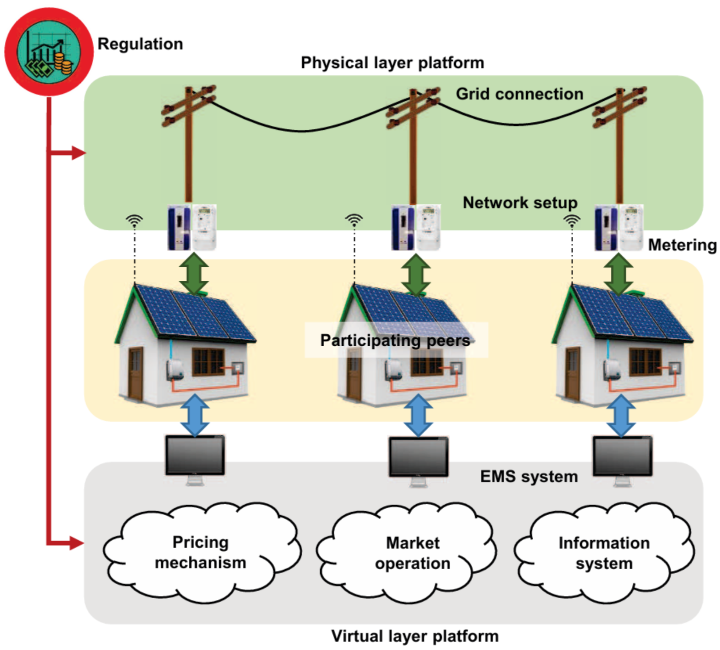

Figure 2.4: Physical and virtual layers of a P2P energy network [6].

Despite its advantages, unconstrained P2P trading may result in technically unpredictable operating points. In LV feeders, extensive P2P exchanges at high PV penetration can cause voltage rises, line congestion, reverse flows, and transformer overloads when network constraints are ignored, as explained in several studies [7]. These limitations highlight the need for network-aware market coordination methods that incorporate distribution system constraints into the P2P negotiation process. Consequently, although P2P trading offers a high degree of flexibility and participant autonomy, its practical implementation in active distribution networks requires additional coordination mechanisms to enforce network constraints. This challenge has motivated the development of more coordinated market architectures, such as CBMs, discussed in the following subsection.

Within these markets, the price of internal transactions can be determined by different mechanisms, such as the Mid-Market Rate (MMR), which sets the local price between the retail buying and selling tariffs, ensuring that both buyers and sellers benefit relative to trading in the external market [5].

2.2.2.2 Community-based Markets

CBMs adopt a more centralized coordination structure, in which a community manager gathers information from prosumers, performs internal market clearing, and interacts with the DSO as needed [10]. This approach enables the implementation of allocation rules that enhance fairness and allow a more transparent distribution of costs and benefits within the community [8, 9].

In contrast to P2P markets, in a CBM, internal trading decisions are cleared up by the community manager, who collects bids from community members, determines internal exchanges, and manages interactions with external markets, as illustrated in the general structure of a CBM in Figure 2.5.

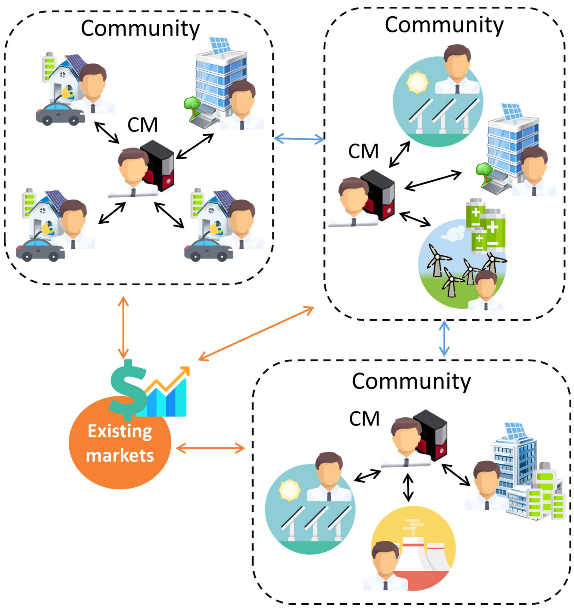

Figure 2.5: CBM structure with a community manager [10].

This coordinated mechanism contributes to more predictable operations and is frequently adopted in practical REC implementations [11, 12]. Because the market-clearing process is performed by a central coordinator, CBMs naturally provide a suitable framework for integrating network-constrained OPF formulations within community operation. This characteristic makes CBMs particularly attractive for optimization-based REC management, including the framework developed in this dissertation.

2.2.2.3 Hybrid Models

Hybrid market structures are a combination of decentralized P2P interactions with centralized coordination, allowing prosumers to trade bilaterally within or across communities, while a higher-level entity supervises system-wide consistency and may step in to ensure viability [6, 10]. These architectures benefit from the autonomy characteristic of P2P markets while maintaining the operational robustness associated with CBMs.

Figure 2.6 presents a typical hybrid P2P design, in which multiple communities coexist and interact with market operators, system operators, and external markets. This layered structure makes hybrid models especially suited to scenarios with heterogeneous user preferences or high DER penetration, where partial coordination can significantly improve both economic and technical performance [7].

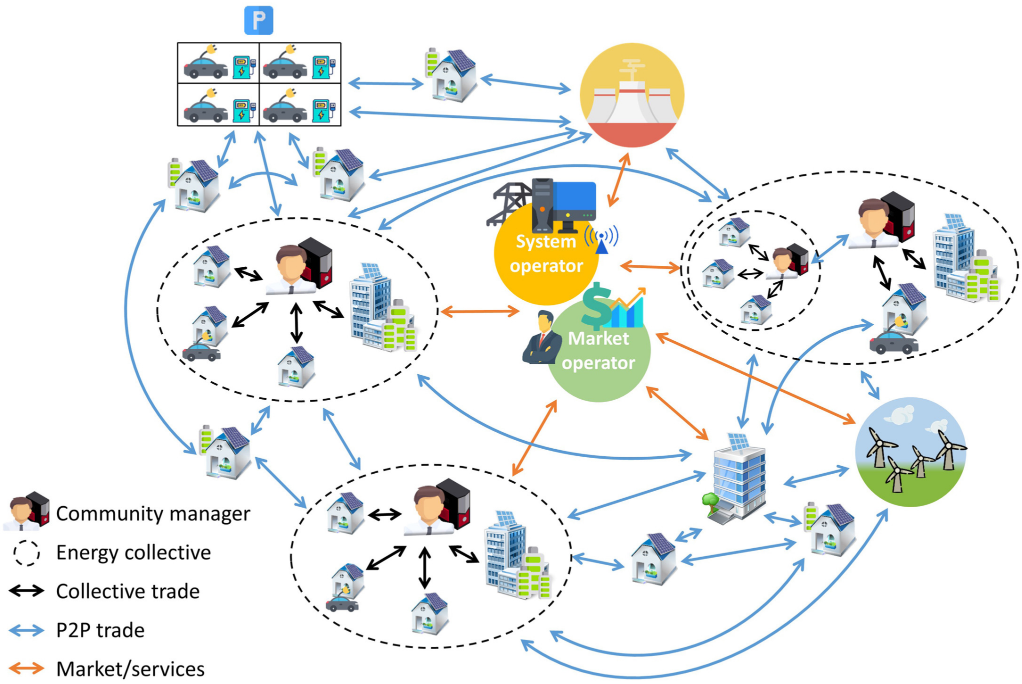

Figure 2.6: Hybrid P2P market design combining community coordination and P2P autonomy [10].

Despite their flexibility, hybrid market structures generally require more sophisticated coordination and communication infrastructure than purely centralized CBMs, thereby increasing implementation complexity while potentially improving scalability and user autonomy.

Table 2.2 summarizes the main characteristics of the local energy sharing models discussed throughout this section. While P2P markets maximize participant autonomy through distributed decision-making, incorporating network constraints into the trading process is considerably more challenging. Conversely, CBMs rely on a central coordinator, facilitating the integration of network-constrained optimization into the market-clearing process. Hybrid models seek to combine the advantages of both approaches, balancing flexibility and coordinated system operation.

Table 2.2: Comparison of the main local energy sharing models for RECs.

Characteristic	**P2P**	**CBM**	**Hybrid**
Coordination Entity	Peer negotiation	Community Manager	Community Manager + Peers
Decision-Making	Distributed	Centralized optimization	Hierarchical
Information Exchange	High (distributed)	Moderate (centralized)	High
Coordination Complexity	High	Moderate	High
Network Constraint Integration	Challenging	Feasible	Moderate
Typical Application	Local energy trading	Operator-coordinated RECs	Multi-community coordination

Given that the proposed framework adopts a centralized optimization approach and explicitly incorporates distribution network constraints within the market-clearing process, the CBM architecture provides the most natural and suitable foundation for the methodology developed in this dissertation.

2.2.3 Technical and Socio-Economic Dimensions of REC Operation

Fairness plays a central role in ensuring the long-term stability of RECs. Given their voluntary participation, it is imperative that members recognize that benefits are allocated in a balanced manner. The literature identifies several dimensions of fairness, including the balance between individual and collective self-consumption, the proportional use of community assets, such as shared batteries, the distribution of economic gains, and various user satisfaction indicators [8, 9, 22]. Implementing fair allocation mechanisms is crucial to preventing any prosumer from consistently benefiting at the expense of others, thereby promoting sustained community engagement and continuity.

The way RECs operate depends a lot on the DERs their members have. PV generation is typically the main resource, but due to its variability, other flexibility tools are needed [11, 24]. Battery Energy Storage Systems (BESS) are particularly relevant because they store surplus PV generation, help prevent voltage rises, reduce reverse flows, and improve collective self-consumption [11, 24]. Additional flexible assets, such as EVs, heat pumps, and responsive loads, also help the community manage local peaks and variability, better aligning local generation and consumption

[11, 24]. The effective coordination of these distributed resources therefore requires optimization frameworks that simultaneously account for market decisions and the physical constraints of the distribution network.

Digital platforms also play a key role in making REC operations scalable and secure. Technologies such as blockchain and smart contracts enable transparent and tamper-proof settlement of P2P transactions [6, 25]. Distributed optimization techniques, such as ADMM, help coordinate markets without exposing private data [23, 26]. Forecasting and monitoring tools also support real-time management of DERs and local imbalances [11]. Together, these technologies provide the digital infrastructure required to support secure information exchange, distributed coordination, and real-time implementation of optimization-based energy management strategies within RECs.

Finally, several studies emphasize that REC operation must remain consistent with the physical constraints of LV networks, meaning that market decisions that ignore voltage limits, line congestion, or transformer loading can result in infeasible or unsafe operating conditions [7, 23]. Embedding network-constrained OPF formulations inside community coordination mechanisms, such as those based on the RBFM, has been shown to mitigate these issues while maintaining satisfactory economic performance [5, 12]. These findings demonstrate that economically efficient REC operation cannot be decoupled from the physical behavior of the underlying distribution network, motivating the development of tractable optimization frameworks that explicitly integrate network constraints into community energy management. Such formulations constitute the focus of the methodology presented in the following chapter.

2.3 Convex Relaxations for Solving OPF in Community Contexts

Convex relaxations offer a more efficient and practical approach to integrating network constraints into REC optimization. While Section 2.1.4 introduced the general ideas of SDP, SOCP, and QC relaxations, their relevance becomes more concrete in the context of community-scale operation, where optimization must be both accurate and computationally efficient.

In particular, convex relaxations enable the direct integration of network-constrained OPF formulations into community energy management frameworks without incurring the computational burden associated with full AC-OPF. Consequently, they constitute one of the key enabling technologies for practical optimization of RECs.

2.3.1 SDP-OPF in Community Networks

As explained before, SDP relaxations provide some of the tightest convex approximations of the AC-OPF, although their role in REC applications is more specific [13, 14]. That is, in community contexts, SDP is mainly used as a reference or a benchmarking tool rather than as the core optimization engine, due to its higher computational cost.

For example, as noted in [17], decentralized SDP-based formulations demonstrate that large distribution networks can be solved using ADMM, making SDP useful only for validating the performance of faster relaxations used in day-ahead community scheduling.

Consequently, in practical RECs, SDP is most valuable to:

- Ensure exactness is critical (e.g., to validate a community market solution);
- Obtain a high-quality reference solution that can be used to determine whether lighter relaxations remain sufficiently accurate.

Beyond these roles, SDP is rarely used for operational REC optimization.

2.3.2 SOCP-OPF and the RBFM

SOCP relaxations are, by far, the most widely used convex formulations in REC optimization since they exploit the BFM structure and scale efficiently to LV networks.

The resulting RBFM is often exact in radial feeders and remains accurate even under practical limits on currents, voltages, and reverse flows. The previously mentioned sufficient condition C1 (proposed in [19]) guarantees exactness in realistic settings, supporting the use of SOCP relaxations when modeling enriched DER communities. From a computational perspective, SOCP relaxations offer an attractive balance between modeling accuracy and solution efficiency, allowing network-constrained optimization problems to be solved repeatedly within the time requirements typically associated with REC scheduling. These characteristics have made SOCP-based formulations the preferred approach for network-constrained REC optimization.

Several studies have successfully adopted this approach. For example, as illustrated in [20], the RBFM can be integrated into robust scheduling frameworks that coordinate energy storage systems, reactive power support, and OLTCs. Similarly, [21] demonstrates that SOCP formulations can be combined with decentralized optimization techniques to efficiently coordinate multiple agents. Together, these studies highlight the versatility of the SOCP-based RBFM, reinforcing its suitability for network-constrained optimization of RECs.

2.3.3 QC-OPF for Distribution-Level Accuracy

In REC applications, the main advantage of QC relaxations is that they offer a middle ground between the tightness of SDP and the scalability of SOCP. This type of relaxation performs particularly well when voltage magnitudes remain close to nominal values, which is how well-regulated LV feeders usually work.

Although it is less common in REC-specific studies, QC-OPF remains relevant when community coordination requires a more accurate approximation than SOCP but cannot afford the computational cost of SDP. It is also useful as an intermediate relaxation or warm start for more demanding OPF algorithms in scenarios involving high DER penetration.

Ultimately, convex relaxations based on the RBFM provide an effective balance between physical modeling accuracy and computational efficiency for REC optimization. As demonstrated in

[12], integrating a relaxed OPF formulation into community energy management enables explicit consideration of network constraints while maintaining computational tractability. These characteristics explain the widespread adoption of RBFM-based SOCP formulations in the REC literature and motivate their selection as the foundation of the optimization framework developed in Chapter 3.

2.4 Distributed Optimization in RECs

Distributed optimization methods have gained increasing attention in REC-oriented research, particularly in contexts where market coordination must remain scalable, preserve user privacy, and operate across several independent decision-makers. Instead of relying on a single central solver, these approaches decompose the OPF or market-clearing problem into smaller subproblems that can be solved locally while maintaining global consistency through iterative message-passing schemes. Although the framework developed in this dissertation adopts a centralized optimization structure, distributed methods are relevant to understanding alternative coordination architectures and potential extensions for larger-scale REC implementations.

One of the most common techniques is the ADMM, which allows convex OPF problems to be solved across multiple areas without exposing private information, such as prosumer preferences or device characteristics. For instance, in [17], it is shown that an SDP-OPF can be decentralized with an accelerated ADMM scheme, achieving good scalability while still maintaining high solution quality. Similarly, the adaptive-core variant of the APP, presented in [21], distributes an SOCP-relaxed OPF across network partitions, improving convergence relative to classical APP variants.

Distributed optimization is also important for Local Energy Markets (LEMs) because, in fully decentralized P2P environments, prosumers negotiate directly, making decentralized algorithms necessary to align bilateral trades with the technical limits of the network. This is illustrated in [23], where P2P trading is combined with distributed OPF updates, allowing participants to trade energy while keeping voltages and currents within acceptable limits. At a higher level of coordination, [26] demonstrates that decentralized decision-making under uncertainty can support communities that self-organize without a central operator.

Finally, although some REC implementations still rely on centralized coordination, as analyzed in the CBM in [12], the results reinforce the importance of incorporating network constraints in local trading. These approaches show a clear convergence between OPF relaxations, decentralized computation, and community-level energy management, whether solved centrally or in a distributed manner. This examined evolution opens the door to future REC coordination mechanisms that are more scalable, privacy-preserving, and better suited to high DER penetration.

2.5 Regulatory Framework for RECs

Besides the technical and optimization aspects discussed in the previous sections, the practical implementation and operation of RECs are also strongly influenced by the applicable regulatory framework. European legislation and its adaptation into Portuguese law establish the legal basis for community organization, energy sharing, market participation, and governance, while also defining several operational mechanisms that directly influence the design of optimization frameworks. The following subsections therefore review the main regulatory developments relevant to RECs and their implications for community energy management.

2.5.1 European Regulatory Framework

The development of RECs in Europe has been strongly supported by the legislative framework introduced under the Clean Energy for All Europeans Package, a comprehensive set of regulatory measures adopted between 2018 and 2019. Among these, Directive (EU) 2018/2001 on the promotion of the use of energy from renewable sources (Renewable Energy Directive II, RED II) plays a key role in formally introducing the concept of RECs [3].

According to RED II, a REC is defined as a legal entity based on open and voluntary participation, controlled by its members, who are typically located in the proximity of the renewable energy projects they are involved in [3]. Notably, their primary objective is not financial profit maximization but rather the delivery of environmental, economic, and social benefits to their members or surrounding areas [3].

Concurrently, Directive (EU) 2019/944, on common rules for the internal electricity market, also referred to as the Internal Market Directive (IMD), introduced the concept of Citizen Energy Communities (CECs). Unlike RECs, CECs have a broader scope and can participate in a wider range of electricity-related activities, such as supply, distribution, and aggregation [4].

Overall, these directives establish the legal foundation for decentralized and consumer-centric energy systems, promoting the active participation of prosumers and enabling local energy-sharing mechanisms. At the same time, they create the need for operational tools capable of coordinating local resources in a technically feasible and economically efficient manner.

2.5.2 Portuguese Regulatory Framework

Building on the European regulatory framework, the mentioned directives have been transposed into national legislation by Member States, resulting in different implementations of RECs across Europe. In Portugal, this framework has evolved progressively, reflecting a transition from simple self-consumption schemes to more structured and integrated energy community models.

The initial legal basis for self-consumption was established by Decree-Law No. 162/2019, which introduced the concepts of individual and collective self-consumption, allowing multiple consumers to share locally generated energy [27]. Although this framework represented a significant step towards decentralized energy management, it remained limited in terms of organizational flexibility and market integration.

For this reason, this limitation was then revised by Decree-Law No. 15/2022, which restructured the Portuguese electricity sector, formally establishing the legal framework for RECs and defining the role of the Collective Self-Consumption Managing Entity (EGAC), responsible for coordinating energy allocation between participants, thus enabling a more organized and scalable operation of these communities [28]. From an optimization perspective, the existence of a centralized management entity also facilitates the implementation of community-level optimization algorithms that coordinate market decisions while enforcing network constraints.

More recently, Decree-Law No. 99/2024 and subsequent revisions have further refined the regulatory framework, particularly by addressing operational aspects such as energy-sharing coefficients, market integration, and administrative procedures [29]. These developments reflect the progressive transition from a purely regulatory definition of RECs towards a framework that supports their practical implementation and operation.

In general, the evolution of the Portuguese regulatory framework reflects the increasing maturity of RECs and their growing role within the national electricity system. At the same time, the resulting operational complexity reinforces the need for optimization frameworks that can coordinate local energy exchanges while explicitly accounting for distribution network constraints.

2.5.3 Operational Mechanisms of RECs in Portugal

The operation of RECs in Portugal is governed by regulatory mechanisms that define how locally generated energy is allocated among members and subsequently settled. These operational rules directly influence the formulation of optimization models for community energy management.

The main mechanism considered is the use of allocation coefficients, which can determine how locally generated energy is distributed between community members [5, 10]. These coefficients can be defined earlier or dynamically updated, thereby allowing different levels of flexibility in the allocation process, as established in the regulatory framework defined by Decree-Law No. 15/2022 and further detailed in the Regulation on Self-Consumption approved by the Portuguese Energy Services Regulatory Authority (ERSE) [28, 30]. While fixed allocation coefficients simplify community operation, dynamically optimized coefficients can improve self-consumption, reduce energy costs, and better accommodate the operational constraints of the distribution network. From an optimization perspective, these coefficients determine how community generation is distributed among participants and, in turn, directly affect both the market's economic outcome and the distribution network's physical loading.

The EGAC plays a central role in this process by defining and communicating the allocation coefficients to the system operator [30]. As the entity responsible for coordinating community operations, the EGAC also provides a natural framework for implementing centralized optimization algorithms that can simultaneously determine energy allocation and enforce network constraints.

Consequently, optimizing REC operation requires not only determining economically efficient allocation coefficients but also ensuring that the resulting energy exchanges remain compatible with the physical constraints of the underlying distribution network. This requirement motivates the integration of network-constrained optimization methods within community energy management platforms.

2.5.4 Deployment of RECs in Portugal

The adoption of self-consumption and energy community models has notably increased in Portugal in recent years. In fact, recent reports from ERSE indicate that, by the end of 2024, there were approximately 237 000 self-consumption systems, resulting in a total installed capacity of around 1.8 GW, which represents about 3% of final energy consumption [30].

These installations represent an increasing share of the national electricity usage and demonstrate the growing importance of decentralized energy solutions.

Despite this growth, the number of fully operational RECs in Portugal remains limited. Existing initiatives, such as the RECs located in Telheiras/Lumiar (Lisbon), Culatra Island (Faro), and Braga, are considered pioneering projects, alongside a small number of LV distribution communities, with most of them being organized as electricity cooperatives, illustrating the challenges associated with the practical implementation of these communities [31]. Most of these initiatives operate as electricity cooperatives, illustrating both the potential of community energy models and the practical challenges associated with their implementation.

Beyond energy sharing, several Portuguese RECs pursue broader social and environmental objectives. A representative example is the Telheiras/Lumiar REC, one of the first citizen-led energy communities in the country, developed within the scope of the EU Energy Poverty Advisory Hub and explicitly including households experiencing energy poverty among its beneficiaries [32, 33]. This example illustrates how REC initiatives may be driven not only by energy-related goals, but also by broader objectives such as social inclusion, community engagement, and local development. At the same time, the experience gained from these pioneering projects highlights the significant administrative, licensing, and operational challenges that continue to limit the widespread deployment of RECs in Portugal.

These early deployment experiences also demonstrate that, beyond regulatory and administrative challenges, the efficient operation of RECs increasingly depends on optimization tools that coordinate local energy exchanges while respecting distribution network constraints.

2.5.5 Legal Barriers and Challenges

Despite the existence of a structured regulatory framework, the practical implementation and operation of RECs continue to face significant challenges. These emerging barriers are caused not only by regulatory design choices but also by the interaction between market design and the physical operation of distribution networks, as highlighted in recent literature [5, 7, 34].

One of the main regulatory limitations is the requirement for electrical proximity among REC members. Within the Portuguese framework, the relevant authority assesses this criterion for each case to ensure that energy sharing aligns with local physical conditions. For this purpose, Article 83 of Decree-Law No. 15/2022 establishes maximum distances between the production unit and the corresponding consumption installation, depending on the voltage level of the connection:

- 2 km for LV networks;
- 4 km for Medium-Voltage (MV) systems;
- 10 km for High-Voltage (HV) networks;
- 20 km for very-high-voltage connections.

For LV installations, sharing the same distribution transformer is also accepted as an equivalent proximity condition, as stated in [28]. Essentially, these requirements preserve the local character of energy sharing but may also restrict the scalability and economic potential of RECs, particularly when geographically dispersed participants could otherwise benefit from cooperation. [34].

A further significant constraint concerns the energy distribution mechanisms that rely on allocation coefficients, which are usually defined as either fixed or automatically proportional to consumption. Even though these methods simplify the implementation, they can limit the flexibility of energy sharing and lead to inefficient outcomes, such as simultaneous energy surpluses and deficits within the same community [5, 34]. This limitation further motivates the adoption of optimization-based allocation strategies that dynamically adapt energy sharing to both market conditions and network operating constraints.

More generally, studies on LEMs highlight that rigid allocation methods limit communities' ability to adapt to real-time modifications in generation and demand, reducing both economic efficiency and system performance [7, 10]. In this context, more flexible approaches, such as dynamically updated coefficients, could enable more efficient and economically attractive community operation, enhancing the overall efficiency of REC operation [5].

Additionally, the current regulatory framework still provides a limited basis for the development of advanced LEMs, such as P2P trading and active participation of aggregators. This limited market maturity currently limits innovation and delays the evolution of RECs towards more flexible and market-oriented structures [5, 10, 34].

From a technical perspective, another critical challenge is the limited integration of REC operations with distribution network constraints. Several studies have shown that when local energy trading mechanisms are not correctly coordinated with the physical grid, it can lead to increased losses, voltage deviations, and network congestion [7, 23]. These effects occur due to market-based decisions being often taken without explicitly considering the physical limitations of the distribution system. Consequently, market-clearing mechanisms that neglect the physical characteristics of the distribution network may produce economically attractive yet technically infeasible operating schedules, reinforcing the importance of network-constrained optimization frameworks.

Overall, the regulatory and technical limitations discussed above reveal a clear gap between the design of a LEM and the physical operation of distribution networks. Addressing this gap requires optimization frameworks that can simultaneously coordinate community energy exchanges and enforce network constraints, which is the primary motivation for the methodology developed in this dissertation.

2.6 Summary, Overview of the reviewed papers and Identified Gaps

This chapter reviewed the main modeling approaches, energy-sharing structures, optimization tools, and regulatory aspects relevant to RECs. Beginning with Section 2.1, OPF formulations and their convex relaxations were analyzed, highlighting the advantages of the BFM for radial networks. Afterward, Section 2.2 examined REC organization and local energy-sharing mechanisms, while Section 2.3 discussed how convex relaxations can allow network-aware community operation. Section 2.4 outlined the role of distributed optimization techniques in coordinating local markets. Finally, the regulatory framework governing RECs was reviewed in Section 2.5, covering both European legislation and the Portuguese implementation, as well as the main operational mechanisms and current challenges associated with REC deployment.

Table 2.3 provides a comparative overview of the main studies reviewed throughout this chapter, highlighting the adopted network models, OPF formulations, market architectures, and their principal technical contributions. The symbol "–" indicates that the corresponding work does not explicitly address the respective dimension.

Table 2.3: Comparison of the main literature related to REC optimization according to network modeling, optimization approach, market architecture, and technical contribution.

Reference	Network Model	OPF / Relaxation	Market Model	Scope and Contribution
[5]	AC-OPF (post-correction)	AC-OPF	Multistage REC	Three-stage REC management with post-hoc OPF correction
[6]	–	–	P2P market (survey)	Survey of P2P architectures, pricing, and trading
[7]	Full AC (simulated)	–	P2P	Impact of P2P trading on LV grid under high PV penetration
[8]	–	–	Energy Collective (CBM)	Fairness-oriented energy collective with community manager
[9]	–	–	Consumer-centric local markets	Consumer-centric fairness indicators for LEMs
[10]	Linear / Unconstrained	–	P2P / CBM	Review of P2P and CBM architectures for local sharing
[11]	LV power-flow simulation	–	CBM	CBM with BESS scheduling under realistic LV conditions
[12]	AC-OPF (RBFM–SOCP)	SOCP	CBM + OPF	Network-constrained CBM with integrated RBFM–SOCP
[13]	AC / Branch Flow	Survey (SDP/SOCP/QC/LP)	–	Comprehensive review of OPF relaxations
[16]	Branch Flow	SOCP	–	BFM formulation and exactness of SOCP relaxation for radial networks
[17]	Radial LV	SDP (distributed)	–	Decentralized SDP-OPF via accelerated ADMM for large networks
[19]	Radial network	SOCP (C1)	–	Sufficient condition (C1) for exactness of SOCP relaxation
[20]	Radial network	Mixed-integer SOCP	Robust coordination	Robust multi-period SOCP with storage and reactive support
[21]	Radial network	SOCP (distributed via APP)	–	Distributed SOCP via adaptive-core APP for multi-agent OPF
[22]	Simplified	–	CBM	BESS scheduling and member engagement in CBM context
[23]	LV network constraints	Distributed OPF	P2P	P2P trading with distributed OPF and ADMM coordination
[24]	Simplified/unconstrained	–	P2P local market	Battery flexibility and P2P trading in LEMs
[25]	–	–	Blockchain P2P	Blockchain-based settlement for P2P energy transactions
[26]	–	–	Decentralized coordination	Decentralized community coordination under uncertainty
This work	AC-OPF (RBFM–SOCP)	SOCP	CBM + P2P (bilateral)	Integration of RBFM–SOCP into OSTEC for network-constrained REC scheduling

As can be observed, most existing studies focus on specific aspects of REC operation, such as market design, network modeling, or OPF formulations, highlighting the limited number of fully integrated optimization frameworks.

Despite the significant progress achieved in recent years, several gaps remain evident in the literature, such as:

- **Simplified representation of distribution networks:** Many REC optimization studies rely on simplified or unconstrained network models, neglecting voltage limits, line loading, and power losses. Although these simplifications reduce computational complexity, they may produce operating schedules that are not physically feasible when implemented in real distribution networks.

- **Limited integration of market operation and network constraints:** While numerous studies investigate either LEM mechanisms or OPF formulations, relatively few integrate both aspects within a unified optimization framework. Consequently, market decisions are often determined independently of the physical operation of the distribution network.

- **Limited implementation in operational community management platforms:** Existing research predominantly focuses on the mathematical development of optimization models, with comparatively fewer studies addressing their integration into operational tools capable of supporting the day-to-day management of RECs.

- **Limited integration of multiple operational dimensions:** Several contributions address specific aspects of REC operation, such as fairness, uncertainty, DER coordination, or network constraints. However, relatively few frameworks combine these dimensions into a single optimization model that supports practical community operations.

These research gaps motivate the methodology proposed in this dissertation, which integrates an RBFM within the OSTEC community energy management platform. By combining community market operation with an explicit representation of distribution network constraints, the proposed framework aims to improve both the technical feasibility and the operational effectiveness of RECs. Building upon the concepts and challenges discussed throughout this chapter, Chapter 3 presents the proposed optimization framework, detailing its mathematical formulation, system architecture, and integration within the OSTEC platform.

Chapter 3

Network-Constrained Formulation of the REC Model

This chapter presents the mathematical formulation developed in this dissertation to represent the operation of a REC while explicitly accounting for the physical constraints of the underlying distribution network. The proposed framework builds upon three complementary components identified throughout the literature review: *(i)* the network-constrained community market model proposed by [12], *(ii)* the second-stage optimization logic of the OSTEC platform [5], and *(iii)* the RBFM model, which provides a computationally efficient representation of power flow in radial distribution networks.

Rather than treating these components independently, this dissertation integrates them into a unified optimization framework that simultaneously coordinates community energy exchanges and enforces network operating constraints. The remainder of this chapter presents the resulting mathematical formulation, including the optimization variables, objective function, and operational constraints that define the proposed network-constrained REC management model.

3.1 Overview of the Community and Network Representation

This section introduces the physical and organizational representation adopted throughout the proposed optimization framework, establishing how REC members and the underlying distribution network are modeled before presenting the mathematical formulation.

The proposed framework considers an REC composed of interconnected members that can consume, generate, and exchange electrical energy within a radial distribution network. As discussed in Chapter 2, each community member is associated with a node of the underlying distribution system and may include DERs, thereby enabling local energy production, storage, and flexibility services.

The distribution network is modeled as a radial distribution system composed of n buses interconnected by a set of distribution lines $(n,m) \in \mathscr{E}$. Active and reactive power flows, nodal voltage magnitudes, and line current limits are represented through the RBFM, enabling the explicit incorporation of network operating constraints within the optimization problem. The radial topology is consistent with the assumptions underlying the SOCP relaxation discussed in Section 2.3 and supports the exactness conditions presented in Subsection 2.1.4.

Community members are necessarily assigned to non-slack network buses, such that each member's economic decisions directly translate into active power injections or withdrawals at the corresponding network node. This one-to-one correspondence between community members and network buses enables the direct coupling of market decisions with the electrical state of the distribution network. The slack bus represents the point of common coupling with the upstream grid, while junction buses with no associated community member are modeled with zero net injection.

Figure 3.1 illustrates the overall structure of the REC considered in this work, where different community members may include local DERs, such as PV systems and BESS units, while remaining sufficiently general to accommodate additional technologies, including wind generation, Combined Heat and Power (CHP) units, and EV charging infrastructure.

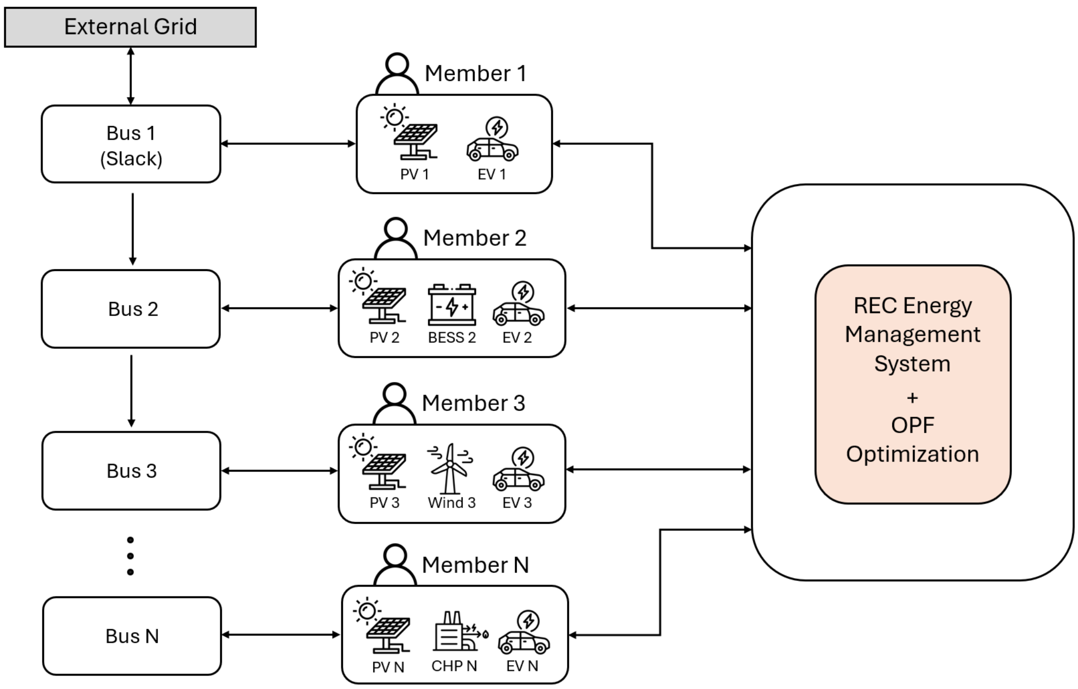

Figure 3.1: Schematic representation of the proposed REC framework, illustrating the integration between community members, their DERs, the underlying radial distribution network, and the unified energy management and OPF optimization system.

3.2 REC Modeling Framework and Workflow

This section presents the overall workflow of the proposed optimization framework before introducing its mathematical formulation. The methodology integrates the economic operation of the REC with the physical constraints of the distribution network within a unified optimization problem. As illustrated in Figure 3.2, the proposed framework combines OSTEC's two-stage optimization procedure with an iterative outer-approximation algorithm to incorporate the SOC constraints associated with the RBFM model.

Unlike conventional sequential approaches, in which market clearing is performed before network feasibility is verified through a subsequent OPF correction stage [5], the proposed framework embeds the network constraints directly into the community optimization problem. Consequently, all economic decisions are guaranteed to satisfy the operational limits of the distribution network during the optimization process itself.

3.2.1 Two-Stage Solution Procedure

The overall optimization procedure follows the two-stage architecture implemented in OSTEC. In Stage 1, each community member $n \in N$ solves an individual Mixed-Integer Linear Programming (MILP) problem to determine its optimal standalone operation, resulting in the individual cost benchmark $\hat{C}_n^{ind}$, subsequently used to enforce the fairness condition in Stage 2. In both the preliminary and main case studies, Stage 1 is solved independently for every community member prior to the collective optimization. The obtained benchmarks are then enforced in Stage 2 through a soft no-worse-off constraint, formally defined in Sub-subsection 3.4.1.2. This stage is independent across members and does not incorporate network constraints, as it represents the baseline each member would achieve operating in isolation.

Building upon these individual benchmarks, Stage 2 solves a single MILP to determine the optimal energy exchanges, storage schedules, and external market interactions for all members simultaneously, while satisfying both economic fairness requirements and the physical constraints of the distribution network.

3.2.2 Iterative Outer-Approximation for the SOC Constraint

The RBFM includes SOC constraints associated with the relationship between branch currents, voltages, and power flows. Although these constraints preserve the convexity of the OPF formulation, they cannot be directly represented within the MILP-based implementation adopted in this work.

To overcome this limitation, an iterative outer-approximation strategy is adopted. The MILP is initially solved with the SOC constraint replaced by linear bounds on branch flows, and the resulting solution is subsequently checked for violations. Whenever a violation is identified, a supporting hyperplane is generated at the violating point and incorporated into the MILP formulation, progressively refining the feasible region. This process is repeated until no further violations are found or a maximum number of iterations is reached. The iterative interaction between the MILP solution stage, the SOC violation check, and the generation of additional supporting hyperplanes is also summarized in Figure 3.2.

This approach enables the incorporation of network-constrained OPF behavior within a computationally tractable MILP framework, while avoiding the direct use of native SOCP solvers and keeping the problem compatible with the mixed-integer linear structure of OSTEC. The mathematical details of this procedure, including the derivation of the supporting hyperplanes and the violation detection criterion, are presented in Sub-subsection 3.4.2.2.

3.2.3 Inputs and Outputs

From a data perspective, the proposed methodology relies on three main sets of inputs. The first category constitutes the member-specific operational profiles, for instance the hourly consumption $\hat{E}^{C}_{n,t}$, the forecasted non-dispatchable renewable generation $\hat{E}^{G}_{n,t}$, and the technical and economic parameters associated with dispatchable CHP generation $E^{G,CHP}_{n,t}$. The following set comprises the economic parameters required for market coordination, including retail tariffs, market prices, grid access tariffs, and DER technical characteristics. Finally, the third set consists of the electrical network data, including the radial distribution topology, branch resistance and reactance parameters, and the operational voltage and current limits for each node and line in the system under study.

The resulting optimization process produces both the REC's economic operating schedules and the distribution network's corresponding electrical state. These outputs include energy exchanges with the retailer and the external market, internal P2P transactions, and the charging and discharging schedules of flexible resources such as BESS and EVs.

The optimization also determines the electrical operating state of the network for each branch and time period. Although the branch flow formulation considers squared quantities as internal decision variables, namely the squared nodal voltage magnitudes $v_{n,t}$ and the squared branch current magnitudes $l_{n,m,t}$, the corresponding physical magnitudes are recovered through square-root transformations for result visualization and analysis. Therefore, the reported network variables comprise nodal voltage magnitudes, branch current magnitudes, and active and reactive branch power flows $P_{n,m,t}$ and $Q_{n,m,t}$.

Finally, the optimization computes the individual operating cost for each REC member, enabling assessment of how network constraints affect the economic performance of different participants. Together with the electrical variables, these results provide the necessary information to evaluate voltage regulation, branch loading, DER utilization, and the effectiveness of the proposed network-constrained optimization framework under different operating scenarios.

The complete workflow of the proposed methodology is summarized in Figure 3.2, which illustrates the required input datasets, the two-stage optimization procedure, the iterative outer-approximation process, and the resulting economic and network-related outputs.

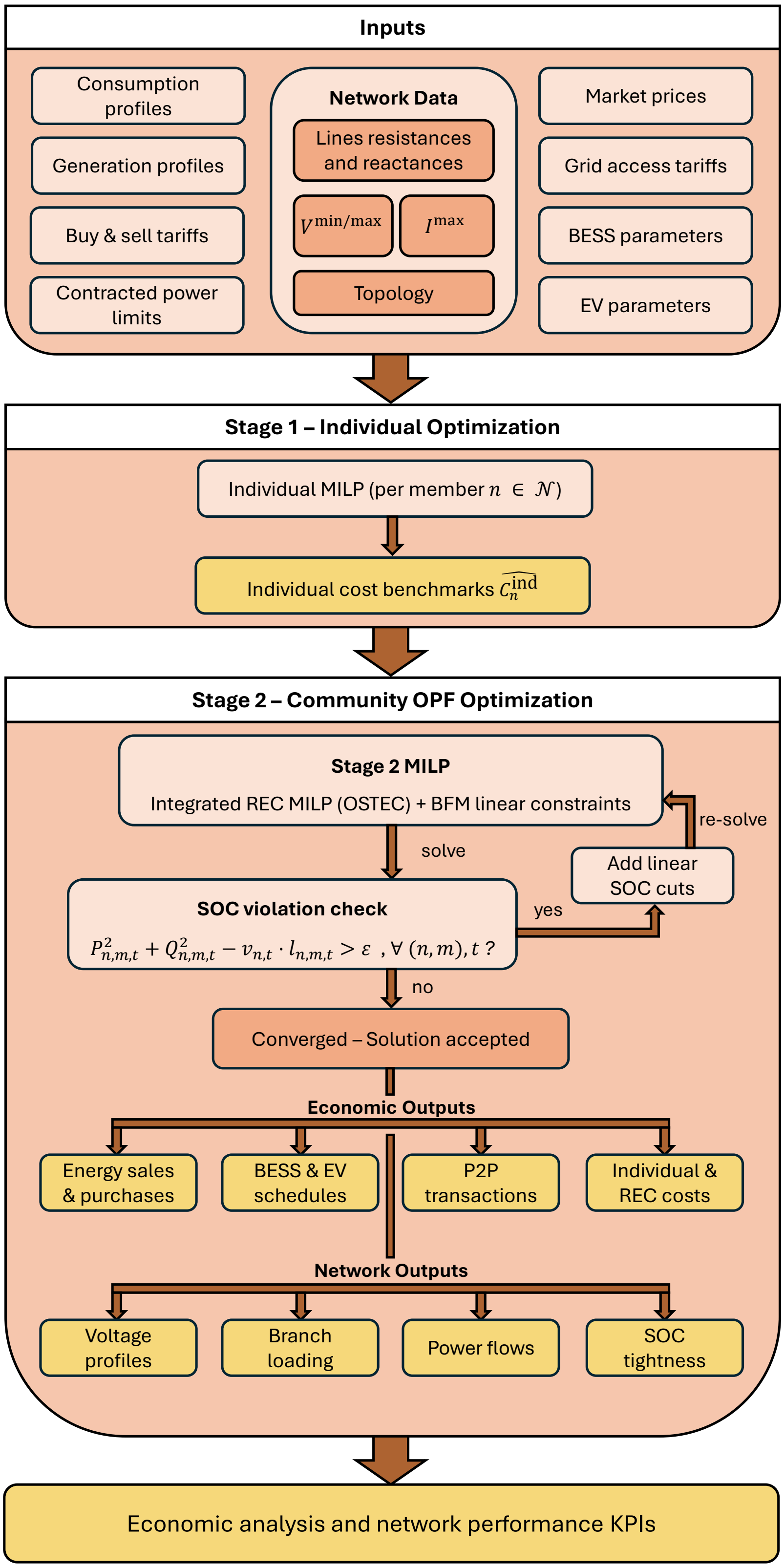

Figure 3.2: Workflow of the proposed REC optimization methodology, illustrating the two-stage solution structure and the resulting economic and network-related outputs.

3.3 REC Model and its relation to OSTEC

The mathematical formulation developed in this dissertation extends the second-stage optimization model of the OSTEC platform. Although OSTEC follows a two-stage optimization architecture, the methodological developments presented in this chapter are incorporated exclusively within the collective optimization performed in Stage 2, while preserving the original framework proposed by [5].

In the original OSTEC implementation, the Stage 2 optimization problem is formulated exclusively in terms of energy variables expressed in kWh and does not explicitly represent the physical distribution network. Consequently, the resulting operating schedules may be economically optimal but physically infeasible, as voltage violations, line overloads, and reverse power flows are not considered during the optimization process. To overcome this limitation, the proposed formulation builds upon the original bilateral Stage 2 structure, in which energy transactions are represented as pair-wise exchanges between individual community members rather than as aggregated community-level flows. This bilateral formulation is subsequently extended by integrating the RBFM, enabling the simultaneous optimization of community energy exchanges and distribution network operations within a unified optimization framework.

The original economic formulation serves as the foundation of the proposed optimization model. It is extended through additional decision variables, constraints, and objective function terms that improve its applicability to network-constrained REC operation. These extensions include, among others, a demand response curtailment variable for flexible load reduction at each metering point, its associated cost term in the objective function, and the no-worse-off constraint. The complete Stage 2 formulation, together with all proposed extensions, is presented in detail in Subsection 3.4.1.

Beyond these economic extensions, the proposed formulation incorporates a set of distribution network variables and constraints that are activated only when network data are available. Otherwise, the optimization problem reduces exactly to the original OSTEC Stage 2 bilateral MILP, thereby preserving full backward compatibility.

The coupling between the economic optimization model and the electrical network is established through the net metered energy variable $E_{n,t}^{CMET}$. This variable consolidates all energy transactions, storage operations, and local generation at each community member's metering point and is then converted to a per-unit active power injection at the corresponding network node. This conversion provides the direct interface between the OSTEC scheduling variables and the BFM. As detailed in Subsection 3.4.2, reactive power injections are modeled separately for each generation technology, namely PV, wind, and CHP units, since the original OSTEC formulation does not include reactive power scheduling.

Finally, when the network-constrained formulation is activated, two small regularization terms are incorporated into the community objective function to promote physically meaningful operating points of the network. The mathematical formulation and role of these regularization terms are presented in Subsection 3.4.2.

3.4 Mathematical Formulation

The proposed optimization model is organized into four main components:

- Objective function with the aim of minimizing the community's operating cost;
- Community energy balance constraints;
- Distribution network constraints through the RBFM model;
- Storage and EV constraints.

3.4.1 OSTEC's Stage 2 Model

This subsection presents the complete Stage 2 formulation adopted in the proposed optimization framework. It first introduces the original economic model implemented in OSTEC, which operates exclusively on energy variables (kWh) over the scheduling horizon, and subsequently describes the methodological extensions developed in this dissertation. These extensions include demand response and generation curtailment mechanisms, along with the additional variables and constraints required to integrate the RBFM, as presented in Subsection 3.4.2.

3.4.1.1 Objective Function

The objective of the REC is to minimize the total operational cost over the optimization horizon [5]:

$$
\begin{aligned}
\min \sum_{t\in T}\Bigg(\sum_{n\in N}\big(&E_{n,t}^{SUP,retail}\,\hat{\lambda}_{n,t}^{buy} - E_{n,t}^{SUR,retail}\,\hat{\lambda}_{n,t}^{sell} + E_{n,t}^{SUP,market}\,\hat{\lambda}_{t}^{marketbuy} - E_{n,t}^{SUR,market}\,\hat{\lambda}_{t}^{marketsell} \\
&+ E_{n,t}^{SLC}\,\hat{\lambda}_{t}^{grid} + P_{n,t}^{EXTRA}\,\hat{\lambda}^{EXTRA} + E_{n,t}^{DR}\,\hat{\lambda}^{DR} + E_{n,t}^{GC}\,\hat{\lambda}^{GC} + \sum_{s\in S} E_{n,s,t}^{B,D}\,\hat{\lambda}_{n,s}^{deg} + E_{n,t}^{G,CHP}\,\hat{\lambda}_{n}^{CHP}\big)\Bigg) \\
&+ \sum_{n\in N} \Delta Y_n\,\hat{\lambda}^{\Delta Y}
\end{aligned}
\tag{3.1}
$$

where, for each member $n \in N$ and time period $t \in T$, $E_{n,t}^{SUP,retail}$ and $E_{n,t}^{SUR,retail}$ represent the energy purchased from and sold to the retailer at tariffs $\hat{\lambda}_{n,t}^{buy}$ and $\hat{\lambda}_{n,t}^{sell}$, respectively, $E_{n,t}^{SUP,market}$ and $E_{n,t}^{SUR,market}$ denote the energy bought from and sold in the external market, at prices $\hat{\lambda}_{t}^{marketbuy}$ and $\hat{\lambda}_{t}^{marketsell}$, respectively, $E_{n,t}^{SLC}$ is the self-consumed energy behind the meter, which is subject to the grid access tariff $\hat{\lambda}_{t}^{grid}$, $P_{n,t}^{EXTRA}$ is the excess power above the contracted limit $\hat{P}_{n}^{CPE,max}$, penalized by the tariff $\hat{\lambda}^{EXTRA}$, $E_{n,t}^{DR}$ is the demand response curtailment variable, representing the load reduction applied at member n at time t to relieve thermal congestion, penalized by $\hat{\lambda}^{DR}$, $E_{n,t}^{GC}$ is the generation curtailment variable, representing the reduction of non-dispatchable renewable generation applied at member n at time t to relieve overvoltage or reverse-flow conditions, penalized by $\hat{\lambda}^{GC}$, $E_{n,s,t}^{B,D}$ represents the discharged energy from battery $s \in S$ of member n, associated with the degradation cost coefficient $\hat{\lambda}_{n,s}^{deg}$, and $E_{n,t}^{G,CHP}$ represents the electrical energy generated by CHP units, associated with its marginal generation cost $\hat{\lambda}_n^{CHP}$. Finally, ΔY_n is the non-negative slack variable associated with the no-worse-off constraint (Equation 3.9), penalized by the coefficient $\hat{\lambda}^{\Delta Y}$ and further detailed in Sub-subsection 3.4.1.2.

The original OSTEC formulation includes a degradation cost parameter for stationary BESS units, although this parameter was set to zero in the simulations considered in this work, as further reported in Table 4.5. No equivalent degradation cost term is included for EV batteries. Since the same cost structure is adopted in both Stage 1 and Stage 2, this omission does not introduce any inconsistency in the no-worse-off condition, represented by Equation 3.9. Nevertheless, the resulting costs do not explicitly account for the economic impact of battery aging, particularly under vehicle-to-grid operation.

The demand response term $E_{n,t}^{DR} \geq 0$ acts as a soft feasibility mechanism for network congestion. When the available generation dispatch, storage flexibility, and P2P reallocation are insufficient to keep branch currents within their thermal limits, the model may reduce the active consumption at congested nodes rather than returning an infeasible solution. The associated cost $\hat{\lambda}^{DR}$ is set to a value high enough to ensure that load reduction is only activated as a last resort. It is important to note that this demand response term is included in the formulation when distribution network constraints are explicitly modeled via the RBFM, as it provides a soft-feasibility mechanism that prevents infeasibility under congested conditions. When network constraints are handled through alternative approaches, such as the sensitivity matrix method described in Subsection 4.1.3, this term is omitted, and the physical balance reduces to its original form.

Similarly, the generation curtailment term $E_{n,t}^{GC} \geq 0$ provides a corrective action on the generation side. While demand response reduces consumption during periods of network congestion, generation curtailment reduces the injection of non-dispatchable renewable generation when an excess of local production would otherwise provoke overvoltage or excessive reverse power flows. The associated penalty $\hat{\lambda}^{GC}$ is set to a positive value that ensures generation curtailment remains a last-resort corrective action. Consequently, since selling surplus energy reduces the community objective while curtailment increases it, the optimization always prefers exporting available generation, resorting to curtailment only when network constraints prevent further export. Although this mechanism is included to ensure the generality of the formulation, it was not required in any of the scenarios considered in this work, since none of the studied networks experienced overvoltage or reverse-flow violations.

3.4.1.2 Community Energy Balance Constraints

The internal operation of the REC is managed by a set of energy-balance constraints that link purchases, sales, self-consumption, and metered energy for each community member at every time interval [5].

3.4.1.2.1 Internal P2P balance

$$\sum_{n} E_{n,t}^{PUR} - \sum_{n} E_{n,t}^{SALE} = 0, \qquad \forall t \in T \tag{3.2}$$

where $E_{n,t}^{PUR}$ and $E_{n,t}^{SALE}$ denote the energy purchased and sold within the REC by member n at time t, respectively.

This constraint ensures that the total internal energy purchases and sales within the REC are balanced, enforcing a constant internal consistency of the P2P market [5].

3.4.1.2.2 Metered energy from economic transactions

$$\begin{aligned} E_{n,t}^{CMET} &= E_{n,t}^{SUP,retail} + E_{n,t}^{SUP,market} - E_{n,t}^{SUR,retail} - E_{n,t}^{SUR,market} \\ &+ E_{n,t}^{PUR} - E_{n,t}^{SALE}, \qquad \forall n \in N,\ t \in T \end{aligned} \tag{3.3}$$

where $E_{n,t}^{CMET}$ is the net metered energy of member n at time t, resulting from all external and internal energy transactions. Purchases made from the retailer or from the market increase the metered consumption, while sales decrease it. Simultaneously, local buying and selling also affect the metered energy level [5].

3.4.1.2.3 Metered energy from physical behind-the-meter quantities

$$\begin{aligned} E_{n,t}^{CMET} &= \hat{E}_{n,t}^{C} - E_{n,t}^{DR} - \left(\hat{E}_{n,t}^{G} - E_{n,t}^{GC} + E_{n,t}^{G,CHP}\right) + \sum_{s \in S} \left(E_{n,s,t}^{B,C} - E_{n,s,t}^{B,D}\right) \\ &+ \sum_{ev \in EV} \left(E_{n,ev,t}^{EV,Charge} - E_{n,ev,t}^{EV,Discharge}\right), \qquad \forall n \in N,\ t \in T \end{aligned} \tag{3.4}$$

where $\hat{E}_{n,t}^{C}$ represents the consumption of member n at time t, $\hat{E}_{n,t}^{G}$ is the forecasted non-dispatchable renewable generation (PV and wind), $E_{n,t}^{G,CHP}$ is the dispatchable CHP generation, $E_{n,s,t}^{B,C}$ and $E_{n,s,t}^{B,D}$ are the charged and discharged energy of battery s, and $E_{n,ev,t}^{EV,Charge}$ and $E_{n,ev,t}^{EV,Discharge}$ are the charging and discharging energy of the EV ev.

Essentially, constraint 3.4 links the physical energy usage to the economic energy measured at the metering point. The term $E_{n,t}^{DR}$ reduces the net active demand at node n, directly decreasing the power injection into the network at that bus and consequently moderating the current magnitude in upstream branches. It is bounded above by the total consumption of member n at each time step. In the absence of storage systems or EVs, the corresponding summation terms are disregarded [5].

As with demand response, the generation curtailment variable $E_{n,t}^{GC}$ is bounded by the available renewable generation at each node and time period:

$$0 \le E_{n,t}^{GC} \le \hat{E}_{n,t}^{G}, \qquad \forall n \in N,\ t \in T \tag{3.5}$$

ensuring that the curtailed generation never exceeds the forecasted non-dispatchable renewable generation $\hat{E}^{G}_{n,t}$ at member n.

3.4.1.2.4 Contracted power limit at the metering point

$$-P^{EXTRA}_{n,t} - \hat{P}^{CPE,max}_{n} \leq \frac{E^{CMET}_{n,t}}{\Delta t} \leq \hat{P}^{CPE,max}_{n} + P^{EXTRA}_{n,t}, \qquad \forall n \in N,\ t \in T \tag{3.6}$$

where $\hat{P}^{CPE,max}_{n}$ is the contracted power limit and Δt is the duration of each time interval.

As expressed in constraint 3.6, the average power at the metering point cannot exceed the contracted limit. Any violation of the contracted power limit is captured by $P^{EXTRA}_{n,t}$ and penalized in the objective function, ensuring feasibility in contractual conditions [5].

3.4.1.2.5 Mutual exclusivity of importing and exporting

$$E^{SUP,retail}_{n,t} + E^{SUP,market}_{n,t} \leq \hat{M}\, \delta^{SUP}_{n,t}, \qquad \forall n \in N,\ t \in T \tag{3.7}$$

$$E^{SUR,retail}_{n,t} + E^{SUR,market}_{n,t} \leq \hat{M}\,(1 - \delta^{SUP}_{n,t}), \qquad \forall n \in N,\ t \in T \tag{3.8}$$

where $\delta^{SUP}_{n,t} \in \{0,1\}$ is a binary variable that enforces that member n cannot simultaneously import and export energy at time t, and $\hat{M}$ is a sufficiently large constant [5].

3.4.1.2.6 No-worse-off constraint

$$\begin{aligned}\sum_{t \in T} \Big(& E^{SUP,retail}_{n,t}\, \hat{\lambda}^{buy}_{n,t} - E^{SUR,retail}_{n,t}\, \hat{\lambda}^{sell}_{n,t} + E^{SUP,market}_{n,t}\, \hat{\lambda}^{marketbuy}_{t} \\ & - E^{SUR,market}_{n,t}\, \hat{\lambda}^{marketsell}_{t} + E^{SLC}_{n,t}\, \hat{\lambda}^{grid}_{t} + P^{EXTRA}_{n,t}\, \hat{\lambda}^{EXTRA} + E^{DR}_{n,t}\, \hat{\lambda}^{DR} + E^{GC}_{n,t}\, \hat{\lambda}^{GC} \\ & + (E^{PUR}_{n,t} - E^{SALE}_{n,t})\, \hat{\lambda}^{p2p}_{t} \Big) \leq \hat{C}^{ind}_{n} + \Delta Y_n, \qquad \forall n \in N\end{aligned} \tag{3.9}$$

where $\hat{\lambda}^{p2p}_{t}$ is the local energy price at time t, while $\hat{C}^{ind}_{n}$ represents the Stage 1 individual energy cost of member n.

This constraint enforces the fairness principle of the original OSTEC formulation by discouraging any community member from incurring a higher operating cost than in its individual Stage 1 solution [5]. Although originally a hard constraint, it is implemented here as a soft constraint by introducing the non-negative slack variable ΔY_n, which absorbs any violation that becomes unavoidable once the network constraints are enforced. Since ΔY_n is penalized in the objective function (Equation 3.1), the optimization ensures that such deviations occur only when strictly necessary. In this way, ΔY_n also provides a direct measure of the economic penalty that the network constraints impose on each member.

3.4.1.2.7 CHP generation limits

$$0 \leq E_{n,t}^{G,CHP} \leq \hat{P}_n^{CHP,max} \Delta t, \qquad \forall n \in N^{CHP},\ t \in T \tag{3.10}$$

where $\hat{P}_n^{CHP,max}$ is the maximum electrical generation capacity of the CHP unit associated with member n.

Unlike renewable generation, which is treated as a fixed forecast profile, CHP generation is modeled as a controllable decision variable, allowing the MILP optimization problem to schedule CHP operation based on the economic conditions and network operating requirements of the REC.

3.4.1.3 Storage and EV dynamics

The behavior of any batteries and EVs considered within this work follows the Stage 2 formulation of OSTEC [5]. For each member n, battery s and time t, the BESS energy content is updated as:

$$E_{n,s,t}^{B} = E_{n,s,t-1}^{B} + (E_{n,s,t}^{B,C}\, \hat{\eta}_{n,s}^{B,C} - \frac{E_{n,s,t}^{B,D}}{\hat{\eta}_{n,s}^{B,D}}), \qquad \forall n \in N,\ s \in S,\ t \in T \tag{3.11}$$

where $E_{n,s,t}^{B}$ is the stored energy in battery s of member n at time t, and $\hat{\eta}_{n,s}^{B,C}$ and $\hat{\eta}_{n,s}^{B,D}$ are the charging and discharging efficiencies of battery s of member n.

Equation 3.11 models the inter-temporal energy evolution of each battery, accounting for charging and discharging efficiencies, while respecting the following State of Charge (SoC) and power limits:

$$\widehat{SoC}_{n,s}^{B,min} \leq SoC_{n,s,t}^{B} = \frac{E_{n,s,t}^{B}}{\hat{E}_{n,s}^{B,N}} \cdot 100 \leq \widehat{SoC}_{n,s}^{B,max}, \qquad \forall n \in N,\ s \in S,\ t \in T \tag{3.12}$$

where $SoC_{n,s,t}^{B}$ is the SoC of battery s of member n at time t, expressed in percentage, $\hat{E}_{n,s}^{B,N}$ is the nominal energy capacity of the battery, and $\widehat{SoC}_{n,s}^{B,min}$ and $\widehat{SoC}_{n,s}^{B,max}$ are the minimum and maximum allowable SoC limits, respectively.

$$\frac{E_{n,s,t}^{B,C}}{\Delta t} \leq \hat{P}_{n,s}^{B,max}\, \delta_{n,s,t}^{B,C}, \qquad \frac{E_{n,s,t}^{B,D}}{\Delta t} \leq \hat{P}_{n,s}^{B,max}\, (1 - \delta_{n,s,t}^{B,C}), \qquad \forall n \in N,\ s \in S,\ t \in T \tag{3.13}$$

where $\hat{P}_{n,s}^{B,max}$ is the maximum charging/discharging power of battery s of member n, and $\delta_{n,s,t}^{B,C} \in \{0,1\}$ is a binary variable that enforces mutually exclusive charging and discharging operations.

These constraints ensure that battery operation remains within acceptable SoC bounds, while charging and discharging power levels are limited by each battery's rated capacity and are mutually exclusive, preventing simultaneous charge and discharge.

Subsequently, for each ev connected at member n, the stored energy evolves according to:

$$E^{EV,Stored}_{n,ev,t} = E^{EV,Stored}_{n,ev,t-1} + \hat{\eta}^{EV,C}_{n,ev}\, E^{EV,Charge}_{n,ev,t} - \frac{1}{\hat{\eta}^{EV,D}_{n,ev}}\, E^{EV,Discharge}_{n,ev,t} - \hat{E}^{Trip}_{n,ev,t}, \qquad \forall n \in N,\ ev \in EV,\ t \in T \tag{3.14}$$

where $E^{EV,Stored}_{n,ev,t}$ is the energy stored in the battery of vehicle ev at member n at the end of period t, $\hat{\eta}^{EV,C}_{n,ev}$ and $\hat{\eta}^{EV,D}_{n,ev}$ are their charging and discharging efficiencies, and $\hat{E}^{Trip}_{n,ev,t}$ represents the energy consumed due to driving during period t.

This equation describes the evolution of the EV battery energy, accounting for charging, discharging, and driving energy consumption, respecting the following technical limits:

$$E^{EV,Stored}_{n,ev,t} \le \hat{E}^{EV,BatCapacity}_{n,ev}, \qquad \forall n \in N,\ ev \in EV,\ t \in T \tag{3.15}$$

$$E^{EV,Stored}_{n,ev,t} \ge \hat{E}^{EV,MinCharge}_{n,ev}, \qquad \forall n \in N,\ ev \in EV,\ t \in T \tag{3.16}$$

$$\frac{1}{\hat{\eta}^{EV,D}_{n,ev}} E^{EV,Discharge}_{n,ev,t} \le \hat{P}^{EV,DischargeLimit}_{n,ev}\, \hat{X}^{EV}_{n,ev,t}\, \Delta t, \qquad \forall n \in N,\ ev \in EV,\ t \in T,\ \hat{X}^{EV}_{n,ev,t} \in \{0,1\} \tag{3.17}$$

$$\hat{\eta}^{EV,C}_{n,ev} E^{EV,Charge}_{n,ev,t} \le \hat{P}^{EV,ChargeLimit}_{n,ev}\, \hat{X}^{EV}_{n,ev,t}\, \Delta t, \qquad \forall n \in N,\ ev \in EV,\ t \in T,\ \hat{X}^{EV}_{n,ev,t} \in \{0,1\} \tag{3.18}$$

where $\hat{E}^{EV,BatCapacity}_{n,ev}$ is the battery capacity of the EV, $\hat{E}^{EV,MinCharge}_{n,ev}$ is the minimum required stored energy, $\hat{P}^{EV,ChargeLimit}_{n,ev}$ and $\hat{P}^{EV,DischargeLimit}_{n,ev}$ are the maximum charging and discharging power limits, and $\hat{X}^{EV}_{n,ev,t} \in \{0,1\}$ is a binary parameter indicating whether the vehicle is connected at time t.

These constraints define the boundaries of both energy and power during EV operation, ensuring that charging and discharging occur only when the vehicle is connected.

In summary, the portrayed relations ensure that all storage and EV schedules are physically feasible and remain consistent with the original OSTEC formulation [5]. The formulation presented in this subsection constitutes the economic layer of the proposed optimization model and provides the variables that are subsequently coupled with the electrical network formulation introduced in the next subsection.

3.4.2 Network-Constrained Operation: RBFM

The OSTEC Stage 2 formulation models the economic interactions within the REC, but it does not explicitly represent the physical behavior of the underlying distribution network. To ensure that the resulting operating schedules are technically feasible, the proposed optimization framework extends the original formulation with a network model based on the RBFM.

The RBFM formulation adopted in this dissertation builds upon the network-constrained model proposed by [12]. It represents active and reactive power flows, squared nodal voltage magnitudes, and squared branch current magnitudes through a combination of linear constraints and SOC relations. Since the implementation must remain compatible with the MILP structure of OSTEC Stage 2, the nonlinear SOC relation is incorporated via an iterative linear outer-approximation procedure using supporting hyperplanes.

The use of the network-constrained formulation requires two small regularization terms to be added to the objective function. The first is associated with the relaxed current-power relation, while the second eliminates redundant bilateral trading patterns that may arise from equivalent economic solutions.

$$\min C_{\text{REC}} + \rho \sum_{(n,m)\in\mathscr{E}} \sum_{t\in T} l_{n,m,t} + \varepsilon \sum_{n\in N} \sum_{\substack{m\in N \\ m\neq n}} \sum_{t\in T} E^{PUR}_{n,m,t} \tag{3.19}$$

where $\rho = 10^{-3}$ and $\varepsilon = 10^{-4}$ are fixed penalty coefficients, C_{REC} denotes the economic objective defined in Equation 3.1, and $l_{n,m,t}$ represents the squared current magnitude of branch (n,m), as introduced before.

The current regularization term is introduced because the relaxed current-power relation imposes $l_{n,m,t}$ as a lower-bounded variable, as detailed in Sub-subsection 3.4.2.2. Without this term, the optimization could select squared current values larger than the physically required minimum without affecting the economic objective or violating the relaxed constraints.

By penalizing the sum of squared branch currents, the regularization term encourages each $l_{n,m,t}$ to approach its minimum admissible value, thereby improving the physical consistency of the network solution. Since active power losses in branch (n,m) are proportional to $R_{n,m} l_{n,m,t}$, penalizing $l_{n,m,t}$ promotes lower branch currents and indirectly discourages high-loss operating points. Moreover, because ρ is several orders of magnitude smaller than the tariff parameters used in the economic objective, this term has a negligible impact on the REC cost minimization while ensuring physically consistent current values.

The second regularization term acts on the gross bilateral purchase volumes $E^{PUR}_{n,m,t}$. Due to the local P2P trading price $\hat{\lambda}^{p2p}$ being fixed and bilateral transactions canceling out at the community level (as seen in Equation 3.2), different trading patterns may lead to the same exact community cost. Some of these equivalent solutions include simultaneous purchases and sales between the same members, which would artificially increase the gross traded volume without producing any physical or economic benefit. Therefore, penalizing the total bilateral purchase volume with a coefficient ε several orders of magnitude smaller than $\hat{\lambda}^{p2p}$ allows the optimization to naturally select the minimum-volume solution among these equivalent optima. Consequently, redundant re-trading is eliminated while the economic results remain unchanged.

It is worth noting that, while the aggregated purchase variable $E^{PUR}_{n,t}$ is used throughout the energy-balance constraints, this regularization term is formulated in terms of the underlying pair-wise variable $E_{n,m,t}^{PUR}$, which represents the energy purchased by member n specifically from member m. Both representations are related by:

$$E_{n,t}^{PUR} = \sum_{m \neq n} E_{n,m,t}^{PUR} \tag{3.20}$$

reflecting the bilateral nature of the OSTEC Stage 2 formulation.

Subsequently, the following constraints define the network-constrained component of the proposed optimization model and its coupling with the community-level energy scheduling variables.

3.4.2.1 Slack Bus Representation

The slack bus represents the point of common coupling between the distribution network and the upstream grid. It provides the network's voltage reference and balances the active and reactive power exchanged with the external electrical system. Accordingly, the active and reactive power exchanged through the slack bus are treated as optimization variables:

$$P_{slack,t}^{inj} = P_t^{slack}, \qquad \forall t \in T \tag{3.21}$$

$$Q_{slack,t}^{inj} = Q_t^{slack}, \qquad \forall t \in T \tag{3.22}$$

where P_t^{slack} and Q_t^{slack} represent the active and reactive power exchanged between the distribution network and the upstream grid at time period t.

This formulation allows the distribution network to exchange active and reactive power with the upstream grid according to the operating conditions determined by the REC optimization, thereby ensuring the overall power balance of the network.

In both the preliminary and main case studies, the slack-bus voltage magnitude is fixed at its nominal value throughout the optimization horizon:

$$v_{\text{slack},t} = 1.0 \text{ p.u.}^2, \qquad \forall t \in T \tag{3.23}$$

providing a well-defined voltage reference for the radial network, from which voltage drops along downstream branches are computed through Equation 3.31.

3.4.2.2 Branch Flow Power Balance Constraints

The BFM ensures conservation of active and reactive power at every network node, linking the injections derived from the community optimization with the flows circulating in the distribution network.

3.4.2.2.1 Active power balance

The net active power injection at node n is obtained from the community-level metered energy as:

$$P_{n,t}^{inj} = -\frac{E_{n,t}^{CMET}}{\Delta t}, \qquad \forall n \in N,\ t \in T$$

where $P_{n,t}^{inj}$ is the net active power injection at node n at time t. $E_{n,t}^{CMET}$ is positive for imports (negative injections) and negative for exports (positive injections). Notably, $E_{n,t}^{CMET}$ is obtained from the previously defined community energy-balance constraints, thereby incorporating external transactions, internal P2P exchanges, storage operations, and EV scheduling. For junction buses without an associated member, the injection is zero, i.e., $P_{n,t}^{inj} = 0,\ \forall n \in \mathscr{N} \setminus N$.

Therefore, the active power balance at each node is then defined as:

$$-\frac{E_{n,t}^{CMET}}{\Delta t} = \sum_{m:(n,m)\in\mathscr{E}} P_{n,m,t} - \sum_{m:(m,n)\in\mathscr{E}} (P_{m,n,t} - R_{m,n}\, l_{m,n,t}) \qquad \forall n \in \mathscr{N},\ t \in T \tag{3.24}$$

where $P_{n,m,t}$ is the active power flow in line (n,m), $R_{n,m}$ is the line resistance, and $l_{m,n,t}$ is the squared current magnitude.

The left-hand side represents the net active injection derived from the OSTEC energy schedule. The right-hand side corresponds to the net power flowing through the connected branches plus ohmic losses $R_{m,n} l_{m,n,t}$.

3.4.2.2.2 Reactive power balance

Reactive injections follow the same structure, replacing resistances with reactances:

$$Q_{n,t}^{inj} = \sum_{m:(n,m)\in\mathscr{E}} Q_{n,m,t} - \sum_{m:(m,n)\in\mathscr{E}} (Q_{m,n,t} - X_{m,n}\, l_{m,n,t}) \qquad \forall n \in \mathscr{N},\ t \in T \tag{3.25}$$

where $Q_{n,t}^{inj}$ is the net reactive power injection at node n at time t, $Q_{n,m,t}$ is the reactive power flow in line (n,m), and $X_{m,n}$ is the line reactance.

Additionally, the net reactive power injection at each node is modeled as the combination of reactive generation and consumption components associated with the corresponding REC member:

$$Q_{n,t}^{inj} = (Q_{n,t}^{G,PV} + Q_{n,t}^{G,W} + Q_{n,t}^{G,CHP}) - Q_{n,t}^{C}, \qquad \forall n \in N,\ t \in T \tag{3.26}$$

where $Q_{n,t}^{G,PV}$, $Q_{n,t}^{G,W}$, and $Q_{n,t}^{G,CHP}$ represent the reactive power generated by PV, wind, and CHP units, respectively, while $Q_{n,t}^{C}$ denotes the reactive power consumption at node n and time t. For junction buses without an associated member, the injection is zero, i.e., $Q_{n,t}^{inj} = 0,\ \forall n \in \mathscr{N} \setminus N$.

Although the original OSTEC formulation does not schedule reactive power, the implemented network-constrained model allows distributed generation resources to provide reactive power support.

As previously noted and as seen in Equation 3.26, reactive power capability is modeled separately for each generation technology, namely photovoltaic, wind, and CHP units.

Subsequently, the reactive power of each generation technology is individually constrained according to the following relations:

$$0 \leq Q^{G,PV}_{n,t} \leq 0.3\,\frac{\hat{E}^{G,PV}_{n,t}}{\Delta t}, \qquad \forall n \in N^{PV},\, t \in T \tag{3.27}$$

$$0 \leq Q^{G,W}_{n,t} \leq 0.3\,\frac{\hat{E}^{G,W}_{n,t}}{\Delta t}, \qquad \forall n \in N^{W},\, t \in T \tag{3.28}$$

$$0 \leq Q^{G,CHP}_{n,t} \leq 0.3\,\frac{E^{G,CHP}_{n,t}}{\Delta t}, \qquad \forall n \in N^{CHP},\, t \in T \tag{3.29}$$

These constraints enforce independent reactive power capability limits for each distributed generation technology, approximating inverter and generator operating limits through a fixed proportional relation between active and reactive power. Reactive power generation is restricted to positive values only, corresponding to capacitive support. Although modern inverters are generally capable of both injecting and absorbing reactive power, this simplification is adopted here for consistency with the dataset used in the case studies and has no material impact on the results, since voltage limits remain non-binding throughout all simulated scenarios.

Lastly, the reactive power consumption at each node is assumed to follow a constant inductive power factor relationship with the corresponding active consumption:

$$Q^{C}_{n,t} = P^{C}_{n,t} \times \tan(\phi), \qquad \forall n \in N,\, t \in T \tag{3.30}$$

where $\tan(\phi) = 0.3$. This value was selected as a representative approximation of the inductive load behavior commonly observed in distribution networks, corresponding to a power factor of approximately 0.96.

3.4.2.2.3 Voltage drop

$$v_{n,t} - v_{m,t} = 2\big(R_{n,m}P_{n,m,t} + X_{n,m}Q_{n,m,t}\big) - (R^2_{n,m} + X^2_{n,m})\, l_{n,m,t}, \qquad \forall (n,m) \in \mathscr{E},\, t \in T \tag{3.31}$$

where $v_{n,t}$ and $v_{m,t}$ are the squared voltage magnitudes at nodes n and m, respectively.

This constraint describes how voltage magnitudes propagate through a radial distribution line. The first term represents the voltage drop caused by active and reactive power flows, while the last term accounts for the quadratic effect of current magnitude.

3.4.2.2.4 Linear Outer-Approximation of the SOC Constraint

The standard SOCP relaxation of the BFM is given by:

$$P_{n,m,t}^2 + Q_{n,m,t}^2 \leq v_{n,t} \cdot l_{n,m,t}, \quad \forall (n,m) \in \mathscr{E},\ t \in T \tag{3.32}$$

This constraint can be equivalently expressed as a rotated SOC:

$$\left\| \begin{pmatrix} 2P_{n,m,t} \\ 2Q_{n,m,t} \\ v_{n,t} - l_{n,m,t} \end{pmatrix} \right\| \leq v_{n,t} + l_{n,m,t} \tag{3.33}$$

Before introducing the iterative outer-approximation procedure, an initial linear relaxation is imposed on the active and reactive branch flows:

$$-S_{n,m}^{\max} \leq P_{n,m,t} \leq S_{n,m}^{\max}, \qquad \forall (n,m) \in \mathscr{E},\ t \in T \tag{3.34}$$

$$-S_{n,m}^{\max} \leq Q_{n,m,t} \leq S_{n,m}^{\max}, \qquad \forall (n,m) \in \mathscr{E},\ t \in T \tag{3.35}$$

where $S_{n,m}^{\max}$ represents the apparent power capacity of branch (n,m).

These constraints define an initial feasible operating region for the MILP formulation, which is then progressively refined through the iterative SOC approximation procedure using linear supporting hyperplanes (cuts).

At a given iteration, let $(\bar{P}_{n,m,t}, \bar{Q}_{n,m,t}, \bar{v}_{n,t}, \bar{l}_{n,m,t})$ denote a solution that violates the SOC constraint. The corresponding normal vector is defined as:

$$\mathbf{u}_0 = \begin{pmatrix} 2\bar{P}_{n,m,t} \\ 2\bar{Q}_{n,m,t} \\ \bar{v}_{n,t} - \bar{l}_{n,m,t} \end{pmatrix} \tag{3.36}$$

with norm:

$$\|\mathbf{u}_0\| = \sqrt{(2\bar{P}_{n,m,t})^2 + (2\bar{Q}_{n,m,t})^2 + (\bar{v}_{n,t} - \bar{l}_{n,m,t})^2} \tag{3.37}$$

The linear cut added to the MILP is then given by:

$$(2\bar{P}_{n,m,t})(2P_{n,m,t}) + (2\bar{Q}_{n,m,t})(2Q_{n,m,t}) + (\bar{v}_{n,t} - \bar{l}_{n,m,t})(v_{n,t} - l_{n,m,t}) \leq \|\mathbf{u}_0\| \cdot (v_{n,t} + l_{n,m,t}) \tag{3.38}$$

This procedure is implemented iteratively. At each iteration, the MILP is solved, and the solution is checked for violations of the SOC constraint, i.e., cases where:

$$P_{n,m,t}^2 + Q_{n,m,t}^2 - v_{n,t} \cdot l_{n,m,t} > \varepsilon^{SOC} \tag{3.39}$$

where $\varepsilon^{SOC} > 0$ is a small numerical tolerance used to detect violations of the SOC constraint. In this work, a value of $\varepsilon^{SOC} = 5 \times 10^{-7}$ is adopted, consistent with the solver tolerance.

For each violating point, a new cut is generated and added to the model. The process is repeated until no further violations are detected or a maximum number of iterations is reached.

In practice, when the strict tolerance cannot be attained within a reasonable number of iterations, the procedure may be terminated once the residual violation becomes physically negligible, as further discussed in the main case study of Chapter 4.

This approach allows embedding convex network constraints within an MILP framework without requiring native SOCP solvers.

3.4.2.2.5 Operating limits

$$(V_n^{\min})^2 \leq v_{n,t} \leq (V_n^{\max})^2, \qquad \forall n \in \mathscr{N},\ t \in T, \tag{3.40}$$

$$0 \leq l_{n,m,t} \leq (I_{n,m}^{\max})^2, \qquad \forall (n,m) \in \mathscr{E},\ t \in T. \tag{3.41}$$

where $V_n^{\min}$ and $V_n^{\max}$ are the minimum and maximum allowable voltage magnitudes at node n, and $I_{n,m}^{\max}$ is the maximum admissible current magnitude in line (n,m).

These constraints impose the standard operational limits of distribution networks. Voltages are restricted to remain within acceptable quality-of-service bounds, while branch currents must respect thermal limits to avoid overloading, ensuring that the optimization produces physically secure operating points.

Although the RBFM incorporates the network representation directly within the community optimization, other approaches can also be used to ensure network feasibility. A common alternative is to separate the economic and network analyses into two sequential steps. First, the community schedule is obtained by solving an economic optimization problem without explicitly accounting for the network. Subsequently, the resulting dispatch is evaluated from an electrical perspective and, if necessary, adjusted with linear sensitivity-based corrections in order to eliminate potential violations.

This decoupled approach serves as a benchmark for comparison in the preliminary case study (Subsection 4.1.3), where it is contrasted with the integrated RBFM approach proposed in this work.

Chapter 4

Case Study

In this chapter, the simulation studies conducted to evaluate the performance of the proposed network-constrained REC optimization framework are presented, with a particular focus on the impact of explicitly considering distribution network constraints.

To assess both the reliability of the implementation and its relevance, two complementary case studies were therefore conducted. The first study focuses on validation, using a small and controlled test system to verify the physical and numerical consistency of the proposed approach. The second study represents the main contribution of this dissertation, applying the validated framework to a more realistic distribution network to quantify the impact of network constraints on community operations.

Together, these two studies cover the validation and application objectives defined in Chapter 1, moving from a validation-oriented environment to a comprehensive analysis of real-world applicability.

Notably, all input datasets and complete simulation results for both case studies and different scenarios, including load, generation, tariffs, BESS, EV, and network parameters, as well as the full hourly economic and electrical outputs, are openly available in the Mendeley Data repository [35] associated with this dissertation. Throughout this chapter, only the most relevant aggregated results are reported.

4.1 Preliminary Case Study: Model Validation

This section presents a preliminary study based on a 10-bus radial distribution network. The main objectives of this case study are to validate the correct implementation of the proposed framework and to assess the numerical behavior of the linear outer-approximation of the SOC constraints.

Rather than providing general conclusions regarding REC operations, this study focuses on three key aspects:

- the tightness of the SOC relaxation;
- the physical consistency of the network response under increasing stress conditions;

- the correct interaction between the individual optimization (OSTEC's Stage 1) and the collective optimization (OSTEC's Stage 2).

The insights obtained in this section denote the foundation for the more comprehensive analysis developed in Section 4.2.

4.1.1 Test Network Description

As described before, the distribution network adopted in this initial study is a 10-bus radial feeder, the same as the test system proposed in [12], representing a single energy community composed of consumers and prosumers. This system, illustrated in Figure 4.1, was originally developed to evaluate distributed network-constrained P2P CBMs and is therefore well suited to validating the proposed framework.

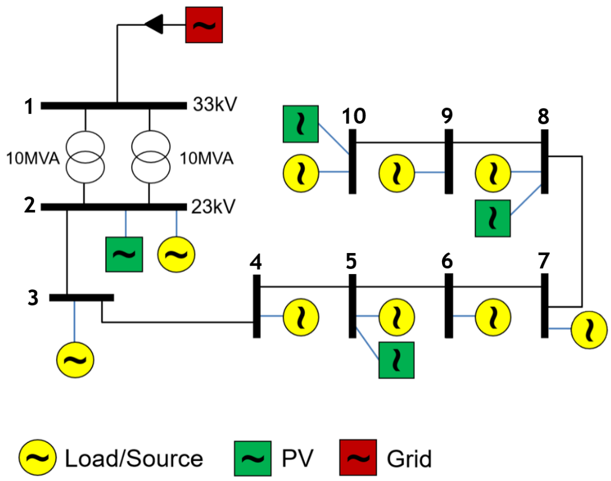

Figure 4.1: Electric diagram of the 10-bus MV radial distribution system, presented in [12].

The slack bus, represented in this case by Bus 1, represents the tie-up with an external supplier [12]. Community agents are located at the remaining buses, where they can either import energy from or export energy to the main grid. The corresponding branch parameters are summarized in Table 4.1.

Table 4.1: Branch parameters of the 10-bus test network [12].

Branch	**R (Ω)**	**X (Ω)**	$I_{\mathbf{max}}$ **(A)**
1–2	0.002331	0.007802	150
2–3	0.000265	0.011439	150
3–4	0.014108	0.022779	150
4–5	0.013202	0.011501	150
5–6	0.037488	0.032658	150
6–7	0.017113	0.014907	150
7–8	0.038851	0.022004	150
8–9	0.090648	0.051342	150
9–10	0.101009	0.057210	150

Even though the network illustrated in Figure 4.1 presents the connection to a higher-voltage network through transformation stages, the implementation adopted in this work follows the per-unit system defined in the available dataset and code of [12], where a base voltage of 23 kV is consistently used across all buses. The system base power is defined as $S_{base} = 10$ MVA, and voltage limits are set to $V_{min} = 0.95$ p.u. and $V_{max} = 1.05$ p.u. for all buses, meaning that their voltages are allowed to vary within $\pm 5\%$ of the nominal value.

Each non-slack node is associated with a deterministic consumption profile over a 24-hour horizon at hourly resolution. Additionally, a subset of nodes (nodes 2, 5, 8, and 10) is equipped with behind-the-meter PV generation [12].

In order to maintain consistency with the data considered in [12], the reactive power consumption at each node for this specific case was defined as:

$$Q^C_{n,t} = 0.2\, P^C_{n,t} \tag{4.1}$$

representing, therefore, a constant inductive power factor. In this preliminary network, the reactive injection at each node corresponds directly to this reactive consumption, since no controllable reactive generation is considered. This contrasts with the main case study, where distributed generation (PV, wind, and CHP) is allowed to provide controllable reactive support, following the technology-specific reactive modeling formulated in Subsection 3.4.2.

Given the characteristics of this illustrative network, the proposed framework was validated using a set of complementary approaches. First, the proposed BFM-based optimization model, coupled with the OSTEC framework, was executed, providing both the community's economic operation and the resulting network state. The obtained physical network solutions were then compared with two independent references: a nonlinear AC power flow, used as an exact physical benchmark, and the PowerWorld Simulator [36], in which the same network was reproduced to confirm the results in an established commercial environment. Finally, the integrated RBFM approach was compared with an alternative sensitivity-based method, in which network feasibility is enforced as a separate correction step rather than as part of the optimization. Together, these approaches assess both the physical accuracy of the network representation and the behavior of the proposed formulation relative to a decoupled alternative.

4.1.2 BFM-based Simulation (OSTEC + RBFM)

The first validation approach consists of executing the proposed optimization framework, which combines the OSTEC methodology with the RBFM. This simulation serves as the core implementation of the dissertation, enabling assessment of both the community's economic coordination and the physical consistency of the network-constrained solution.

The analysis is structured into four main components. Primarily, the implementation framework is described, detailing the integration of Stage 1 and Stage 2. Then, the tightness of the SOC relaxation is evaluated to verify the accuracy of the linear approximation. Afterward, a stress test is performed to observe how the system responds as demand increases, helping to pinpoint the network's operational limits. Finally, the resulting network state is validated against external power flow tools to confirm its physical accuracy.

4.1.2.1 Implementation Framework

The optimization framework was implemented in Python using the PuLP modeling library [37], with Gurobi [38] as the main MILP solver.

The solution procedure follows the two-stage structure introduced in Chapter 3:

- As briefly mentioned before, in **Stage 1**, each community member solves its standalone optimization problem, resulting in the individual cost benchmarks $\hat{C}_n^{ind}$. As in the main case study, Stage 1 is executed for all community members prior to the collective optimization, and the resulting benchmarks are used to enforce the soft no-worse-off constraint (Equation 3.9) in Stage 2.

- In **Stage 2**, the community-level problem is solved by combining its OSTEC economic formulation (Subsection 3.4.1) with the network constraints described by the RBFM (Subsection 3.4.2).

The integration between both stages is enforced through the soft no-worse-off constraint (Equation 3.9), which discourages any participant from being penalized by the collective solution and, when a penalty becomes unavoidable, quantifies it through the slack variable ΔY_n.

Moreover, another crucial feature of the implementation is the incorporation of the SOC constraint associated with the RBFM. As described in Subsection 3.4.2, this nonlinear constraint is handled through a linear outer-approximation approach based on iteratively generated supporting hyperplanes.

In practice, the MILP is solved iteratively, and the solution is checked for violations of the SOC constraint. Whenever violations are detected, additional linear cuts are introduced to refine the approximation. This process is repeated until no further violations are identified or a maximum number of iterations is reached.

4.1.2.2 Validation of Relaxation Tightness

The accuracy of the SOC relaxation was evaluated by analyzing the extent to which the obtained solution satisfies the corresponding equality condition:

$$P_{n,m,t}^2 + Q_{n,m,t}^2 = v_{n,t} \cdot l_{n,m,t} \tag{4.2}$$

Notably, in the context of the adopted outer-approximation approach, this equality is not enforced explicitly but is expected to hold at optimality if the relaxation is tight.

For the base-case scenario, the algorithm converged after only 18 linear SOC cuts. The procedure was iterated until the maximum absolute SOC violation across all branches and time periods fell below the defined numerical tolerance of 5×10^{-7} p.u.^{2}, at which point convergence was declared. This corresponds to a relative violation on the order of 10^{-5}%, confirming that the linear outer-approximation reproduces the exact conic relation with negligible error.

Additionally, the consistency between the current variable and its physical definition was verified by comparing $l_{n,m,t}$ with $(P_{n,m,t}^2 + Q_{n,m,t}^2)/v_{n,t}$, yielding a maximum deviation on the order of 10^{-7}.

From a physical perspective, the tightness of the relaxation ensures that the computed branch currents are consistent with the corresponding active and reactive power flows, avoiding artificial distortions that could otherwise arise from a loose relaxation.

Essentially, these results confirm that the proposed linear outer-approximation approach achieves high accuracy, effectively recovering the behavior of the original SOC constraint within the MILP framework and ensuring physically consistent network solutions.

4.1.2.3 Stress Testing and Feasibility Boundary

Thereafter, to evaluate the model behavior under increasing system stress, due to a low percentage of network usage in its base case, a parametric analysis was conducted by scaling the active and reactive load profiles with a stress factor α, while maintaining PV generation unchanged. This asymmetric stress test reflects real-world scenarios where increasing demand is not matched by proportional growth in local generation, progressively pushing the network towards its operational limits.

The stress factor α was progressively increased in steps until infeasibility was reached. Coarser increments were initially used to identify the approximate feasibility boundary, after which finer adjustments were applied to determine more accurately the critical value at which the transition from feasible to infeasible operation occurs. The key results obtained for representative values of α are summarized in Table 4.2.

As the stress factor increases, the results show a physically consistent evolution of the system, with the upstream branch (1–2), which carries the aggregated power flow of the entire downstream

Table 4.2: Stress test results: branch 1–2 maximum loading and voltage profiles at selected stress levels.

Stress Factor (α)	Status	Branch 1–2 Loading (%)	Min. Voltage (p.u.)	Max. S (p.u.)
1.0 (Base Case)	Optimal	18.925	0.9997	0.1131
2.0	Optimal	38.261	0.9995	0.2286
3.0	Optimal	57.937	0.9992	0.3462
5.0	Optimal	97.300	0.9987	0.5814
⋮	⋮	⋮	⋮	⋮
5.137	Optimal	99.997	0.9986	0.5975
5.138	Infeasible	—	—	—

network, being consistently the most heavily loaded element. For this reason, only the loading of branch 1–2 is reported in Table 4.2, as it represents the critical constraint across all scenarios.

Additionally, as is expected in radial distribution networks, the voltage profiles decrease gradually as load increases. However, voltage limits remain non-binding throughout the feasible region, indicating that the system feasibility is driven by thermal constraints rather than voltage violations.

A sharp feasibility boundary is observed between $\alpha = 5.137$ and $\alpha = 5.138$, where the model transitions from feasible to infeasible. It should be noted that in this stress test, the demand response (load curtailment) mechanism was intentionally disabled to isolate the purely physical feasibility boundary of the network. The behavior of the system beyond this boundary, once corrective curtailment is enabled, is examined later in Subsection 4.1.3.

The maximum loading distribution across all branches for the near-limit case ($\alpha = 5.137$) and its comparison to the base case are illustrated in Figure 4.2, highlighting another characteristic behavior of radial networks, where upstream branches carry higher power flows due to load aggregation.

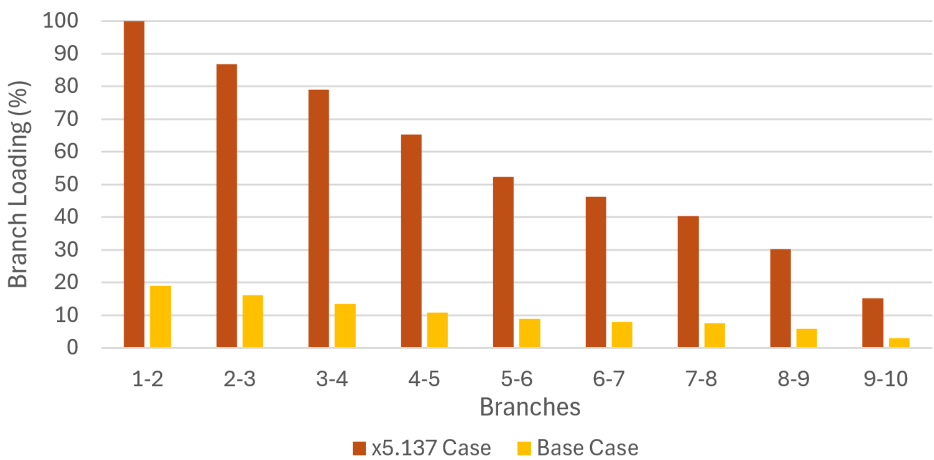

Figure 4.2: Branch maximum loading distribution for the base case and near-limit operating condition ($\alpha = 5.137$).

The comparison between the two operating conditions clearly shows how the branch loading evolves as the system becomes more stressed. Although the loading pattern remains unchanged, with the upstream branches consistently carrying the highest loading, their magnitude increases significantly. For instance, branch 1–2 rises from below 20% in the base case to nearly 100% with $\alpha = 5.137$, while the downstream branches, which carry only local power, remain comparatively lightly loaded even at the feasibility boundary. This confirms that the network limit is reached at the head of the feeder, where the aggregated demand of all downstream nodes converges.

Overall, the stress test confirms that the model preserves a physically coherent network response across the entire feasible range, from the lightly loaded base case to the feasibility boundary, thereby supporting the reliability of the formulation before its application to the main case study.

4.1.2.4 Physical Validation of the Network Solution

The previous analysis focused on the numerical behavior of the proposed framework, namely, the tightness of the SOC relaxation and the response of the network under increasing stress conditions. Although these results indicate that the model behaves consistently, they do not demonstrate that the network state obtained from the optimization accurately reflects the behavior of a real electrical network.

Therefore, to verify that the underlying physical representation of the network is correct, the network state obtained from the BFM was independently validated against two external power-flow tools: a nonlinear AC power-flow tool and the PowerWorld Simulator [36]. Unlike the proposed framework, these tools do not include any market mechanisms, DER scheduling decisions, or community-level optimization, being limited to solving only the electrical behavior of the network.

The validation procedure is the same in both cases. The active and reactive power injections corresponding to the community operating point are imposed as fixed inputs in the external tool, which then computes the resulting voltages and branch flows purely from the network physics. An agreement between these results and those of the BFM confirms that the physical network behavior incorporated in the proposed framework is correctly modeled.

4.1.2.4.1 AC Power Flow Validation

Rather than solving a full AC-OPF problem, the AC power flow model was used as a nonlinear benchmark, where the nodal active and reactive power injections obtained from the dataset were imposed, and the resulting voltage magnitudes, phase angles, and branch flows were computed. This approach allows a direct comparison between the physically accurate nonlinear solution and the approximation provided by the RBFM.

The AC power flow model was implemented in Python using the Pyomo optimization framework and solved with IPOPT. The formulation follows the standard nonlinear power flow Equations 2.1 and 2.2 introduced in Subsection 2.1.1, considering both active and reactive power balances at each node. The slack bus voltage was fixed at 1.0 p.u., while voltage magnitude limits were enforced for all remaining buses. The model was solved independently for each hour of the 24-hour horizon, allowing the extraction of time-dependent voltage profiles and branch loading conditions.

The comparison between the BFM-based results and the AC power flow solution reveals an almost perfect agreement, as illustrated in Figure 4.3 for two representative buses, where the BFM and AC power flow voltage profiles are visually indistinguishable. Across all buses and time periods, the maximum deviation in nodal voltage magnitudes was on the order of $10^{-5}\%$, while the deviation in branch current magnitudes was less than 0.1% of the thermal limit, with the largest relative differences occurring only on branches carrying negligible current. This near-exact correspondence is consistent with the theoretical exactness of the SOCP relaxation of the BFM on radial networks (Subsection 2.1.4): when the relaxation is tight, the recovered voltages and currents coincide with the true nonlinear AC solution.

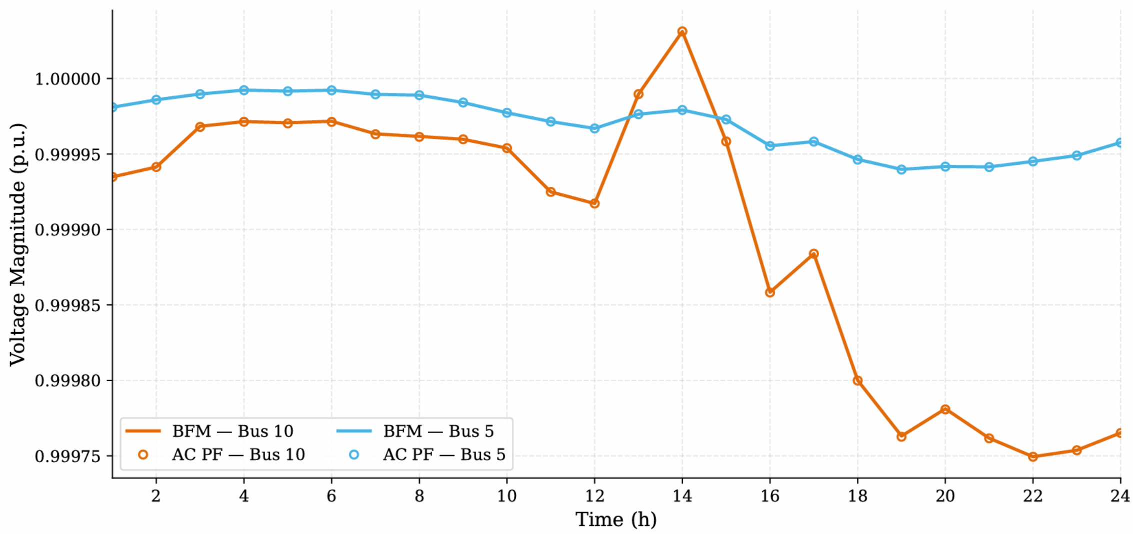

Figure 4.3: Comparison of nodal voltage magnitudes between the BFM-based model (solid lines) and the AC power flow solution (markers) for representative buses.

These results further confirm that the proposed RBFM-based formulation reproduces the network's physical behavior with the same fidelity as a nonlinear AC power flow while preserving the computational advantages of a linear formulation.

4.1.2.4.2 PowerWorld Validation

The same 10-bus network was also implemented in PowerWorld, a widely used commercial tool for power system analysis [36]. To ensure full consistency with the stress-testing analysis, the input data were scaled according to the previously identified critical operating condition, with the active and reactive load components adjusted using a stress factor of $\alpha = 5.137$.

Two representative operating points were selected, corresponding to hours 12 and 20, which are associated with high loading conditions in the daily profile. For each case, the active and reactive power injections from the dataset, together with the per-unit branch parameters shown in Table 4.1, were manually introduced into the software, ensuring consistency with the previously analyzed scenarios.

The resulting network state for the near-limit operating condition at hour 20 is illustrated in Figure 4.4, which shows the corresponding voltage magnitudes and branch power flows, thereby confirming the consistency of the implemented model across different simulation environments.

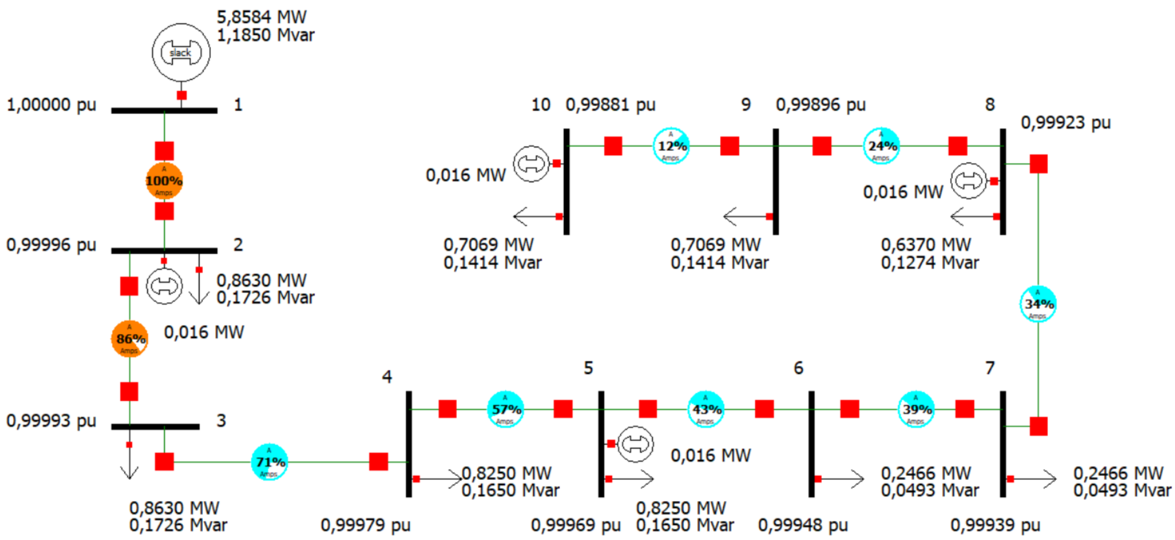

Figure 4.4: PowerWorld simulation network for the near-limit operating condition ($\alpha = 5.137$, $t = 20$).

The comparison between the proposed BFM model and the PowerWorld simulation results is illustrated in Figure 4.5, which presents the branch loading levels for the near-limit operating condition.

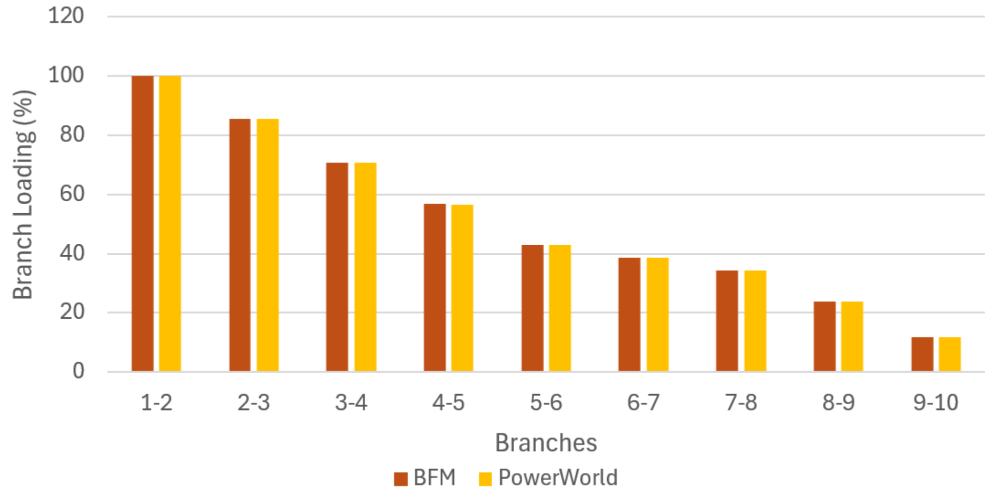

Figure 4.5: Comparison of branch loading between the BFM-based model and PowerWorld simulation for the near-limit operating condition ($\alpha = 5.137$, $t = 20$).

As observed, the results from both approaches are nearly identical, with all branches exhibiting the same loading pattern and very similar magnitudes. Specifically, the upstream branch, identified as the limiting element in the stress-testing analysis, consistently reaches its maximum load in both models.

A complementary comparison of voltage magnitudes across all network buses was produced, further confirming the same level of agreement: the maximum deviation between the BFM-based model and PowerWorld remains on the order of $10^{-5}\%$, consistent with the accuracy already observed against the AC power flow benchmark and therefore physically negligible.

Together with the AC power-flow analysis, these results demonstrate that the adopted linear outer-approximation approach accurately reproduces the behavior of the electrical network, even under stressed operating conditions.

4.1.3 Comparison with a Decoupled Sensitivity-Based Approach

To conclude the analysis of the preliminary network, the integrated RBFM approach adopted in this work is compared with an alternative method for enforcing network feasibility that uses linear sensitivity matrices. Besides providing additional validation of the obtained network results, this comparison also illustrates the practical differences between handling network constraints during optimization and as a separate post-processing correction step.

4.1.3.1 Method Overview

Unlike the RBFM formulation, which considers network constraints directly during the optimization process, the sensitivity-based approach separates the economic and network layers into two consecutive stages. The community schedule is first obtained by solving the Stage 2 economic problem, without any network representation. The resulting dispatch is then evaluated from a network perspective to determine whether any operational limits are violated and, if a violation is found, corrective load curtailment is applied to restore a feasible operating point.

This verification relies on a pair of sensitivity matrices that linearly relate the nodal active power injections to the resulting network state, namely the nodal voltage magnitudes and the branch currents:

$$S^V_{n,j} = \frac{\partial V_n}{\partial P_j}, \qquad S^I_{(n,m),j} = \frac{\partial I_{n,m}}{\partial P_j}. \tag{4.3}$$

where $S^V_{n,j}$ is the sensitivity of the voltage magnitude at bus n to an active power injection at bus j, $S^I_{(n,m),j}$ is the sensitivity of the current magnitude in branch (n,m) to an active power injection at bus j, V_n is the voltage magnitude at bus n, $I_{n,m}$ is the current magnitude in branch (n,m), and P_j is the active power injected at bus j.

These matrices were obtained numerically, through a perturbation procedure. Starting from a representative operating point of the network, a small active power variation (i.e., 1kW) is applied to one bus at a time, and an AC power-flow calculation is performed to observe how the nodal voltages and branch currents respond. The sensitivity coefficients are then calculated as the ratio of each obtained variation to the applied perturbation, and repeating this process for every bus produces the complete sensitivity matrices. One of the main advantages of this approach is its simplicity and linearity, since it only requires repeated evaluations of a conventional power-flow model.

Once the sensitivity matrices have been computed, the impact of any dispatch schedule on the network can be estimated directly, without solving a new power flow, simply by multiplying the matrices by the corresponding change in power injections. Based on these estimates, a linear correction problem is solved to determine the minimum amount of load curtailment required to keep all voltages and currents within their admissible limits while remaining as close as possible to the original Stage 2 schedule.

The main conceptual distinction is therefore one of timing: the sensitivity-based approach applies a corrective action after the economic optimization, while the RBFM guarantees feasibility within the optimization itself.

4.1.3.2 Results and Cross-Validation

Under the base-case operating conditions, the network is lightly loaded and the Stage 2 economic schedule is already physically feasible. Consequently, the sensitivity-based verification does not require any corrective curtailment, and the resulting voltage profiles and branch loadings are identical to those obtained using the RBFM. This agreement confirms that both approaches provide a consistent representation of the network when no congestion is present.

A more meaningful comparison can be made under stressed operating conditions, where network constraints become active. Since the feasibility boundary of the network was previously identified at $\alpha \approx 5.137$ (Sub-subsection 4.1.2.3), the load was deliberately scaled beyond this point, to $\alpha = 6$, with the curtailment mechanism enabled in both methods. Under these conditions, the evening demand peak causes branch 1–2 to exceed its thermal limit without corrective action. Therefore, both approaches must actively reduce load to restore feasibility. The resulting curtailment obtained with each method is summarized in Table 4.3.

Table 4.3: Applied load curtailment under stress ($\alpha = 6$) on both the RBFM and the Sensitivity-based approaches.

Bus	Hour	RBFM (kWh)	Sensitivity (kWh)
9	20	229.57	222.20
10	18	413.52	418.27
10	19	626.45	633.71
10	20	807.55	825.60
10	21	894.31	904.45
Total		**2 971.40**	**3 004.24**

The results obtained show strong agreement, with both methods identifying the same congestion pattern, applying curtailment at the same downstream buses (9 and 10), and doing so during the same evening hours. The total curtailed energy differs by only about 1%, with 2 971.40 kWh obtained considering the RBFM and 3 004.24 kWh using the sensitivity-based approach.

Moreover, Figure 4.6 compares the resulting loading of the critical branch 1–2 over the full scheduling horizon, showing that the two loading profiles progress with no difference apart from the evening peak (hours 18 to 21). In both cases, the branch operates at its thermal limit, however, while the RBFM reaches exactly 100% loading during those hours, the sensitivity-based correction keeps the branch slightly below the limit, between 99.8% and 99.9%.

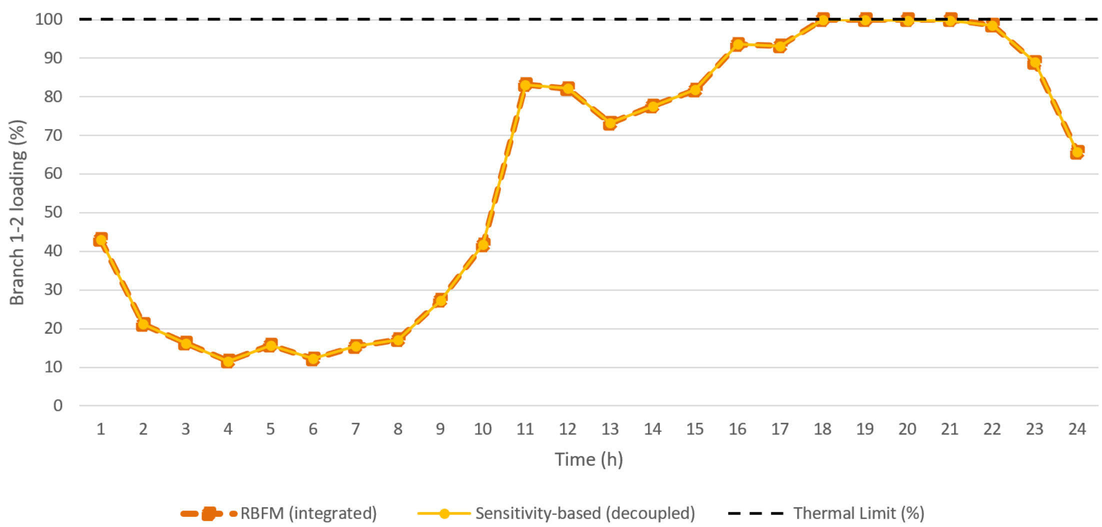

Figure 4.6: Loading of the critical branch 1–2 over the 24-hour horizon under stress ($\alpha = 6$), on RBFM and sensitivity-based approaches.

This small difference can be explained by the linear nature of the sensitivity model. Since the corrective curtailment is determined from a linear approximation of the branch currents, the resulting solution is slightly conservative, therefore applying marginally more load curtailment than strictly necessary. Nevertheless, the deviation remains extremely small, confirming that the sensitivity-based approach remains highly accurate even under significant stress and provides an independent cross-validation of the RBFM results.

4.1.3.3 Decoupled versus Integrated Network Handling

Beyond the agreement between the numerical results, this comparison also highlights an important difference regarding how network feasibility can be addressed. Essentially, the sensitivity-based method is a decoupled approach in which the economic schedule is determined first, and any network violations are corrected afterward in a separate feasibility stage, similar to the OPF-correction procedure proposed in [5]. In contrast, the adopted RBFM incorporates the network constraints directly into the market optimization, ensuring the resulting schedule is feasible from the outset, in line with the approach presented in [12].

For the preliminary network considered, both methodologies yield very similar results, primarily because congestion is associated with a single critical branch and the only available corrective action is load curtailment. Under these conditions, both approaches identify essentially the same solution.

4.1.4 Discussion and Key Observations

The results obtained throughout this preliminary case study provide a comprehensive validation of the proposed network-constrained optimization framework, both numerically and physically.

Firstly, the tightness of the SOC relaxation confirms that the adopted linear outer-approximation approach accurately reproduces the nonlinear behavior of the BFM, as evidenced by the negligible deviations observed in the representation of power flows and branch currents.

Secondly, the stress-testing analysis highlights the network's physically consistent response under increasing-demand conditions. The progressive loading of the upstream branch, together with the smooth voltage degradation, reflects the expected behavior of radial distribution systems. The identification of a sharp feasibility boundary at $\alpha \approx 5.137$ further confirms that the model correctly captures the operational limits of the network, with infeasibility being driven by thermal constraints rather than voltage violations.

Moreover, the comparison with the AC power flow solution demonstrates that the proposed formulation continues to represent the system with high accuracy, indicating that the RBFM preserves the essential physical characteristics of the system, even under stressed operating conditions. The additional validation using PowerWorld further reinforces these findings, showing a strong agreement between the proposed framework and an industry-standard simulation tool.

Finally, the comparison with the sensitivity-based approach provides an additional confirmation of the obtained network results, with both methods identifying the same congestion and applying nearly identical curtailment under stress conditions. At the same time, an important methodological distinction is highlighted. In this small network, where congestion is associated with a single critical branch and curtailment is the only corrective measure, both approaches produce almost the same outcome. In larger systems with multiple flexible resources, however, the integrated formulation is able to coordinate generation, storage, and P2P trading together with the network limits, relieving congestion through a combination of actions before resorting to curtailment, an advantage that is explored in the main case study of Section 4.2.

Overall, these results demonstrate that the proposed BFM-based optimization framework provides an accurate and computationally efficient representation of network-constrained REC operations. This validation step, therefore, establishes a solid foundation for the more advanced and realistic case study presented in the following section.

4.2 Main Case Study: Network-Constrained REC Operation

Following the illustrative example validation presented in the previous section, the proposed network-constrained REC framework is now applied to a larger distribution system. The objective of this main case study is to evaluate the capability of the integrated REC market and network operation model to coordinate DERs while simultaneously respecting the physical constraints of the distribution grid.

The adopted case study allows the assessment of the interactions among local energy trading mechanisms, distributed renewable generation, flexible resources, and network operational constraints under realistic operating conditions.

4.2.1 37-Bus Network and REC Description

The main case study considers the 37-bus distribution network firstly presented in [39] and illustrated in Figure 4.7. The network operates at a nominal MV level of 11 kV and is connected to the upstream utility grid through a 33/11 kV substation. Bus 0 corresponds to the HV side of the substation, while Bus 1 represents the 11 kV distribution bus from which the radial feeders originate and therefore acts as the slack bus of the system. Since the network is operated entirely at 11 kV, the analysis focuses on Bus 1 and its downstream feeders.

The distribution network is represented as a balanced three-phase system using a single-phase equivalent model. Under this assumption, the three phases have identical voltage and current magnitudes and are separated by 120°, while loads and generation are considered symmetrically distributed across the phases. Consequently, only one representative phase is explicitly modeled in the RBFM.

The corresponding system comprises 37 buses and 36 distribution lines arranged according to a radial topology, representing a realistic MV distribution network with geographically distributed loads and DERs.

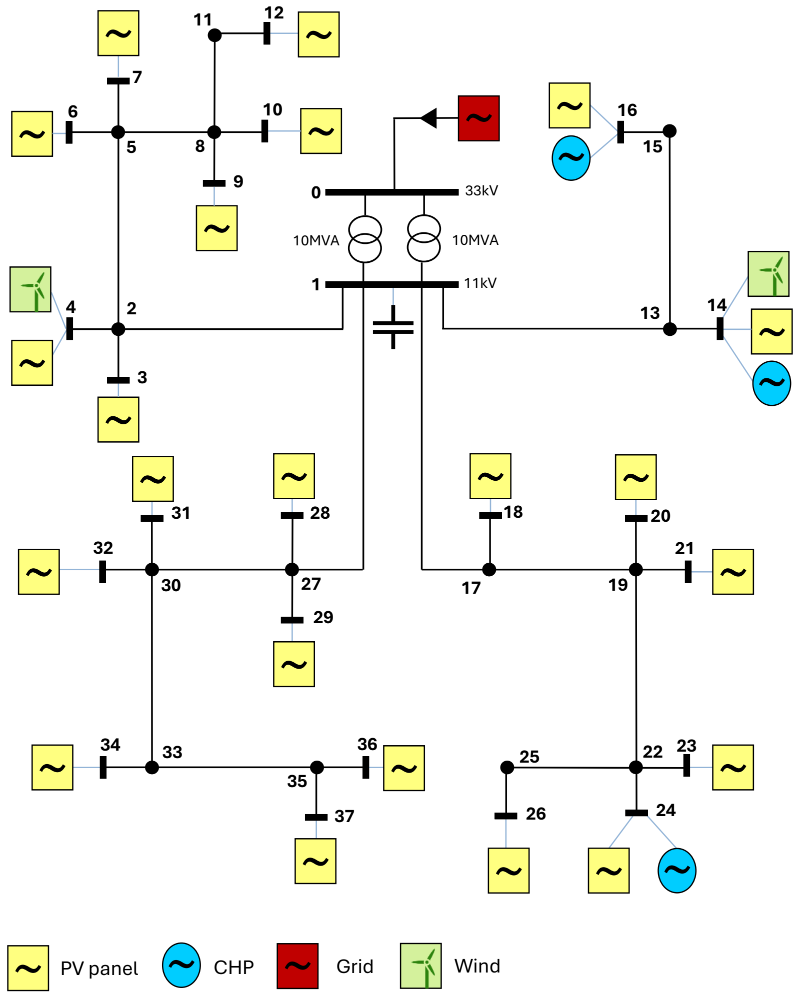

Figure 4.7: 37-bus radial distribution network considered in the main case study [39].

The distribution lines were modeled using the electrical parameters of LX95 underground cables. The corresponding resistance and reactance values were converted to per unit considering the base quantities summarized in Table 4.4. Additionally, the thermal limit for each branch was defined by the maximum admissible current for the adopted cable type.

Table 4.4: Base values adopted for the 37-bus distribution network.

Parameter	Value
Base apparent power (S_{base})	1 MVA
Base voltage (V_{base})	11 kV
Base impedance (Z_{base})	121 Ω
Base current (I_{base})	52.49 A
Branch thermal limit	245 A
Voltage limits	0.95–1.05 p.u.

Accordingly, S_{base} represents the total three-phase apparent power and V_{base} the line-to-line voltage, leading to $I_{\text{base}} = S_{\text{base}}/(\sqrt{3}V_{\text{base}})$.

Regarding the REC considered in this work, 22 community members were allocated across all of the leaf buses (i.e., buses located at the extremities of the radial feeders and directly associated with end-user consumption and generation). Each member may also simultaneously include local demand, renewable generation, storage systems, and EVs, while the remaining buses correspond exclusively to network interconnection nodes. This spatial distribution of REC members allows the proposed framework to capture the interaction between local energy exchanges and the physical operation of different areas of the distribution system.

The REC generation portfolio includes 22 PV systems, 2 wind farms, and 3 CHP plants distributed across the entire network. Specifically, PV generation is connected at all REC member buses, while wind generation units are installed at Buses 4 and 14. Additionally, the CHP plants, rated at 500 kW each, are connected at Buses 14, 16 and 24, providing dispatchable local generation capacity within different areas of the network.

Besides renewable generation resources, the model also incorporates flexible assets in the form of BESS units and EVs. In the first place, four BESS units were connected to Buses 12, 16, 26, and 36. Each unit has an energy capacity of 250 kWh and operates under the charging, discharging, and SoC constraints formulated in Sub-subsection 3.4.1.3.

Additionally, an EV aggregation model comprising 1979 EVs was considered and distributed among all community members according to predefined mobility and connection patterns. The inclusion of these flexible resources allows the proposed framework to capture the interaction between distributed storage operations, local energy exchanges, and network constraints over the scheduling horizon.

Furthermore, to support the spatial analysis of network operations, the distribution system was divided into four main feeder areas, each supplied by a distinct branch connected to the primary substation. This organization, illustrated in Figure 4.8, enables the identification of localized congestion points, the interpretation of feeder-dependent power exchange patterns, and the distinction between intra-feeder and inter-feeder P2P transactions, providing a structured way to relate economic results to the network's physical regions.

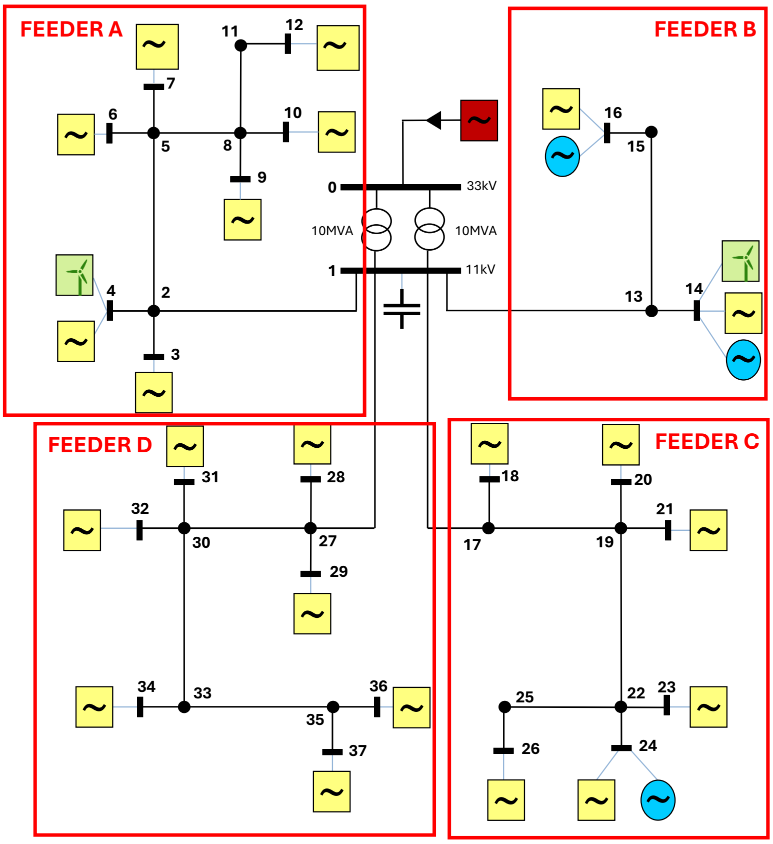

Figure 4.8: 37-bus radial distribution network divided into four main feeder areas.

As can be observed in Figure 4.8:

- Feeder A comprises buses 2–12;
- Feeder B includes buses 13–16;
- Feeder C covers buses 17–26;
- Feeder D consists of buses 27–37.

4.2.2 Data and Simulation Setup

This subsection summarizes the datasets, operating assumptions, and simulation parameters adopted throughout the main case study. While the mathematical formulation of the optimization problem was presented in Chapter 3, the focus here is on the specific data used to characterize the operation of the considered REC.

4.2.2.1 Distributed Generation Resources

The REC considered in this case study includes both non-dispatchable renewable generation resources and dispatchable conventional generation units. Specifically, as previously stated, the community comprises a total of 27 generation units, including 22 PV systems, 2 wind turbines, and 3 CHP units. While the PV and wind generators are modeled as non-dispatchable resources based on forecasted generation profiles (as in [39]), the CHP units are represented as dispatchable generation assets whose operating schedules are determined by the optimization process.

The renewable generation profiles considered correspond to hourly forecast data ($\Delta t = 1$ h) over a 24-hour scheduling horizon. Consequently, PV and wind generation are treated as fixed parameters within the optimization model and do not appear as decision variables. Furthermore, no generation costs are assigned to these resources, reflecting their must-take nature and negligible marginal operating costs.

However, to create operating conditions with significant local energy exchange inside the REC, the renewable generation levels were adjusted. More specifically, PV generation profiles were multiplied by a factor of four, while wind generation profiles were scaled by a factor of three.

In contrast, CHP units are modeled as controllable generators and participate actively in the optimization process. Their active power output is represented by the decision variable $E_{n,t}^{G,CHP}$, whose operation respects the following limits:

$$0 \leq E_{n,t}^{G,CHP} \leq 500 \text{ kW} \cdot \Delta t, \tag{4.4}$$

while also being associated with the marginal generation cost $\hat{\lambda}_n^{CHP}$, which is incorporated into the objective function whenever CHP generation exists and is preferable. This allows the optimization model to determine the optimal CHP dispatch according to both economic and network operating conditions.

Although the active power output of PV and wind generators is treated as fixed, forecast values, their reactive power injections are represented as optimization variables in the network model to avoid convergence issues. As defined in Equation 3.26 and in Constraints 3.27, 3.28, and 3.29, PV, wind, and CHP units are allowed to provide reactive power support, with their reactive generation bounded between 0 and 30% of their active power output.

4.2.2.2 Load Profiles

The active power demand profiles of the 22 REC members adopted in this case study correspond to the original consumption data provided with the 37-bus distribution network and are the same as those employed by [39]. These profiles are treated as fixed input parameters throughout the optimization process, thereby defining the community's baseline energy requirements and constituting one of the main drivers of energy exchanges and network utilization.

Reactive power consumption is modeled following the approach presented in Chapter 3. Rather than relying on independent reactive demand measurements, the reactive load at each bus and at each hour is assumed to be proportional to the corresponding active power demand according to:

$$Q_{n,t}^{C} = 0.3\,P_{n,t}^{C} \tag{4.5}$$

which corresponds to the relationship defined in Equation 3.30. Consequently, reactive power demand varies throughout the day following the same temporal pattern as the active load profiles. This representation enables the network-constrained optimization model to capture the effects of reactive power flows on voltage regulation and branch loading while maintaining a consistent and computationally tractable load representation.

4.2.2.3 Flexible Assets

The operational flexibility available within the REC is provided by BESS units and EVs. The four BESS units considered in this work are characterized by their nominal energy capacity, charging and discharging efficiencies, power limits, SoC bounds, and degradation costs. These parameters directly affect the scheduling decisions made by the optimization model and determine the amount of flexibility each storage unit can provide. All BESS units share the same input values for these parameters, as properly summarized in Table 4.5.

Table 4.5: BESS parameters for the main case study.

Parameter	**Value**
Number of units	4
Connected buses	12, 16, 26, 36
Nominal capacity	250 kWh
Maximum charge/discharge power	250 kW
Charging efficiency ($\hat{\eta}^{B,C}$)	80 %
Discharging efficiency ($\hat{\eta}^{B,D}$)	80 %
Minimum SoC	10 %
Maximum SoC	100 %
Initial stored energy	200 kWh
BESS degradation cost	0 €/kWh

Regarding EVs, the aggregation model is composed of 1979 vehicles distributed across all 22 community member buses, with 21 EVs from the original dataset excluded due to them being assigned to junction nodes. Each EV is characterized by its battery capacity, minimum stored energy (set to 10% of capacity), charging and discharging efficiencies of 88%, maximum charging and discharging power limits, a binary availability profile indicating its connection periods, and a trip energy consumption profile representing driving activity.

The dataset comprises EVs with six distinct battery capacities: 4.4, 12.0, 15.0, 16.0, 22.0, and 24.0 kWh. While these capacities are relatively low compared to those of many contemporary EVs, they are retained from the original dataset adopted in this work. The EVs also present different charging and discharging power limits, reflecting the heterogeneous technical characteristics represented in the dataset. The connection periods reproduce typical commuting behavior, with vehicles being disconnected mainly during working hours and available for charging during overnight and evening periods. The initial stored energy of each EV is set according to the dataset, representing the pre-optimization SoC conditions.

4.2.2.4 Market and Simulation Parameters

The optimization process adopted in this work follows the standard day-ahead scheduling methodology of the OSTEC framework. The resulting MILP was solved using Gurobi, with a Mixed Integer Programming Gap (MIPGap) tolerance of 0.1% to ensure a high-quality solution while limiting the optimality gap, and a solver time-out of 300 seconds per solve. During the iterative SOC cutting-plane procedure, this gap was tightened to 0.01% to improve the numerical stability of the successive solves.

As for the market structure, all REC members participate in a bilateral P2P market, where internal energy exchanges are valued at a LEM price of $\hat{\lambda}^{p2p} = 0.10$ €/kWh. Following the MMR principle, this value is placed between the retail and market buy and sell tariffs to provide mutual trading incentives [5].

Two tariff configurations are adopted to assess the sensitivity of the community operation to economic signals:

- **Flat tariffs**: uniform prices throughout the day, serving as the baseline reference scenario;
- **Time-of-Use (TOU) tariffs**: time-varying prices reflecting a typical day/night differentiation, designed to create economically driven load-shifting and storage dispatch incentives.

The complete tariff structure for both scenarios is summarized in Table 4.6.

Table 4.6: Tariff structures adopted in the main case study simulations.

Tariff	**Period**	**Hours**	**Flat**		**TOU**	
			Buy	**Sell**	**Buy**	**Sell**
Retail	Off-peak	1–7, 23–24	0.15	0.05	0.08	0.03
	Mid-peak	8–16	0.15	0.05	0.15	0.07
	Super-peak	17–22	0.15	0.05	0.25	0.12
Market	Off-peak	1–7, 23–24	0.12	0.08	0.06	0.04
	Mid-peak	8–16	0.12	0.08	0.12	0.08
	Super-peak	17–22	0.12	0.08	0.22	0.15
LEM (P2P, flat, both scenarios)			0.10			

All values are in €/kWh.

The TOU tariff structure is intentionally designed to create economically driven load-shifting and storage-dispatch incentives, which are particularly relevant for assessing how BESS and EV flexibility interact with physical network constraints under time-varying price signals.

The remaining penalty and cost parameters are defined as follows. The demand response penalty $\hat{\lambda}^{DR}$ presented in Subsection 3.4.1 is set to 5.00 €/kWh, ensuring that load curtailment is only activated as a last resort when network congestion cannot be relieved through available generation or storage flexibility. Similarly, the contracted power violation penalty $\hat{\lambda}^{EXTRA}$ is set to a high value of 10.00 €/kW, reflecting its role as a soft feasibility mechanism rather than a realistic tariff. That is, violations of the contracted power limit are therefore economically discouraged while maintaining numerical tractability. Additionally, the no-worse-off penalty coefficient $\hat{\lambda}^{\Delta Y}$ is set to 1, so that one euro of individual-rationality violation is penalized by exactly one euro in the objective. Finally, the generation-curtailment penalty $\hat{\lambda}^{GC}$ was set to 0.13 €/kWh. Consistent with the formulation in Chapter 3, this mechanism was never activated, since no overvoltage or reverse-flow conditions emerged in any of the simulations.

Regarding dispatchable generation, the three CHP units are associated with marginal generation costs of 0.03, 0.02, and 0.01 €/kWh for the units connected at Buses 14, 16, and 24, respectively, allowing the optimization to preferentially dispatch lower-cost units while accounting for both economic and network operating conditions. Finally, the regularization coefficient is $\rho = 10^{-3}$, consistent with the formulation defined in Chapter 3.

Furthermore, to assess the impact of network constraints on the community operation, three simulation configurations are considered throughout this case study:

The main simulation uses the physical thermal limit of the LX95 cable ($I_{\max} = 245$ A) with flat tariffs, representing the baseline operating scenario with the original dataset parameters. Afterward, a TOU scenario, under the same network configuration, is conducted, replacing the flat tariff structure with the time-varying prices defined in Table 4.6, to assess how dynamic price signals affect the connection of flexible assets when network constraints are active. Ultimately, an unconstrained simulation is considered under the flat tariff conditions but with the network constraints disabled, as the reference for the primary comparison of the case study: quantifying the impact that explicitly considering distribution network constraints, such as the ones on the RBFM, has on the economic and physical operation of the REC.

In all network-constrained simulations, the SOC outer-approximation procedure is initialized with linear flow bounds and iterated until the maximum SOC violation across all branches and time periods either falls below the strict tolerance $\varepsilon^{SOC} = 5 \times 10^{-7}$ p.u.^{2} or becomes physically negligible (below a practical acceptance threshold of 10^{-3} p.u.^{2}, whose negligible physical impact is verified in Section 4.2.4), with up to 300 supporting hyperplanes added per iteration and a maximum of 30 iterations.

4.2.3 Economic Operation of the REC: Results and Analysis

In this subsection, the economic operation of the REC under the baseline simulation is presented, corresponding to flat tariffs with the physical network constraints active. Essentially, the analysis covers the community energy balance, the composition of the generation mix, the role of dispatchable assets, and the activation of the demand response mechanism. A targeted comparison with the TOU tariffs scenario is subsequently introduced to highlight the effect of dynamic pricing on the dispatch of flexible assets.

4.2.3.1 Energy Balance and Generation Mix

The community power balance over the one-day simulation reflects the typical behavior of a REC with significant renewable generation capacity.

Figure 4.9 presents the hourly supply mix, including grid imports, CHP, wind and PV generation, together with the aggregated discharge of stationary BESS units and EV batteries. In addition, the figure includes three cumulative demand-side curves. The first corresponds to the served community consumption, obtained after subtracting demand-response curtailment from the original demand. Storage charging is then added to this profile, producing the "Consumption + Charge" curve. Finally, the upper curve, denoted as "Consumption + Charge + Export + Losses", further includes the power exported to the upstream grid and the active distribution network losses, therefore coinciding with the upper boundary of the stacked supply areas.

Wind power provides a stable contribution throughout the day, while PV output becomes the dominant renewable source during daylight hours (between hours 6–20), reaching its maximum around midday. Notably, the three CHP units operate at their maximum rated output of 0.5 MW each throughout all 24 time periods, due to the fact that marginal CHP costs are well below both the market buy price and the retail tariff, making CHP generation always economically preferable over external acquisition, and therefore resulting in a constant dispatchable generation of 1.5 MW and a total of 36 MWh on the full day.

Storage discharge is most relevant during the evening period, when EV batteries, together with the smaller contribution of the stationary BESS units, supply part of the community demand and reduce the required grid imports. In contrast, the separation between the served-consumption and consumption-plus-charging curves during the daylight period reflects the charging of these flexible resources using the available generation surplus.

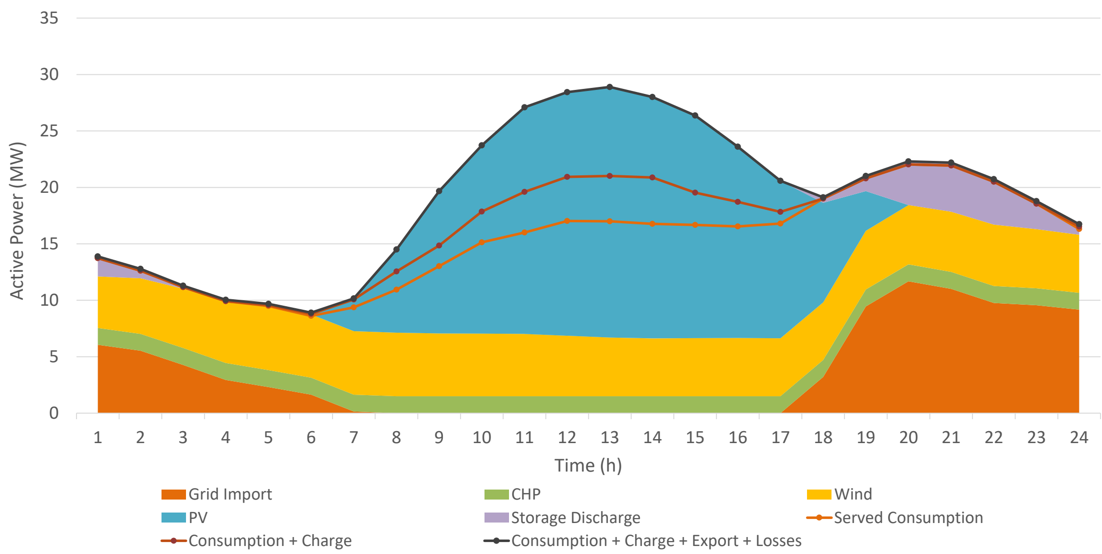

Figure 4.9: Hourly active-power supply mix and cumulative community demand components for the baseline simulation, including storage operation, grid exports, and network losses.

Regarding the community's net position with respect to the upstream grid, Figure 4.10 reveals a clear transition between two operating regimes. During the early morning hours (hours 1-7) and evening periods (hours 18-24), the REC acts as a net importer, relying on external energy purchases to satisfy local demand. In contrast, during the central hours of the day (hours 8-17), the combined generation from PV, wind, and CHP exceeds the served community consumption and the charging requirements of the flexible assets (as shown in Figure 4.9), making the REC a net exporter of electricity. The strongest export condition occurs around hour 13, when PV production reaches its highest level, whereas the largest import is observed during the evening peak (hour 20).

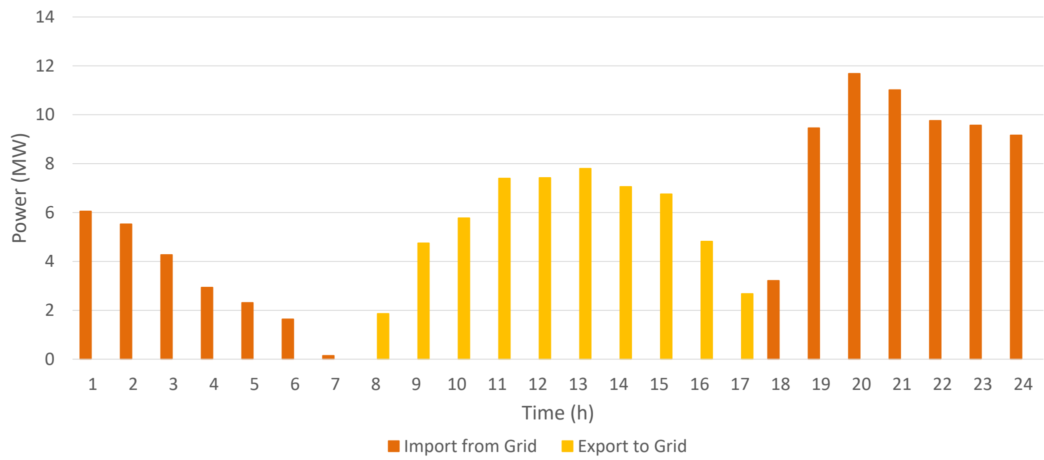

Figure 4.10: Community net power exchange with the upstream grid over the 24-hour scheduling horizon (baseline simulation).

This behavior highlights the strong temporal mismatch between renewable generation and consumption. While local resources are sufficient to create substantial energy surpluses during midday, considerable grid imports remain necessary during the evening peak, once PV production disappears and demand reaches its highest levels.

4.2.3.2 Market Interactions and P2P Trading

Regarding external market interactions, a prominent outcome is that no community member purchases energy from or sells energy to the retailer over the entire scheduling horizon, with all external transactions conducted exclusively through the wholesale market channel. This behavior is a direct consequence of the tariff price structure adopted: as seen in Table 4.6, the market buy price (0.12 €/kWh) is consistently lower than the retail buy tariff (0.15 €/kWh), while the market sell price (0.08 €/kWh) exceeds the retail sell tariff (0.05 €/kWh), making the market channel strictly dominant for all members under both import and export conditions.

Internal P2P trading is active throughout the day, with bilateral exchanges occurring between members across all four feeder areas, resulting in a total of approximately 82.79 MWh exchanged bilaterally in the community. As represented in Figure 4.11, the pattern that can be observed reveals a strongly inter-feeder ratio: approximately 86.3% of all P2P energy transitions are between different feeders, while only 13.7% correspond to intra-feeder exchanges. This result shows an uneven distribution between where energy is produced and where it is used on the network. This behavior indicates that the location of generation resources does not prevent energy from being redistributed across the entire REC, with highly productive members effectively supplying demand beyond their local feeder area.

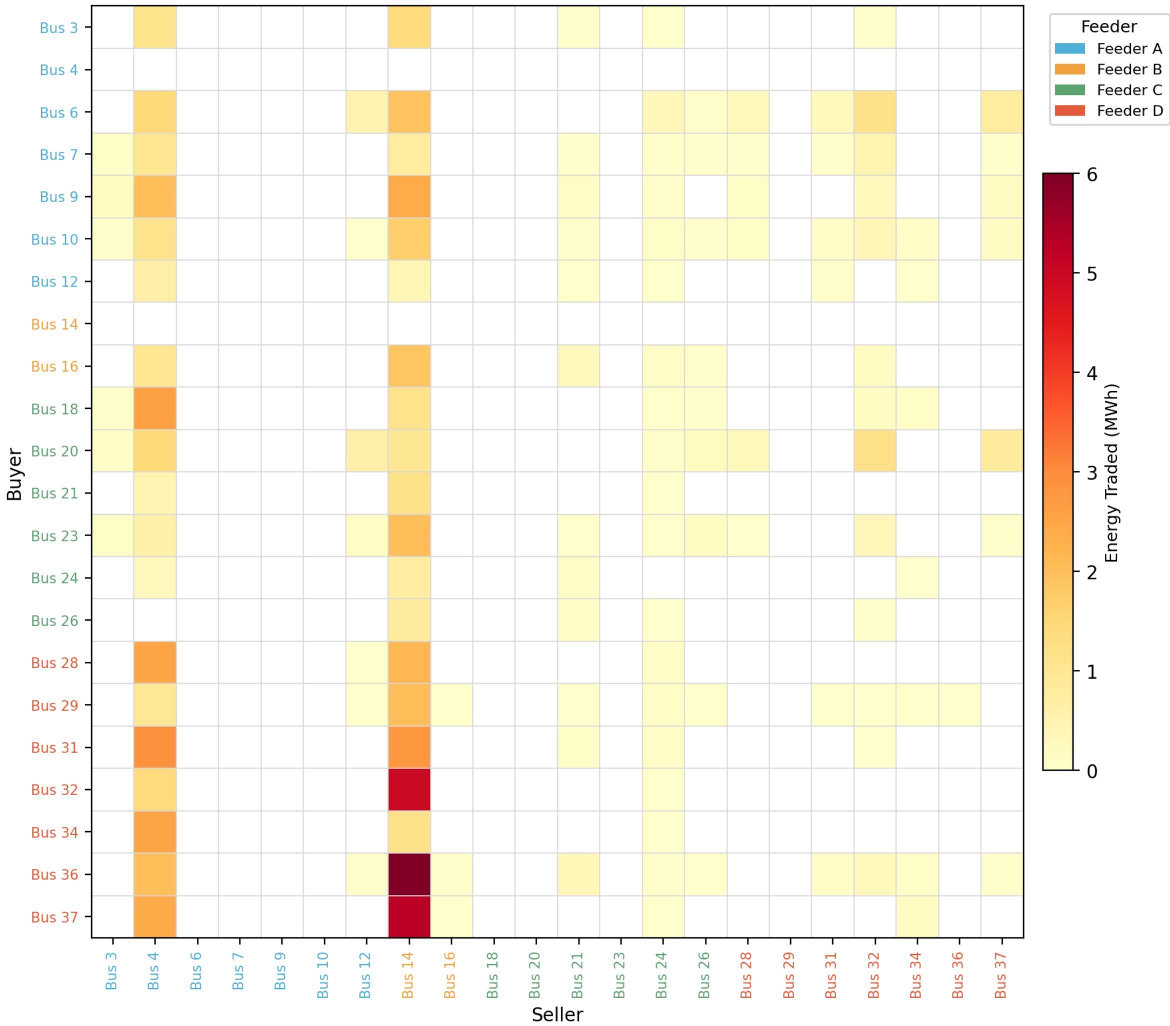

Figure 4.11: Bilateral P2P energy trading matrix for the baseline simulation, showing the total energy exchanged between each buyer–seller pair over the scheduling horizon.

The trading matrix is highly concentrated around a limited number of participants. Specifically, on the supply side, Bus 14 (41.5 MWh sold in total) and Bus 4 (28.3 MWh), both equipped with wind generation, emerge as the dominant sellers, together accounting for 84.3% of all the energy sold within the community, therefore confirming the central role of wind resources in the internal market. Bus 14 additionally hosts a CHP unit, strengthening its position as the main supplier within the REC. On the demand side, the most active buyers are all located in Feeder D, namely Buses 36 (9.1 MWh bought), 37 (7.8 MWh), 32 (6.4 MWh), and 31 (5.9 MWh), which combine high demand with limited local generation and, therefore, depend heavily on energy imported from the rest of the community.

Notably, high gross demand does not by itself translate into high P2P purchases. Bus 16 illustrates this clearly: despite having one of the greatest gross demands in the community, its local combination of PV generation and a CHP unit covers the majority of its consumption, so it relies only marginally on internal purchases (around 3.4 MWh). The determining factor for P2P purchases is therefore each member's net load rather than its gross consumption.

For these buyers, the high purchase volumes observed under flat tariffs reflect their underlying consumption, as none of them actively uses storage for arbitrage under uniform pricing.

It should be noted that, while the aggregated traded volumes and the inter- versus intra-feeder shares are robust across solver runs, the exact pair-wise allocation between individual buyers and sellers does not have a unique solution. Under a constant local energy price, the P2P market admits multiple economically equivalent trading patterns that lead to the same aggregate traded volume and community cost. Therefore, although the bilateral-volume regularization introduced in Equation 3.19 removes the redundant re-trading that would otherwise inflate the gross traded volume, multiple minimum-volume trading patterns may still exist. For this reason, the aggregate quantities reported here are stable and meaningful, while the assignment of specific buyer–seller pairs among the most central buses may vary between equivalent solutions.

Beyond these aggregate trading patterns, the resulting economic outcomes can now be examined. The total community energy cost for the baseline scenario amounts to 9476.57 €, while the objective value, which additionally includes the individual-rationality penalty (i.e., the term $\sum_{n\in N} \Delta Y_n \hat{\lambda}^{\Delta Y}$ and a negligible contribution from the regularization terms presented in Equation 3.19, added to the objective function), amounts to 11 658.92 €. The full individual Stage 1 and Stage 2 costs of all 22 members are reported in the corresponding repository file [35].

Members with large renewable generation capacity, particularly Bus 14 (wind and CHP) and Bus 4 (wind), present negative individual costs of −6 549.69 € and −3 891.05 € respectively, reflecting their role as net energy exporters within the community. In contrast, Bus 37 presents the highest individual cost (2 351.63 €), followed by Bus 16 (1 880.01 €) and Bus 36 (1 690.38 €). However, the reasons behind these costs are different. The high cost of Bus 16 originates from its great demand rather than from the network, while the costs of Buses 36 and 37 are directly affected by the enforcement of an additional economic penalty. This is made explicit by the no-worse-off slack variable ΔY_n, which is non-zero only at these two buses (620.57 € at Bus 36 and 1 551.90 € at Bus 37, totaling 2 172.47 €). More precisely, Buses 36 and 37 are the only members whose operating costs increase above their individual Stage 1 benchmarks, both located in Feeder D, the most congested area of the system, as further discussed in Subsection 4.2.4.

4.2.3.3 BESS Operation and Demand Response

Regarding BESS units, considering flat tariffs, three of the four BESS units (i.e., those located at Buses 12, 16, and 26) remain inactive throughout the entire day, maintaining their initial SoC of

80% unchanged. This result is economically consistent: with uniform prices throughout the day, the round-trip efficiency losses associated with charging and discharging make any arbitrage cycle economically unattractive. In the absence of a congestion incentive for these buses, the optimizer correctly identifies storage cycling as unfavorable.

The exception is the BESS unit at Bus 36, located in Feeder D. As shown in Figure 4.12, this unit is charged by 62.5 kWh at hour 13, reaching its maximum SoC of 100%, and discharged by 180 kWh at hour 20, dropping to the minimum SoC of 10%. Unlike the remaining storage units, this dispatch pattern is not driven by price arbitrage but by congestion management. As discussed in Section 4.2.4, branch 1→27 reaches its thermal limit at hour 20, and the BESS discharge at Bus 36 reduces the local net demand, alleviating the downstream power flow through the congested branch.

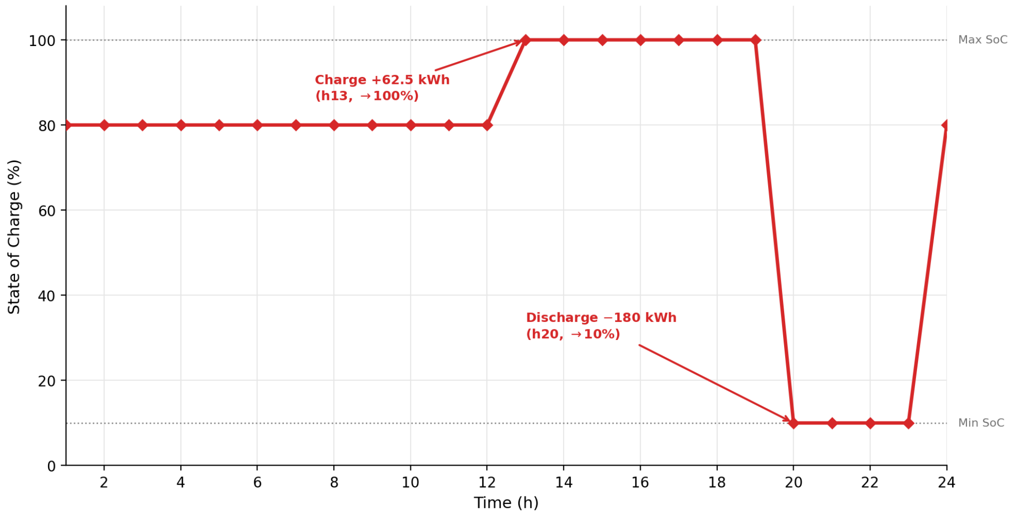

Figure 4.12: SoC of the BESS unit at Bus 36 over the 24-hour horizon (baseline simulation).

Despite this storage contribution, the flexibility available at Bus 36 is insufficient to eliminate the congestion occurring at hour 20. Consequently, as shown in Figure 4.13, the demand response mechanism is activated across every member of Feeder D (Buses 28, 29, 31, 32, 34, 36, and 37), totaling 640.06 kWh of load reduction during that single time period. The fact that curtailment is distributed over the entire feeder rather than being isolated at a single node indicates that the binding constraint is the shared upstream branch 1→27, whose relief depends on the aggregate demand reduction across the whole feeder. This activation provokes 3 200.28 € of penalty costs, representing a significant fraction of the total community objective value.

Notably, this activation occurs despite the high demand response penalty of 5.00 €/kWh, which is substantially higher than any energy purchase or generation cost considered in the market. The fact that the optimizer still chooses to curtail load indicates that all other available flexibility resources have been exhausted and that demand reduction becomes necessary to maintain network feasibility.

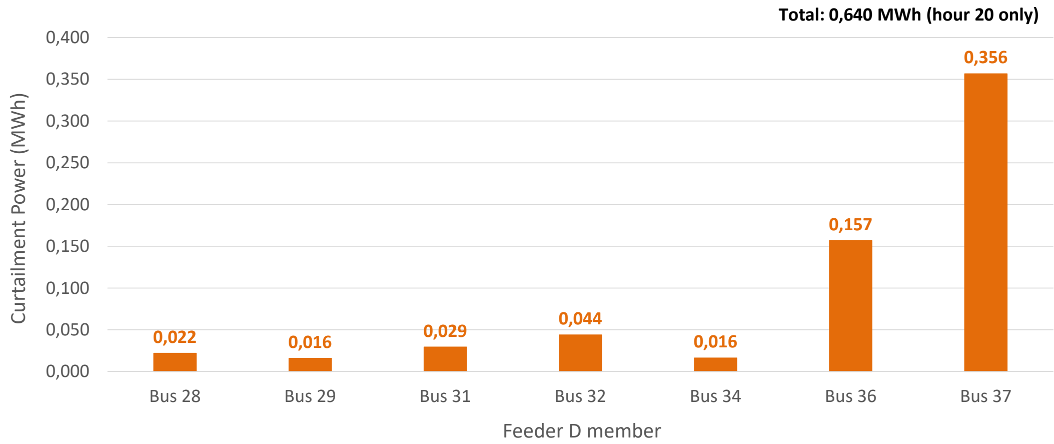

Figure 4.13: Demand response curtailment per Feeder D member at hour 20 (baseline simulation).

Ultimately, the fact that demand response is activated exclusively at hour 20 further confirms that the critical operating condition of the network occurs during the evening peak, when branch 1→27 reaches thermal saturation and local flexibility resources are no longer sufficient to maintain a feasible operating point.

4.2.3.4 Demand Flexibility from EVs

The aggregated EV fleet constitutes the largest source of flexible demand within the REC and therefore plays a significant role in shaping the daily energy balance. As illustrated in Figure 4.14, the charging and discharging behavior of the 1979 vehicles follows a clear temporal pattern aligned with the availability of local renewable generation. During daylight hours (approximately hours 8–17), the fleet charges intensively, reaching an aggregated charging peak of 4.10 MWh at hour 14. In contrast, during the evening period (hours 18–24), the vehicles operate predominantly in discharge mode, with a maximum aggregated discharge of 4.36 MWh observed at hour 21.

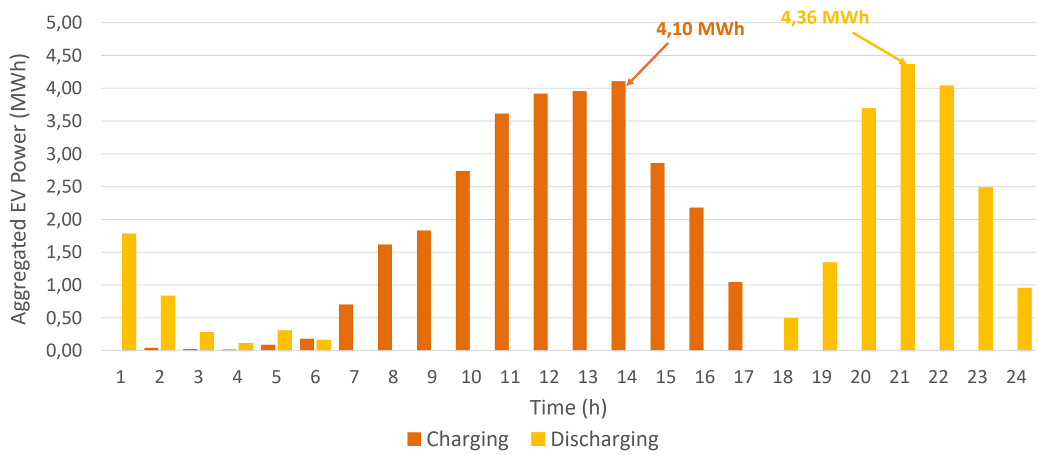

Figure 4.14: Aggregated EV charging and discharging profile over the 24-hour horizon (baseline simulation).

This behavior is economically intuitive. That is, charging the EV fleet during the central hours of the day allows locally generated renewable energy to be absorbed rather than exported to the external market at relatively low selling prices. Later, during the evening peak, the stored energy is returned to the community, reducing the amount of electricity that would otherwise need to be imported from the upstream grid. The underlying economic driver is therefore the spread between the low price at which midday surplus would be sold and the higher price at which evening energy would have to be purchased. Whenever this difference exceeds the round-trip efficiency losses, temporal energy shifting becomes profitable. As a result, the optimization schedules charging during periods of generation surplus and discharging during periods of higher demand.

An important observation is that, despite their different operation under flat tariffs, both stationary BESS units and EV batteries can, in principle, store local renewable surpluses. This is essentially explained by their round-trip efficiencies. For the stationary BESS units, the charging and discharging efficiencies of 80% result in a round-trip efficiency of 64%. Consequently, storing 1 kWh that could otherwise be exported at 0.08 €/kWh, as reported in Table 4.6, allows only 0.64 kWh to be subsequently delivered, avoiding an energy purchase worth 0.0768 € at the market buy price of 0.12 €/kWh. Since this value is slightly lower than the immediate export revenue, stationary storage arbitrage is not economically attractive.

Conversely, the EV charging and discharging efficiencies of 88% correspond to a round-trip efficiency of approximately 77.4%. Under the same prices, storing 1 kWh of surplus generation allows approximately 0.774 kWh to be delivered later, avoiding a purchase cost of about 0.0929 €, which exceeds the 0.08 € revenue that would be obtained through immediate export. Therefore, EV flexibility remains economically attractive under flat tariffs, while the stationary BESS units are only activated when required for congestion management.

Besides reducing energy costs, the EV fleet also contributes to more balanced network operations. By shifting demand towards the midday period and supplying energy during the evening peak, EV flexibility helps reduce the net load seen by the upstream branches and partially mitigates network congestion.

However, unlike stationary storage units, EVs are not available throughout all day. Their availability depends on the mobility needs of each user, meaning that vehicles are disconnected from the network during travel periods and consume part of their stored energy for mobility purposes. Consequently, EVs can only participate in charging or discharging actions while connected to the network, making the flexibility they provide more limited in both time and magnitude than that offered by dedicated storage systems.

As a result, this contribution is insufficient to fully eliminate the thermal saturation on branch $1 \rightarrow 27$ at hour 20, and demand response curtailment is still required to maintain network feasibility under the baseline scenario.

4.2.3.5 Effect of TOU Tariffs

The introduction of TOU tariffs leads to a noticeable change in the economic operation of the REC. The total community energy cost increases from 9 476.57 € in the baseline scenario to 10026.01 €, representing an increase of approximately 549 € (5.8%). Although the TOU tariff creates additional flexibility opportunities, a large share of the community demand still occurs during the super-peak evening period (hours 17–22), when electricity prices are significantly higher. Consequently, energy that cannot be supplied locally becomes more expensive, increasing the community's overall cost.

The most visible difference between the two scenarios is observed in the operation of the BESS units, as illustrated in Figure 4.15. Under flat tariffs (Figure 4.15a), the units located at Buses 12, 16, and 26 remain inactive throughout the day, maintaining their initial SoC of 80%, therefore appearing as a single overlapping flat line, while only the BESS at Bus 36 is activated to support congestion management. Under TOU pricing (Figure 4.15b), however, all four storage units become involved in the scheduling process. All batteries charge during the low-price off-peak hours, reaching full capacity before midday, and discharge during the super-peak evening period.

The discharge profile, however, differs across the network. While the batteries at Buses 26 and 36 reach the minimum SoC of 10% at the peak hour 20, those present at Buses 12 and 16 distribute their discharge over two consecutive hours, passing through intermediate SoC levels at hour 20 before reaching the minimum at hour 21. This difference reflects the stronger congestion requirements in Feeder D, where the batteries are fully discharged at the time of maximum network stress, while the remaining units respond solely to the price signal. This behavior confirms that the price difference between off-peak and super-peak periods is sufficient to compensate for the storage efficiency losses, making energy arbitrage economically attractive across the network rather than only at locations affected by congestion.

A similar effect is observed for the EV fleet, whose charging profile shifts towards the cheaper off-peak hours. Together, the BESS units and EVs demonstrate a clear response to the economic signals introduced by the TOU structure, increasing local energy shifting and reducing the dependence on expensive electricity purchases during peak-price periods.

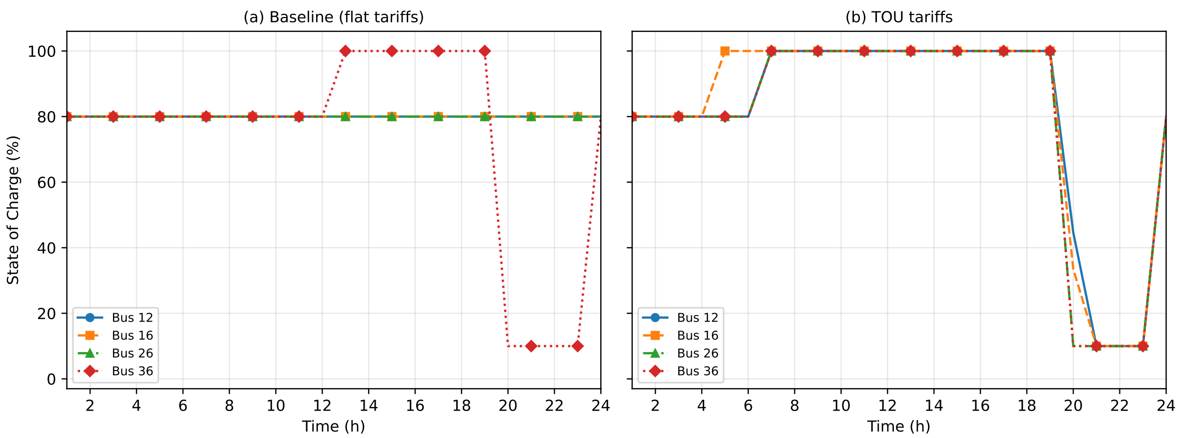

Figure 4.15: SoC profiles of the four BESS units under the baseline (a) and TOU (b) scenarios.

Despite these changes in asset scheduling, the demand response activation remains essentially unchanged: the total curtailed energy is approximately 640 kWh in both scenarios and continues to occur exclusively at hour 20 across Feeder D. This result is especially revealing, as it shows that the congestion responsible for the curtailment is determined primarily by the network's physical characteristics rather than by the tariff structure.

Although the physical congestion remains essentially unchanged, its economic impact on individual community members does not. Under TOU tariffs, ΔY_n decreases to 963.04 € and is now incurred exclusively at Bus 37, compared to 2 172.47 € shared between Buses 36 and 37 under flat tariffs. This suggests that although time-varying prices cannot eliminate structural thermal congestion, they do improve the distribution of its economic consequences. By encouraging a more flexible use of the available resources, TOU tariffs reduce the extent to which members connected to Feeder D exceed their individual Stage 1 benchmarks, thereby partially mitigating the additional cost imposed by the network.

While TOU prices clearly influence how flexible resources are scheduled, they do not eliminate the thermal saturation of branch 1→27, which remains the binding constraint in both scenarios. Overall, this comparison highlights one of the main findings of the case study: economic incentives can significantly modify the scheduling of flexible assets, but they cannot completely overcome physical network limitations when congestion becomes structurally binding.

4.2.4 Network-Constrained Operation: Results and Analysis

This subsection analyses the physical operation of the distribution network under the baseline simulation, focusing on the branch loading distribution, the nodal voltage profiles, and the convergence behavior of the iterative SOC approximation. The analysis concludes with the main comparison of this case study, contrasting the network-constrained solution with an unconstrained version to quantify the impact of explicitly modeling the distribution grid.

All voltage and current results reported in this section correspond to physical magnitudes, recovered from the squared optimization variables $v_{n,t}$ and $l_{n,m,t}$ as $V_{n,t} = \sqrt{v_{n,t}}$ and $I_{n,m,t} = \sqrt{l_{n,m,t}}$. In particular, branch loadings are expressed as the ratio between the recovered current magnitude and the corresponding thermal limit, $\sqrt{l_{n,m,t}}/I_{n,m}^{\max}$.

4.2.4.1 Branch Loading Distribution

The loading of all 36 distribution branches throughout the 24-hour horizon is presented in Figure 4.16, expressed as a percentage of their thermal limit. As can be seen, the highest loading levels are observed in the branches directly connected to the primary substation (Bus 1), namely branches 1→27, 1→17, 1→2, and 1→13, which aggregate the power flows of their respective downstream feeders. This behavior is characteristic of radial distribution networks, where upstream branches carry the combined power of all downstream nodes.

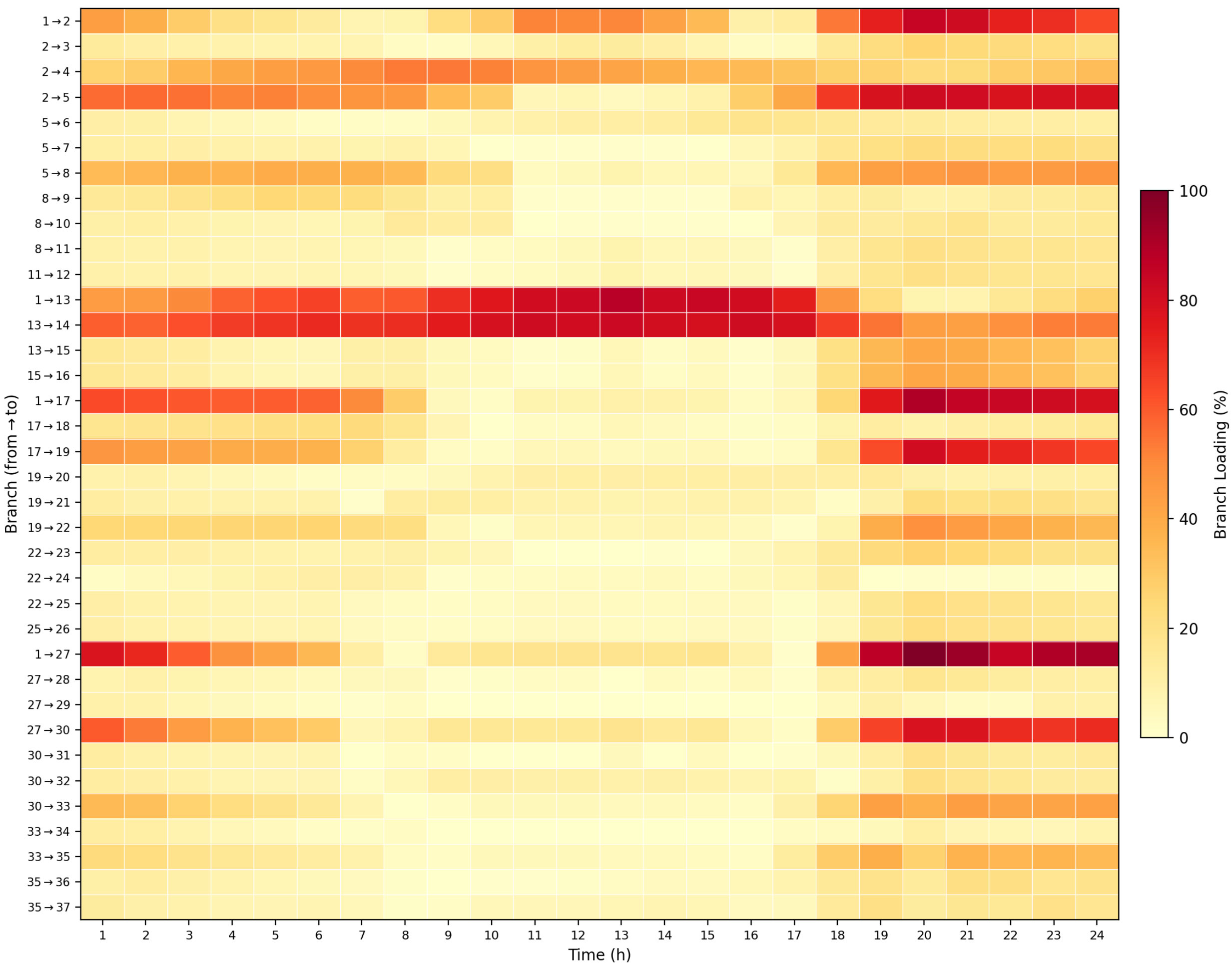

Figure 4.16: Branch loading distribution heatmap across all 36 branches over the 24-hour horizon (baseline simulation).

Moreover, a closer look at the heatmap reveals two different loading patterns throughout the day. During its central hours (approximately hours 11 to 16), the branches connected to the main generation hubs, particularly branches 1→13 and 13→14, present a significant loading increase. This behavior is associated with the high concentration of generation resources at Bus 14, including PV, wind, and CHP units, which create a local surplus that must be transported to other parts of the network and, when applicable, exported upstream.

A distinct situation occurs during the evening peak (hours 19–22), in which the loading shifts towards the branches supplying the high-demand feeders, with branch 1→27 reaching exactly 100% of its thermal capacity at hour 20 in the network-constrained solution. This branch, which supplies the entire Feeder D, constitutes the binding network constraint of the system and is the direct cause of the demand response activation across this feeder discussed in Section 4.2.3.

The fact that branch 1→27 reaches its thermal limit during the evening demand peak, when PV generation is no longer available and local flexibility resources have already been utilized, confirms the physical consistency of the model. At this operating point, the network is no longer capable of supplying the required downstream demand without violating the branch rating.

4.2.4.2 Voltage Profile Analysis

The nodal voltage behavior is summarized in Figure 4.17, which shows the evolution of the minimum and maximum nodal voltages across the network at each time period. Throughout the entire horizon, the results indicate a stable voltage profile, with all bus voltages remaining within the defined limits of 0.95–1.05 p.u.

The highest voltage is observed at Bus 14, reaching approximately 1.016 p.u. around midday. This coincides with the period of maximum renewable generation, when injecting active power into the network raises the voltage at generation-rich nodes. On the other hand, the lowest voltage occurs at Bus 36, reaching approximately 0.973 p.u. during the evening peak (hour 21), reflecting the voltage drop along the heavily loaded Feeder D.

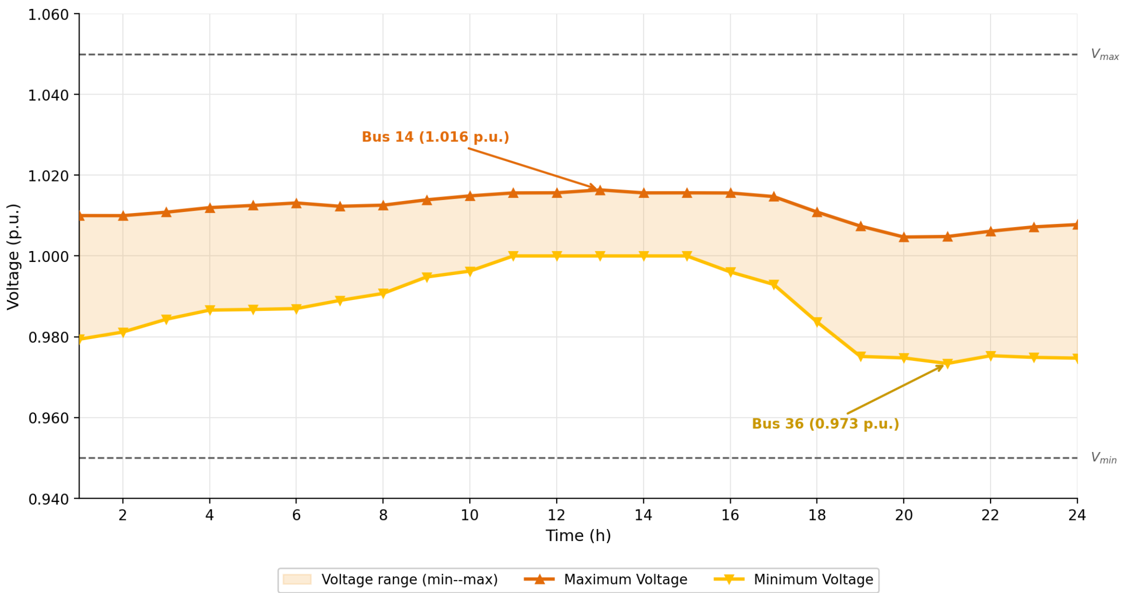

Figure 4.17: Voltage envelope (minimum and maximum nodal voltages) over the 24-hour horizon (baseline simulation), bounded by the regulatory limits of 0.95–1.05 p.u.

An important observation is that the voltage limits never become binding during the simulation. That is, although voltage variations follow the expected daily changes in generation and demand, they remain sufficiently far from the admissible boundaries, indicating that, for this network and operating conditions, the system feasibility is essentially constrained by thermal (current) limits rather than by voltage constraints, which is consistent with the observations obtained in the preliminary case study in Section 4.1.

4.2.4.3 Convergence of the SOC Approximation

Regarding the iterative outer-approximation procedure used to represent the SOC constraint, detailed in Subsection 3.4.2.2, it was used to tighten the linear representation on the 37-bus network. The procedure was controlled by two stopping criteria: a strict numerical tolerance of 5×10^{-7} p.u.^{2}, below which the SOC relation is considered fully satisfied, and a practical acceptance threshold of 10^{-3} p.u.^{2}, adopted to avoid the numerical instability that can arise when a very large number of nearly redundant cuts accumulate in the model.

Starting from an initial maximum violation of approximately 25 p.u.^{2}, the approximation improved progressively as additional supporting hyperplanes were introduced. After 19 iterations and a total of 5 700 supporting hyperplanes, the maximum residual SOC violation across all 36 branches and 24 time periods was reduced to 5.11×10^{-4} p.u.^{2}, at which point the procedure was stopped. Although this value remains above the strict tolerance, it is below the practical acceptance threshold and was therefore considered sufficiently small for the purposes of the present study.

Compared with the 10-bus validation network of Section 4.1, this larger system naturally required a significantly greater number of cuts. This is expected, since the 37-bus case contains 864 simultaneous SOC constraints (36 branches $\times$ 24 periods), making the approximation problem considerably more demanding. Moreover, beyond this point, the residual violation no longer decreased consistently, and additional cuts only increased the numerical complexity of subsequent solves. For this reason, the procedure was terminated once the residual violation became physically negligible.

To confirm that this residual violation has no impact on the reported results, the consistency between the optimized branch currents and the corresponding power flows was evaluated after the optimization process. The largest discrepancy that the residual violation could introduce in any branch loading was found to be only 0.25% of the thermal limit, occurring on a lightly loaded branch (branch 30→31 at hour 10, more precisely). More importantly, the SOC relation is satisfied with negligible error in branch 1→27, the most critical branch in the network, which reaches its thermal limit at hour 20. Therefore, the residual approximation gap does not affect the network loading results, the congestion analysis, or any of the conclusions drawn throughout this case study.

4.2.4.4 Impact of Network Constraints: Constrained vs. Unconstrained Operation

The final and most important comparison in this case study evaluates the impact of considering network constraints on the community optimization. For this purpose, the network-constrained solution presented in this chapter is compared with an unconstrained version, in which the RBFM is disregarded from the optimization, with the community therefore being scheduled exclusively according to economic criteria while using exactly the same demand, generation, and market data.

Moreover, to assess the physical consequences of this unconstrained dispatch, a linearized DistFlow was subsequently applied to the resulting economic solution, providing an estimation of the branch flows and nodal voltages that would physically arise if the resulting dispatch were implemented in the actual distribution network.

From an economic perspective, the unconstrained solution performs considerably better, with a total energy cost of 6 307.89 €, compared to the 9 476.57 € value obtained in the network-constrained case. This difference of 3 169 € is almost entirely explained by the absence of demand response activation. While the constrained solution requires approximately 640 kWh of load curtailment, corresponding to about 3 200 € in penalty costs, in the unconstrained formulation no curtailment is scheduled at any time period. Therefore, and presumably, the unconstrained solution would appear to be the preferable option.

However, this apparent economic benefit comes with a cost to the physical feasibility. Figure 4.18 compares the maximum loading of the most heavily used branches under both formulations. While all branches remain within their thermal limits in the network-constrained solution, the unconstrained dispatch reveals four overloaded branches at the evening peak (hour 20). The most extreme case occurs in branch 1→27, which reaches 130.8% of its thermal capacity. Additional overloads are observed in branches 27→30 (102.4%), 1→17 (102.1%), and 1→2 (101.7%). Moreover, branch 1→27 remains overloaded beyond this single hour, exceeding its rating for three consecutive evening hours (reaching 130.8%, 117.4%, and 100.5% at hours 20, 21, and 22, respectively), confirming that the violation is structural rather than a momentary peak. Notably, the largest violations occur in Feeder D, the same area previously identified as the most critical part of the network and the location where demand response activation became necessary.

For comparison, the figure also includes branch 1→13, which supplies Feeder B, the area with the highest generation concentration. Although this branch remains below its thermal limit, its loading still increases noticeably from 88.27% to 95.95% when the network model is removed. This shows that the unconstrained dispatch affects loading across the network, and not only on the four branches that exceed their thermal ratings.

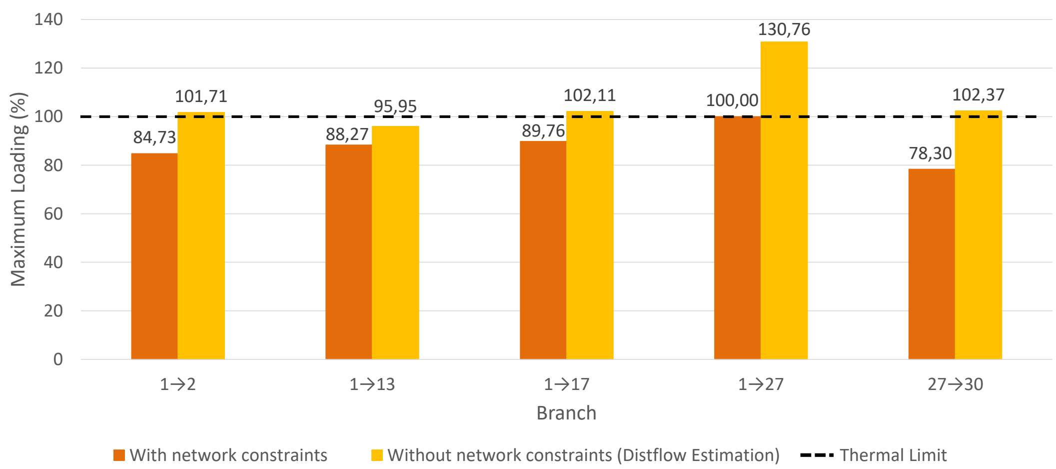

Figure 4.18: Maximum loading of the most heavily used branches with and without network constraints.

Another interesting observation emerges from the internal P2P market activity. The total volume of bilateral energy traded is nearly the same in both cases (82.79 MWh with the network modeled versus 83.60 MWh without it), indicating that the network constraints barely affect the total amount of energy exchanged within the community. Instead, their main effect is on the distribution of these exchanges across the network. In particular, the share of inter-feeder trading increases from 77.8% in the unconstrained case to 86.3% when the network constraints are considered.

This shows that, rather than increasing the overall level of P2P trading, the network constraints change the direction of the energy exchanges. More energy is traded between different feeders, helping to relieve the loading on the critical branches before demand-response curtailment becomes necessary.

These results highlight the importance of considering the distribution network during the optimization process. Although the unconstrained solution achieves a lower operating cost, it does so by relying on power flows that the physical network cannot support. This type of schedule would require corrective actions from the DSO, such as re-dispatch measures or additional load curtailment, before it could be safely implemented.

In contrast, the proposed network-constrained formulation produces a solution that is fundamentally aligned with the physical capabilities of the grid. The additional operating cost observed in the constrained case can therefore be interpreted as the cost of maintaining network feasibility. Ultimately, this comparison demonstrates that economic optimality alone is not sufficient when operating RECs. Network constraints must also be considered to ensure that the resulting schedules remain physically achievable.

4.2.5 Discussion and Main Findings

The results from this case study provide a comprehensive view of how an REC operates when market decisions and distribution network constraints are considered simultaneously. The analysis also helps to identify the main factors driving both the economic and physical behavior of the community, highlighting the importance of considering market and network interactions within a unified framework.

The most relevant outcome of the case study emerges from the comparison between the constrained and unconstrained solutions. Although the unconstrained formulation achieves a cost reduction of approximately 3 169 € (about 33.4% lower than the constrained case), the resulting dispatch is not physically feasible. When evaluated through a post-hoc power flow analysis, four branches exceed their thermal limits, with branch 1→27 reaching 130.8% loading. The network-constrained formulation, in contrast, produces a fully feasible schedule at the cost of a moderate increase in the community objective. This confirms that economic optimality alone is insufficient when operating a REC, since market decisions that ignore network limits may lead to schedules that cannot be safely implemented in practice.

The analysis also shows that the congestion observed in the network is largely structural, due to the fact that regardless of whether flat or TOU tariffs are considered, branch 1→27 remains the critical element of the system, and demand response activation remains practically unchanged at 640 kWh, concentrated entirely at hour 20. This demonstrates that the observed congestion is essentially determined by the network topology and the spatial distribution of demand rather than by the economic incentives applied. Consequently, tariff-based flexibility can mitigate operating costs, but it cannot completely eliminate a binding physical constraint.

Thereafter, the operation of the flexible resources reveals an interesting distinction between how stationary storage and EV flexibility contribute to community operation. Under flat tariffs, the BESS units remain inactive unless required for congestion relief, whereas the EV fleet actively shifts energy from periods of surplus generation to periods of high demand. This difference highlights that the economic value of flexibility depends not only on the asset itself but also on the operating context that activates it, namely the price spread for EVs and the congestion relief for the BESS at Bus 36. The strong inter-feeder character of the P2P trading further confirms that locally generated energy is effectively redistributed throughout the network, with Bus 14 acting as the main supplier due to its combination of wind and CHP generation. Notably, the network constraints do not change the total volume of bilateral trading (about 83 MWh in both the constrained and unconstrained cases), but they do influence how this energy is exchanged across the network. The share of inter-feeder trading increases from 77.8% to 86.3% when the network is modeled, indicating that P2P exchanges are redirected between feeders to help relieve congestion rather than simply increasing in volume.

Another important observation, consistent with the preliminary validation of Section 4.1, is that the feasibility of this network is managed by thermal limits rather than by voltage constraints. Throughout all simulations, the nodal voltages remain comfortably within the admissible range, never becoming binding, while the branch currents become the active limiting factor. This suggests that, for compact MV distribution networks of this type, congestion management is the dominant network concern in REC scheduling.

Ultimately, from a methodological perspective, the SOC outer-approximation proved sufficiently accurate for the considered application. Although the larger 37-bus system required substantially more cuts than the validation network and did not meet the strict numerical tolerance of 5×10^{-7}, the remaining violation was shown to have a negligible impact on the physical results. In particular, the loading error introduced by the approximation was around 0.25% and effectively zero on the binding branch. These results support the use of the cutting-plane approach while also referencing the growing computational effort associated with larger networks.

Overall, these findings demonstrate that modeling the distribution network significantly impacts REC operations. The proposed framework successfully coordinates local generation, storage resources, EV flexibility, and P2P trading while ensuring compliance with network limits. More importantly, the results show that network constraints are not a secondary modeling detail, but a necessary component for obtaining realistic and implementable community schedules.

Chapter 5

Conclusions

This final chapter summarizes the main conclusions drawn from the work developed throughout this dissertation. It begins by revisiting the problem that motivated the research and the approach adopted to address it, followed by a discussion of the main findings and contributions. Finally, an outline of the several directions for future work is presented.

5.1 Main Conclusions and Contributions

The increasing penetration of DERs and the emergence of prosumers have reinforced the role of RECs in the energy transition. However, as discussed throughout this dissertation, a significant amount of the optimization models considered for REC operation rely on simplified or unconstrained network representations, potentially leading to schedules that are economically attractive but physically infeasible. Addressing the gap between market operations and physical network behavior was the main motivation for this work.

To overcome this gap, a network-constrained optimization framework was developed and integrated into INESC TEC's OSTEC platform. The proposed formulation combines the RBFM constraints directly within the community's economic optimization, ensuring that the resulting energy schedules are not only economically efficient but also physically feasible. Furthermore, to preserve compatibility with OSTEC's existing MILP-based architecture, the SOC constraint was handled via an iterative linear outer-approximation procedure, enabling the network-constrained formulation to be embedded within the original optimization framework without requiring a native SOCP implementation.

The proposed framework was validated through two complementary case studies. The preliminary 10-bus radial network focused on validating the correct implementation of the model and the numerical behavior of the linear outer-approximation to accurately reproduce AC power-flow behavior. The results showed excellent agreement with nonlinear power-flow calculations, PowerWorld simulations, and an alternative sensitivity-based network representation, thereby establishing the reliability of the implementation before its application to a larger, more realistic scenario.

The main case study applied the validated framework to a realistic 37-bus distribution network that hosts an REC equipped with renewable generation, battery storage systems, and an aggregated EV fleet. The comparison between the constrained and unconstrained solutions ultimately revealed the most important conclusion of this work. Although the unconstrained formulation achieved a lower operating cost (a reduction of approximately 33%), a subsequent power flow evaluation indicated that it relied on power flows that the network could not physically support, leading to severe branch overloads (reaching up to 130.8% of the thermal limit) that would not be acceptable in a real network. In contrast, the proposed formulation produced a fully feasible schedule, at the cost of a moderate increase in the community objective. This result clearly shows that economic optimality alone is insufficient for REC operation and that the distribution network must be considered directly during scheduling.

Besides this central comparison, one of the main findings of the study concerns how congestion develops within the community. The critical congestion remained concentrated on the same branch and during the same evening period under both flat and TOU tariffs, indicating that the congestion was primarily caused by the network topology and the location of demand rather than by the tariff structure considered. This indicates that, while economic incentives can influence the behavior of flexible assets, they cannot eliminate a structurally binding network limitation.

Moreover, although the volume of bilateral P2P trading remained almost unchanged when network constraints were considered (about 83 MWh in both cases), the share of inter-feeder exchanges increased considerably (from 77.8% to 86.3%), indicating that network constraints alter the spatial distribution of energy exchanges rather than the overall trading volume. This result suggests that the integrated optimization exploits the redistribution of energy flows, together with the coordinated operation of flexible resources, as part of the overall congestion management strategy, thereby reducing the need for load curtailment.

The coordinated operation of flexible resources also differed according to the operating conditions. Battery storage remained largely inactive when price arbitrage alone was insufficient to justify its operation, becoming active only when required to relieve network congestion. In contrast, the aggregated EV fleet consistently shifted surplus midday renewable generation towards the evening demand peak. These results highlight the complementary roles of different flexibility resources, whose utilization depends on both economic incentives and network operating requirements.

Beyond confirming the results obtained, the comparison with the sensitivity-based procedure also revealed a broader methodological distinction between the two approaches to handling network feasibility. In the small validation network, where curtailment was the only available corrective action, both approaches produced very similar outcomes. However, in larger systems, the integrated formulation can coordinate generation, storage, and P2P trading with network limits, thereby relieving congestion through several flexibility mechanisms before curtailment becomes necessary.

Overall, the work developed in this dissertation highlights not only the technical but also the practical significance of explicitly considering the distribution network when optimizing REC operations. By integrating a tractable network-constrained OPF formulation into the OSTEC platform, it became possible to align market decisions and network operations within a single optimization framework. The obtained results demonstrate that such integration leads to more realistic, technically consistent, and practically implementable schedules, supporting the operation of future RECs under increasingly constrained distribution network conditions. Nevertheless, the proposed framework remains subject to some limitations. The current formulation assumes balanced radial distribution networks and deterministic operating conditions, while the iterative outer-approximation adopted to preserve compatibility with the MILP-based OSTEC architecture still imposes a significant computational burden on larger systems. These limitations do not affect the validity of the proposed methodology but rather identify opportunities for further methodological development, which are discussed in the following subsection.

5.2 Future Work

Building upon the limitations identified in the previous section, several research directions can be envisaged to further extend the proposed framework and improve its applicability to practical REC operation, namely:

- Reduce the computational burden of the proposed framework, whose current execution time exceeds one hour for the 37-bus case. This includes investigating strategies to limit the growth in the number of supporting hyperplanes generated by the cutting-plane procedure, as well as exploring warm-starting, cut-management, decomposition techniques, or alternative solution strategies to accelerate the successive MILP solves;
- Assess the scalability of the proposed framework by applying it to larger distribution systems comprising several hundred buses, evaluating both the computational performance and the effectiveness of the proposed methodology under increasingly complex network conditions;
- Incorporate uncertainty in renewable generation, demand, and EV availability, moving from the current deterministic formulation to a stochastic or robust approach better suited to real-time operation, thereby accounting for forecast errors in renewable generation, electricity demand, and EV availability;
- Replace the simplified proportional reactive power model with inverter capability curves and, where appropriate, coordinated Volt/Var control strategies;
- Extend the network-constrained formulation to a decentralized solution scheme, in which the optimization is decomposed across community members, preserving the privacy of individual data while maintaining network feasibility;
- Assess the impact of REC operation on non-participating network users in order to evaluate whether the benefits achieved within the community create positive or adverse externalities for consumers outside the REC;

- Validate the framework using data from operational REC pilots or DSO demonstrators, in order to refine the modeling assumptions and confirm its applicability under practical operating conditions.

References

[1] United Nations. *Sustainable Development Goals*. Accessed: 2026-02-11. URL: https://www.un.org/.

[2] European Commission et al. *Energy communities in the clean energy package – Best practices and recommendations for implementation*. Publications Office, 2020. DOI: doi/10.2833/51076.

[3] European Union. *Directive (EU) 2018/2001 of the European Parliament and of the Council of 11 December 2018 on the Promotion of the Use of Energy from Renewable Sources (Recast) (Text with EEA Relevance)*. Accessed: 2026-04-12. 2018. URL: https://eur-lex.europa.eu/eli/dir/2018/2001/oj/eng.

[4] European Union. *Directive (EU) 2019/944 on common rules for the internal market for electricity and amending Directive 2012/27/EU*. Accessed: 2026-04-18. URL: https://eur-lex.europa.eu/legal-content/EN/TXT/?uri=CELEX:32019L0944.

[5] Rogério Rocha et al. "A Three-Stage Model to Manage Energy Communities, Share Benefits and Provide Local Grid Services". In: *Energies* 16 (3 Jan. 2023), p. 1143. ISSN: 1996-1073. DOI: 10.3390/en16031143.

[6] Wayes Tushar et al. "Peer-to-Peer Trading in Electricity Networks: An Overview". In: *IEEE Transactions on Smart Grid* (Jan. 2020). URL: http://arxiv.org/abs/2001.06882.

[7] Marthe Fogstad Dynge et al. "Impact of local electricity markets and peer-to-peer trading on low-voltage grid operations". In: *Applied Energy* 301 (Nov. 2021), p. 117404. ISSN: 0306-2619. DOI: 10.1016/J.APENERGY.2021.117404. URL: https://www.sciencedirect.com/science/article/pii/S0306261921008035.

[8] Fabio Moret and Pierre Pinson. "Energy Collectives: A Community and Fairness Based Approach to Future Electricity Markets". In: *IEEE Transactions on Power Systems* 34 (5 Sept. 2019), pp. 3994–4004. ISSN: 15580679. DOI: 10.1109/TPWRS.2018.2808961. URL: https://ieeexplore.ieee.org/document/8301552.

[9] Carlos Oliveira et al. "Consumer-centric electricity markets: A comprehensive review on user preferences and key performance indicators". In: *Electric Power Systems Research* 210 (Sept. 2022), p. 108088. ISSN: 0378-7796. DOI: 10.1016/J.EPSR.2022.108088. URL: https://www.sciencedirect.com/science/article/pii/S0378779622003121.

[10] Tiago Sousa et al. "Peer-to-peer and community-based markets: A comprehensive review". In: *Renewable and Sustainable Energy Reviews* 104 (Apr. 2019), pp. 367–378. ISSN: 18790690. DOI: 10.1016/j.rser.2019.01.036.

[11] Rubi Rana et al. "Modelling and Simulation Approaches for Local Energy Community Integrated Distribution Networks". In: *IEEE Access* 10 (2022), pp. 3775–3789. ISSN: 21693536. DOI: 10.1109/ACCESS.2022.3140237.

[12] Carlos Oliveira et al. "Distributed Network-Constrained P2P Community-Based Market for Distribution Networks". In: *Energies* 16 (3 Feb. 2023), p. 1520. ISSN: 1996-1073. DOI: 10.3390/en16031520.

[13] Daniel K Molzahn and Ian A Hiskens. "A Survey of Relaxations and Approximations of the Power Flow Equations". In: *Foundations and Trends R in Electric Energy Systems* 4 (2 2019), pp. 1–221. DOI: 10.1561/3100000012.

[14] Steven H. Low. "Convex Relaxation of Optimal Power Flow-Part I: Formulations and Equivalence". In: *IEEE Transactions on Control of Network Systems* (1 Mar. 2014), pp. 15–27. DOI: 10.1109/TCNS.2014.2309732.

[15] Tianqi Hong, Dongbo Zhao, and Yichen Zhang. "A Relaxed PV Bus Model in Linear Power Flow". In: *IEEE transactions on power delivery* (2 Apr. 2021), pp. 1249–1252. DOI: 10.1109/TPWRD.2020.3031758.

[16] Masoud Farivar and Steven H. Low. "Branch Flow Model: Relaxations and Convexification—Part I". In: *IEEE Transactions on Power Systems* 28.3 (2013), pp. 2554–2564. DOI: 10.1109/TPWRS.2013.2255317.

[17] Biswajit Dipan Biswas, Md Shamim Hasan, and Sukumar Kamalasadan. "Decentralized Distributed Convex Optimal Power Flow Model for Power Distribution System Based on Alternating Direction Method of Multipliers". In: *IEEE Transactions on Industry Applications* 59.1 (1 2023), pp. 627–640. DOI: 10.1109/TIA.2022.3217023.

[18] M.E. Baran and F.F. Wu. "Network reconfiguration in distribution systems for loss reduction and load balancing". In: *IEEE Transactions on Power Delivery* 4.2 (1989), pp. 1401–1407. DOI: 10.1109/61.25627.

[19] Shaojun Huang et al. "A Sufficient Condition on Convex Relaxation of AC Optimal Power Flow in Distribution Networks". In: *IEEE Transactions on Power Systems* 32 (2 Mar. 2017), pp. 1359–1368. ISSN: 08858950. DOI: 10.1109/TPWRS.2016.2574805.

[20] Hongjun Gao, Junyong Liu, and Lingfeng Wang. "Robust Coordinated Optimization of Active and Reactive Power in Active Distribution Systems". In: *IEEE transactions on smart grid* (5 Sept. 2018), pp. 4436–4447. DOI: 10.1109/TSG.2017.2657782.

[21] Hui Du et al. "Decentralized optimal power flow based on auxiliary problem principle with an adaptive core". In: *Energy Reports* 8 (Nov. 2022), pp. 755–765. ISSN: 2352-4847. DOI: 10.1016/J.EGYR.2022.08.152.

[22] Wanessa Guedes et al. "Community Energy Markets with Battery Energy Storage Systems: A General Modeling with Applications". In: *Energies 2022, Vol. 15,* 15 (20 Oct. 2022). ISSN: 1996-1073. DOI: 10.3390/EN15207714. URL: https://www.mdpi.com/1996-1073/15/20/7714.

[23] Jaysson Guerrero, Archie C. Chapman, and Gregor Verbič. "Decentralized P2P Energy Trading Under Network Constraints in a Low-Voltage Network". In: *IEEE Transactions on Smart Grid* 10 (5 Sept. 2018), pp. 5163–5173. ISSN: 19493061. DOI: 10.1109/TSG.2018.2878445.

[24] Alexandra Lüth et al. "Local electricity market designs for peer-to-peer trading: The role of battery flexibility". In: *Applied Energy* 229 (Nov. 2018), pp. 1233–1243. ISSN: 03062619. DOI: 10.1016/j.apenergy.2018.08.004.

[25] Gijs van Leeuwen et al. "An integrated blockchain-based energy management platform with bilateral trading for microgrid communities". In: *Applied Energy* 263 (Apr. 2020), p. 114613. ISSN: 0306-2619. DOI: 10.1016/J.APENERGY.2020.114613. URL: https://www.sciencedirect.com/science/article/pii/S0306261920301252.

[26] Jose Luis Crespo-Vazquez et al. "A Community-Based Energy Market Design Using Decentralized Decision-Making Under Uncertainty". In: *IEEE Transactions on Smart Grid* 12.2 (2021), pp. 1782–1793. DOI: 10.1109/TSG.2020.3036915.

[27] Portuguese Government. *Decreto-Lei n.º 162/2019*. Accessed: 2026-04-18. URL: https://dre.pt/dre/detalhe/decreto-lei/162-2019-125692189.

[28] Portuguese Government. *Decreto-Lei n.º 15/2022*. Accessed: 2026-04-18. URL: https://diariodarepublica.pt/dr/detalhe/decreto-lei/15-2022-177634016.

[29] Portuguese Government. *Decreto-Lei n.º 99/2024*. Accessed: 2026-04-19. URL: https://diariodarepublica.pt/dr/detalhe/decreto-lei/99-2024-898705893.

[30] *Regulamento de Autoconsumo de Energia Elétrica - ERSE*. Accessed: 2026-04-19. URL: https://www.erse.pt/atividade/regulamentos-eletricidade/autoconsumo/.

[31] Edifícios e Energia. *Comunidades de Energia Renovável ganham peso no futuro orçamento da União Europeia*. https://edificioseenergia.pt/noticias/comunidades-de-energia-renovavel-ganham-peso-no-futuro-orcamento-da-uniao-europeia/. Accessed: 2026-06-21. (2026).

[32] Viver Telheiras. *Comunidade de Energia Renovável de Telheiras/Lumiar*. https://vivertelheiras.pt/certelheiras/. Accessed: 2026-06-21. (2024).

[33] M. M. Sequeira et al. *Guia Prático: Desenvolvimento de comunidades de energia renovável por cidadãos, associações e autarquias — O exemplo da Comunidade de Energia Renovável de Telheiras/Lumiar*. http://vivertelheiras.pt/certelheiras/. Accessed: 2026-06-21. (2024).

[34] Rogerio Rocha et al. "Comparative Analysis of Self-Consumption and Energy Communities Regulation in the Iberian Peninsula". In: *2021 IEEE Madrid PowerTech, PowerTech 2021 - Conference Proceedings* (June 2021). DOI: 10.1109/POWERTECH46648.2021.9494916. URL: https://ieeexplore.ieee.org/abstract/document/9494916.

[35] Gonçalo Coelho, Tiago Soares, and António Sérgio Faria. *Relaxed Branch Flow Model Applied to Renewable Energy Communities — Research Dataset*. Version 2. 2026. DOI: 10.17632/zfrrnh8m4d.2.

[36] PowerWorld Corporation. *PowerWorld Simulator Version 23*. 2024. URL: https://www.powerworld.com.

[37] Stuart Mitchell et al. *PuLP: A Linear Programming Toolkit for Python*. The University of Auckland. 2011. URL: https://coin-or.github.io/pulp/.

[38] Gurobi Optimization, LLC. *Gurobi Optimizer Reference Manual*. 2026. URL: https://www.gurobi.com.

[39] Tommaso Orlandini. "Mutual-Benefit Coordination of P2P Market and Distribution Grid Management". Master's thesis. Politecnico di Milano, 2018.